



A STUDY OF FLOW SURFACE BOILING

by

WALTER TARLETON BROWN, JR.

S.B., United States Military Academy
(1959)

S.M., New Mexico State University
(1963)

SUBMITTED IN PARTIAL FULFILLMENT
OF THE REQUIREMENTS FOR THE
DEGREE OF DOCTOR OF
PHILOSOPHY

at the

MASSACHUSETTS INSTITUTE OF TECHNOLOGY

January 5, 1967

Signature of Author:

Department of Mechanical Engineering, January 5, 1967

Certified by Thesis Supervisor

Accepted by Chairman, Departmental Committee on Graduate Students

A STUDY OF FLOW SURFACE BOILING

by

Walter Tarleton Brown, Jr.

Submitted to the Department of Mechanical Engineering on January 5, 1967, in partial fulfillment of the requirements for the degree of Doctor of Philosophy in Mechanical Engineering

ABSTRACT

A study of surface variables in boiling has been completed. An instrument was developed which allowed the measurement of both the number and size of nuclei on an arbitrary surface. The orientation of surface scratches with respect to advancing liquid-gas interfaces is shown to be the dominant cause for the creation of these nuclei. Experimental work is presented which gives a further understanding of the surface effects.

A new means by which heat is removed in boiling is analyzed and shown to have considerable influence on many aspects of boiling. This phenomenon, which is referred to as thermocapillarity, results from an interaction between the velocity and temperature gradients existing around bubbles produced at surfaces.

The above two studies have lead to a further understanding of the conditions which will produce boiling. Eleven different theories concerning the inception of boiling are found to be special cases of a more generalized model. The basic assumptions of this generalized model are shown to be oversimplifications. These oversimplifications explain the lack of agreement between these models and experimental evidence.

Several techniques were developed for use in the experimentation associated with this work. The first was an instrument for detecting the onset of boiling. The second was an analytical method for solving a large class of nonlinear differential equations.

Thesis Supervisor: Arthur Edward Bergles

Title: Assistant Professor of Mechanical Engineering

DEDICATION

To my wife
whose encouragement and
help made this work possible

ACKNOWLEDGMENTS

The author acknowledges the receipt of a National Science Foundation Graduate Fellowship and the release from normal duties by the Army in order to attend M.I.T.. This study was supported by the National Magnet Laboratory of the Massachusetts Institute of Technology. The facilities of the Computation Center were also relied upon.

Professor Arthur Bergles, my thesis advisor, has given freely of his time and counsel. Professors Warren M. Rohsenow and Peter Griffith were extremely helpful in several aspects of this research. My indebtedness to them cannot be overstated.

Mr. Michael Cooper, lecturer at Cambridge University, provided many thought provoking and penetrating discussions. Professor Lloyd Trefethen, Chairman of the Mechanical Engineering Department at Tufts University, has given graciously of his time and experience. Both gentlemen contributed much to the understanding of thermocapillarity.

The technical staff of the Engineering Projects Laboratory has continually given prompt and cheerful assistance. A particular note of appreciation is due to Mr. Fred Johnson.

Finally, I would like to acknowledge the many graduate students in the Heat Transfer Laboratory whom I have had the privilege of knowing. The innumerable discussions which we have had on all aspects of our work have been quite valuable and broadening. A special thanks in this regard to Captain Robert F. Lopina.

TABLE OF CONTENTS

| | Page |
|--|--------|
| Title Page | 1 |
| Abstract | 2 |
| Dedication | 3 |
| Acknowledgments | 4 |
| Table of Contents | 5 |
| List of Figures | 7 |
| Symbols | 9 |
| Chapter I - Introduction | 14 |
| Chapter II - The Measurement of Cavity Size Distributions | 17 |
| A. Introduction | 17 |
| B. Theory | 18 |
| C. Apparatus | 19 |
| D. Results | 20 |
| E. Conclusions | 23 |
| Chapter III - Thermocapillarity | 24 |
| A. Bubble Boundary Layer | 24 |
| B. Jetting | 25 |
| C. Order of Magnitude Calculations | 26 |
| 1. Model Formulation | 26 |
| 2. Interfacial Temperature Drop | 31 |
| 3. Applicability of Model | 34 |
| D. Other Proposed Mechanisms for Heat Transfer | 36 |
| E. "Anomilies" Explainable by Thermocapillarity | 39 |
| F. Conclusions | 41 |
| Chapter IV - The Measurement of Temperatures at the Heat Transfer Surface for Electrically-Heated Tubes | 43 |
| A. Introduction | 43 |
| B. Problem Formulation | 45 |
| C. The Rapid-Convergence Solution | 47 |
| D. The Application of the Rapid-Convergence Technique for Electrically-Heated Tubes | 41 |
| E. The Measurement of Thermal Conductivity Appropriate for Electrically-Heated Tubes | 53 |

TABLE OF CONTENTS

(continued)

| | Page |
|--|------|
| Chapter V - Experimental Equipment and Procedure | 58 |
| A. Boiling Apparatus | 58 |
| B. Thermocouple Design | 62 |
| C. Bubble Detector | 63 |
| D. Measurement of Gas Concentration | 65 |
| E. Experimental Procedure | 67 |
| Chapter VI - The Inception of First Significant Boiling | 70 |
| A. Introduction | 70 |
| B. Literature Survey | 71 |
| C. Analytical Solution | 74 |
| D. Experimental Results of Other Investigators | 83 |
| E. A Reexamination of the Model's Assumptions | 86 |
| F. The Existence of Metastable States at Inception | 90 |
| G. Conclusions | 92 |
| Chapter VII - The Effect of the Surface on Boiling | 94 |
| A. Introduction | 94 |
| B. Pool Boiling | 94 |
| 1. Apparatus | 94 |
| 2. Results | 95 |
| C. Flow Boiling | 96 |
| 1. General Results | 96 |
| 2. Hysteresis | 98 |
| D. Conclusions | 100 |
| References | 101 |
| Appendices | |
| A: Application of the Rapid-Convergence Technique to the Solution of the Gravity Pendulum | 108 |
| B: The Thickness of the Laminar Sublayer | 112 |
| C: Sample Reduction of Data of McAdams, et al. | 114 |
| D: Original Inception Data | 115 |
| Figures | 117 |
| Biographical Note | 151 |

LIST OF FIGURES

| Fig. No. | Title | Page |
|----------|---|------|
| 1 | Various States During the Growth of a Bubble | 117 |
| 2 | Bubble Meter for Use in Measuring the Cavity Size Distribution | 118 |
| 3 | Some Quantitative Results from Measurements of Cavity Sizes | 119 |
| 4 | Cavity Size Distributions for Various Finishes | 120 |
| 5 | Bankoff's Mechanism of Nuclei Formation | 121 |
| 6 | Some Results of Jiji and Clark ¹² | 122 |
| 7 | The Mechanism of Thermocapillarity | 123 |
| 8 | Jetting in Acetone - Trefethen ¹⁸ | 124 |
| 9 | Jetting in Water - Farello ¹⁹ | 125 |
| 10 | The Influence of Flow Velocity on Thermocapillarity | 126 |
| 11 | Comparison of Burnout Heat Flux with the Expected Thermocapillarity Heat Flux | 127 |
| 12 | Temperature Dependence of Thermal Conductivity for 304 Stainless Steel | 128 |
| 13 | Schematic Layout of Experimental Facility | 129 |
| 14 | Test Section Assembly | 130 |
| 15 | Schematic of Bubble Detector | 131 |
| 16 | Influence of Dissolved Gas on Inception of Flow Surface Boiling | 132 |
| 17 | Generalized Flow Diagram for Prediction of Boiling Inception | 133 |
| 18 | Schematic Representation of Bubble Growth in Flow Surface Boiling | 134 |
| 19 | Dimensionless Representation of Inception | 135 |

LIST OF FIGURES
(continued)

| Fig. No. | Title | Page |
|----------|--|------|
| 20 | Flow Boiling Inception Data of McAdams' Project ⁵¹ | 136 |
| 21 | Flow Boiling Water Data of Various Investigators | 137 |
| 22 | Flow Boiling Data of Various Investigators for Fluids Other than Water | 138 |
| 23 | Inception of Flow Surface Boiling when there is an Absence of Large Cavities | 139 |
| 24 | Dimensionless Inception Loci when the Largest Cavity is r_{\max} | 140 |
| 25 | Flow Boiling Inception Data for Water from Present Investigation | 141 |
| 26 | Some Conditions for Bubble Growth and Collapse | 142 |
| 27 | Illustration of Metastable States for Nuclei | 143 |
| 28 | Influence of Surface Finish when Pool Boiling from the Outside of a Horizontal Tube | 144 |
| 29 | Flow Surface Boiling Data - Moderate Heat Flux | 145 |
| 30 | Flow Surface Boiling Data - Low Heat Flux | 146 |
| 31 | Flow Surface Boiling Data - Very Low Heat Flux | 147 |
| 32 | Expected Influence of Surface Finish - Pool vs. Flow Boiling | 148 |
| 33 | Data Illustrating Hysteresis in Flow Boiling | 149 |
| 34 | Comparison of Linear and Nonlinear Solutions for the Gravity Pendulum | 150 |
| 35 | Some Flow Surface Boiling Data of McAdams, et al. ³⁰ | 151 |

SYMBOLS

Arabic

| | | |
|-----------------|---|---|
| a | = | power series coefficients defined by Eq. 35 |
| A | = | surface area |
| A_b | = | projected bubble area, defined by Eq. 11 |
| A_{cs} | = | cross-section area of a tube |
| AR | = | axial scratches - rough finish |
| AS | = | axial scratches - smooth finish |
| b | = | power series coefficients defined by Eq. 43 |
| C_1, C_2, C_3 | = | constants defined by Eqs. 8, 9, and 10 respectively |
| C | = | dissolved gas concentration |
| \bar{C} | = | a constant defined by Eq. 1 |
| CR | = | circumferential scratches - rough finish |
| CS | = | circumferential scratches - smooth finish |
| c_p | = | constant pressure specific heat |
| d | = | constant defined by Eq. 73 |
| D | = | hydraulic diameter |
| D_b | = | bubble diameter |
| E | = | voltage drop across tube length |
| f | = | friction factor defined by Eq. 28 |
| h_H | = | heat transfer coefficient |
| H | = | height of bubble |
| h_{fg} | = | latent heat of vaporization |
| I | = | electrical current |

| | |
|--------------|--|
| k | = thermal conductivity |
| k_L | = thermal conductivity of the liquid |
| k_o | = defined by Eq. 27 |
| $K(T)$ | = Henry's Law Constant |
| l | = liter |
| ℓ | = length |
| L | = the solution to a linearized differential equation |
| m | = defined by Eq. 1 |
| M | = molecular weight |
| \dot{m}/A | = mass flux |
| n | = defined by Eq. 63 |
| N/A | = number of bubbles per unit area |
| $(N/A)_m$ | = number of metastable nuclei per unit area |
| p | = pressure |
| p_{atm} | = atmospheric pressure |
| p_{Hg} | = pressure head of mercury |
| p_{hs} | = hydrostatic pressure |
| P | = defined by Eq. 29c |
| Pr | = Prandtl number |
| q/A | = heat flux |
| $(q/A)_{BO}$ | = heat flux at burnout |
| $(q/A)_i$ | = heat flux at inception |
| $(q/A)_j$ | = heat flux resulting from jetting |
| r | = radius |
| R | = defined by Eq. 29b |
| R_1, R_2 | = principal radii of curvature |
| r_{max} | = maximum cavity radius |
| R_v | = gas constant |

| | | |
|------------------|---|---|
| Re | = | Reynolds number |
| Res | = | electrical resistance |
| t | = | time |
| T | = | temperature |
| T_{air} | = | air temperature |
| T_{b} | = | bulk temperature |
| T_{cr} | = | critical temperature |
| T_{s} | = | saturation temperature |
| T_{w} | = | wall temperature |
| v | = | specific volume |
| v_{cr} | = | critical volume |
| V | = | mean stream velocity |
| V_{b} | = | velocity of bubble |
| v_{cr} | = | critical volume of a gram-mole |
| V_{j} | = | velocity of thermocapillarity induced jet |
| W_{i} | = | heat generated per unit volume |
| y | = | distance measured from solid wall into liquid |

Greek

| | | |
|------------|---|--|
| α | = | defined by Eq. 26 |
| A | = | defined by Eq. 30 |
| β | = | defined by Eq. 27 |
| B | = | defined by Eq. 30 |
| γ | = | defined by Eq. 86 |
| δ | = | thickness of thermal boundary layer |
| ϵ | = | natural logarithm base |
| Δp | = | pressure difference across phase interface |

| | | |
|------------------|---|---|
| Δt_w | = | tube wall thickness |
| ΔT_b | = | temperature drop across a bubble |
| ΔT_{sub} | = | saturation temperature minus bulk temperature |
| ΔT_s | = | wall temperature minus saturation temperature |
| θ | = | bubble lifetime (in Chapter III) |
| θ | = | defined by Eq. 29a (in Chapter IV) |
| θ | = | angle of pendulum from the vertical (in Appendix A) |
| ν | = | kinematic viscosity |
| λ | = | accommodation coefficient |
| ρ | = | electrical resistivity |
| ρ_L | = | density of liquid |
| ρ_o | = | defined by Eq. 26 |
| ρ_v | = | density of vapor |
| σ | = | surface tension |
| τ_o | = | wall shear stress |
| ω | = | defined by Eq. 2A |

Subscripts

| | | |
|---|---|---|
| A | = | designates a specific temperature profile |
| B | = | designates a specific temperature profile |
| c | = | cold wall |
| C | = | designates a specific temperature profile |
| g | = | gas |
| h | = | hot wall |
| i | = | at inception |

L = liquid
r = rough
s = smooth
v = vapor

Superscripts

* denotes a dimensionless quantity

Chapter I - Introduction

Despite the extensive research, both experimental and theoretical, into the boiling phenomenon, it is still not well understood. The motivation for this research is caused, first, by the increasing number of heat-limited systems being designed which are characterized by a large heat generation per unit volume and, second, by the extremely high heat fluxes obtainable in boiling. This last motivating factor is made apparent when one realizes that boiling surfaces are able to have higher heat fluxes than the energy flux leaving the sun's surface without even approaching the 10,000°F temperature of that surface.

Flow boiling, when measured in terms of heat removed per volume of coolant space, has the greatest capacity for removing heat for applications in systems with high heat generation per unit volume. Very early in the study of boiling it was felt that an understanding of flow boiling could be best gained if one first eliminated the flow velocity and studied boiling in a stagnant liquid. This was the impetus given to the thousands of studies which have been made of pool boiling over the past twenty years. Many other studies have approached the flow boiling problem by eliminating the temperature gradients and associated heat fluxes, and have concentrated on two-phase isothermal phenomena. These efforts have produced substantial information from which a study of flow boiling can proceed. However, it is now known (see Chapter III) that there is a significant interaction between the velocity field, the liquid-vapor interface, and the high temperature

gradients at the solid-liquid interface. Therefore, eliminating either the temperature or flow velocity fields appears to be an oversimplification of the problem.

The present study was initially aimed at determining the conditions (in the most general sense) under which boiling began. It soon became apparent that the size and number of cavities on the boiling surface was an important variable in this problem. Techniques were then developed to quickly measure the cavity size distribution of any given surface. This allowed one to then vary all possible factors which might effect the cavity size distribution and thereby determine which were significant. With this ability to control the nuclei population, an experimental program was initiated to see what effect different populations had upon boiling. This experimentation also yielded the inception data needed to supplement that already in the literature, which when taken as a whole, allowed a new understanding of the original problem. In the course of these experiments, unexpected bubble behavior was observed which upon closer examination lead to the study of thermocapillarity. Thermocapillarity allowed further understanding of surface effects upon boiling as well as upon inception. However, its significance appears to lie well beyond these two problems.

The present **experimental** work indicated the need for two developments which may prove of value in other areas of research. The first was an instrument which allowed the detection of the extremely small bubbles which exist under certain flow boiling conditions. The second development was a compact and accurate analytical technique for solving a large class of nonlinear differential equations. Two examples

of this nonlinear technique are given: the temperature drop across an electrically-heated tube wall, and the classical large amplitude pendulum (which until now has not been solved).

Chapter II - The Measurement of Cavity Size Distributions

A. Introduction

Surface conditions have long been known to play a major role in boiling. A generalized expression for the boiling heat flux is

$$q/A = \bar{C} (T_w - T_s)^m \quad (1)$$

where $(T_w - T_s)$ is the wall superheat and both \bar{C} and m are "constants". The Rohsenow nucleate boiling correlation^{1*} as well as the work of Berenson² suggest that both the coefficient and exponent in Eq. 1 depend on surface variables. A number of investigators attempted to gain some understanding of the surface effects by using such devices as electron microscopes, highly magnified still photos, and high speed motion pictures.^{3,4,5} Still others have resorted to extensive experimentation and bubble counting techniques, hoping to gain some understanding as to what quantities characterize the surface insofar as nuclei are concerned.^{6,7,8,9} It is herein proposed that the main difficulties in understanding the effects caused by natural surfaces are (1) the inability to determine which variables, such as material and finish, control the formation of nucleation sites and (2) the inability to measure the size and number of nucleation sites. In what follows a method is presented for quickly making nucleation site measurements and thereby determining the variables which control the formation of nucleation sites.

*Numbers denote References listed beginning on p. 101

B. Theory

It is commonplace to see small bubbles clinging to the side of a glass of water. If closely observed, these bubbles appear suddenly, are at first below the resolving ability of the eye, and appear only when the water is being warmed. It is reasonable to assume that the nucleation sites on a clean surface from which these gas bubbles appear would also be the nucleation sites if boiling were to begin.

These gas bubbles, which are of course saturated with vapor, have the following desirable characteristics which make them useful in identifying cavities:

1. They grow slowly by gas diffusion and can be easily counted.
2. They grow in a constant temperature liquid thereby avoiding certain problems associated with temperature gradients (to be discussed in Chapters III and VI).
3. Their slow growth in a relatively stagnant liquid avoids any dynamic problems which might tend to hide the characteristics of the cavities themselves.

The force balance on any of the possible states of the bubble emerging from an irregular shaped depression (Fig. 1) is

$$\pi r^2 (p_{\text{atm}} + p_{\text{hs}}) + 2\pi r\sigma = \pi r^2 (p_{\text{v}} + p_{\text{g}}) \quad (2)$$

or

$$r = \frac{2\sigma}{p_{\text{v}} + p_{\text{g}} - p_{\text{atm}} - p_{\text{hs}}} \quad (3)$$

As the bubble of Fig. 1 passes from state (1) to state (2), its radius of curvature decreases which, by Eq. 3, requires the net pressure difference across the interface to increase. If this pressure difference

increases sufficiently, state (3) is reached. The hemispherical bubble of state (3) has the special characteristic of having the smallest radius of curvature. If the net pressure difference is increased further, which it will if the bubble grows by gas diffusion, and if p_v is held constant, the force equilibrium requirement of Eq. 3 would require the radius of curvature to decrease below the cavity mouth radius. Since the radius can only increase in going to state (4a) or (4b), force equilibrium is not satisfied and the bubble is therefore unstable. This instability will result in growth which is governed by the rate of gas diffusion into the bubble. Microscope observations were made of gas bubbles growing from this unstable condition. Rapid initial growth was observed which made the bubbles visible to an unaided eye within less than a minute. By evaluating the terms on the right side of Eq. 3 at the time when this instability at the cavity occurs, the equivalent radius of that particular cavity can be measured.

C. Apparatus

To simplify the evaluation of the right hand side of Eq. 3, the manometer type instrument shown in Fig. 2 was constructed. The porous disk of this manometer allows vapor and gas to exist between it and the surface of mercury. It essentially serves the same function as a semipermeable membrane except that the gas diffusion process is faster. Since the long arm of the manometer is open to the atmosphere, the mercury pressure head is

$$P_{Hg} = p_v + p_g - P_{atm} \quad (4)$$

The only restriction on p_v and p_g within the manometer equaling the same properties within the nuclei on some surface within the liquid is (1) that the temperature in the liquid be uniform and (2) that all processes proceed slowly enough to insure equilibrium. With these assumptions, Eq. 3 can be substituted into Eq. 4 to give

$$r = \frac{2 \sigma}{P_{Hg} - P_{hs}} \quad (5)$$

The right hand side of Eq. 5 can easily be evaluated to give the equivalent cavity radius.

To obtain an independent check on all measurements, artificial cavities of known dimensions were placed on three mirror finish stainless steel plates (2" x 2"). In each plate was drilled a set of cavities of one particular size ($r = 0.001$ in., 0.0004 in., and 0.00025 in.) in the pattern of a diagonal cross. The depth of the artificial cavities was usually about ten times the diameter, thereby giving a high probability that gas would be trapped. The artificial cavities were in the shape of cylindrical pits whose radii were felt to be close to the effective radii of natural cavities. The drilling was done through the courtesy of the M.I.T. Instrumentation Laboratory with an electric-discharge drilling machine.

The appearance of the cross pattern on a plate containing the 0.00025 inch cavities, for example, would indicate the sufficient pressure existed within all nucleation sites to "pop" all cavities of radii greater than 0.00025 inches. These plates containing artificial cavities of known dimensions gave results which typically are as shown in Fig. 3a.

D. Results

The specimens from which data were collected generally consisted of flat plates (1" x 1"). Typical measurement results are shown in Figs. 3 and 4. The scatter of the points in these figures is representative of all the data collected. For example, in Fig. 3b are shown the total number of nucleation sites per unit area which have a cavity radius greater than r . The scatter is evidently the result of some variable (experimental or physical) which is uncontrolled.

The variation of nucleation site populations for different materials (stainless steel-316, copper, and aluminum) is shown in Fig. 3c. There is no indication that any one of these materials of a given finish has more ability to form nucleation sites than another.

Figures 3b, 3d, 4a, and 4b show representative populations for each of these three materials. The 80-grit finish is rough to the touch while the B finish is a bright mirror finish which is made with a three-micron aluminum oxide abrasive.

Figure 4c compares the populations found on a copper mirror finish with those found on the inside of two plug drawn copper tubes. This inside surface was prepared by cutting open a 1/4" ID tube and merely cleaning the inside surface with acetone. The unexpected result was that this inside surface had fewer nucleation sites than a highly polished surface. The same result was observed with stainless steel tubes. A visual examination of the internal surface of these tubes showed many axial extrusion grooves. Since the liquid came in contact with the surface by traveling axially down the tube segment it was suspected that merely by traveling parallel to grooves fewer nuclei

would result. It is noted that a collection of long grooves is a common type of gross surface roughness for metals since almost all metal forming operations, such as machining, drawing, extruding, polishing, and pressing, produce grooved surfaces.

To explore this possibility, specimen plates were prepared in an identical manner as previously. They were then placed in the liquid so that the direction of liquid advance over the surface took place in two different ways: parallel to the polishing grooves and perpendicular to the grooves. The resulting populations were then compared with prior results when random loading took place (Fig. 4d). Identical qualitative results to those shown in Fig. 4d were obtained for all materials and all finishes where grooves could be observed.

Bankoff¹⁰ has analyzed the formation of nucleation sites by a film of liquid traveling perpendicular to a groove. He visualized a nucleation site being formed when the liquid surface trapped gas by touching the far side of the groove or pit before it touched its base (Fig. 5). With this explanation in mind, it appears logical that liquid traveling parallel to the majority of grooves would create fewer nucleation sites than by traveling perpendicular to these grooves.

In his paper Bankoff suggested that someone attack the other half of the trapping phenomenon, i.e., gas trapping by liquid flowing parallel to grooves. From the present results, the answer may well be that trapping does not occur unless a microscopic groove or pit lies sufficiently perpendicular to the path of liquid advance.

E. Conclusions

1. The number and distribution of nucleation sites on a metallic surface do not appear to be affected by the particular metal.
2. Smoother finishes result in fewer nucleation sites being created.
3. The direction of travel of the liquid when it comes in contact with the surface has a strong effect upon the resulting nucleation site population.
4. The largest cavity radii for the surfaces of this work were approximately .001 inches. For smaller radii the populations increase very rapidly.

Chapter III - Thermocapillarity

A. Bubble Boundary Layer

For some time it has been observed that bubbles produced in flow surface boiling remain quite near the hot wall while flowing downstream. Gunther,¹¹ in 1950, was the first to observe this surprising fact. Furthermore, his high speed photographs recorded that increased subcooling caused the bubbles to stay even closer to the hot wall. When this subcooling reached 150°F, he reported that the bubbles did not appear to detach and would only slide downstream.

Jiji and Clark,¹² in observing this phenomenon, described the region occupied by these bubbles moving next to the wall as a "bubble boundary layer". Their observations, which will be discussed later in this chapter, included the following unexplained facts:

1. The temperature within the bubble boundary layer is generally well below the saturation temperature (Fig. 6a).
2. The temperature throughout the bubble boundary layer fluctuates over a wide range (Figs. 6a and 6b).
3. The frequency of this fluctuation is virtually constant throughout both the bubble boundary layer and the single phase core (Fig. 6b).
4. The magnitude of this temperature fluctuation decreases as the distance from where boiling begins is increased (Fig. 6c).
5. The temperature at the edge of the bubble boundary layer decreases as the heat flux increases (Fig. 6d).

Kirby, et al.,¹³ in observing the puzzling attraction of the bubbles to the hot wall, attributed it to the inertia resulting from positive growth of the bubbles as they move downstream. Since this attraction has also been observed (1) in the present work when no significant growth was taking place and (2) in the work of Gunther when collapse was occurring, one can conclude that inertia cannot completely explain this observation. Kirby applied the following test to determine whether the attracting force was either thermally or hydrodynamically induced. While bubbles were moving next to the heated wall, the power was quickly shut off. Had the bubbles remained at the wall, one could conclude that some hydrodynamic force was acting on the bubbles. What actually happened was that the bubbles immediately began to drift away from the wall. In light of this result and Gunther's observations on the effect of subcooling, it is safe to conclude that this attraction phenomenon is thermally induced.

B. Jetting

It was first reported by Marangoni,¹⁴ about 100 years ago, that motion can be induced by a variation in surface tension at a liquid-vapor interface. This variation produces a force imbalance which tends to move the interfacial liquid film. Through the action of viscosity the liquid film drags adjacent liquid which produces an observable flow. Scriven and Sternling,¹⁵ for example, have shown that the flow observed in liquid Benard cells is due to this phenomenon and not to buoyancy forces. Of interest in flow boiling is flow resulting from variations in surface tension caused by a temperature gradient along the phase interface of a bubble.

Sugden¹⁶ has suggested that surface tension is a derived property, that is, it is directly related to more basic properties. This relationship is

$$\sigma = \left[\frac{.78 v_{cr}}{M} (\rho_L - \rho_V) \right]^4 \quad (6)$$

As this equation indicates, σ decreases with an increase in temperature for all fluids (i.e., $\frac{d\sigma}{dT}$ is negative) and becomes zero at the critical point (Fig. 7a). Therefore, if the bubble of Fig. 7b has a temperature gradient across it, liquid will be pulled in the cold direction. The motion of the liquid in the cold direction causes the bubble to move in the opposite direction as a result of continuity. In other words, a bubble in a nonuniform temperature field will throw hot liquid in the cold direction and will move in the hot direction.

This effect has been simply demonstrated by Young, Goldstein, and Block,¹⁷ who caused air bubbles in water to travel downward between two horizontal plates when the lower plate was heated. Trefethen,¹⁸ in his excellent film, Surface Tension In Fluid Mechanics, has dramatically demonstrated jetting (see Fig. 8) along an electrically heated wire immersed in an acetone (plus 2% water) bath. He has estimated that the velocity of this jet is on the order of 1000 diameters a second. Farello¹⁹ has photographed bubbles sitting on an electrically heated wire immersed in distilled water (Fig. 9). His photographic technique is such that density changes in the liquid appear as different colors and consequently the jets are clearly seen. The lack of downward jetting in his pictures is simply a consequence of the natural convection and the thermocapillarity induced flow impinging on the bottom of the wire.

Semeria,²⁰ using Schlieren techniques, has photographed jetting in stagnant water. In this reference he attributed the phenomenon to micropumping or vibrations of the bubble itself. In a later paper,²¹ he, along with Behar, et al., reproduced the same photographs and suggested that surface tension variations may also account for it. The word thermocapillarity appears to have been first mentioned in that paper. It further appears to be the most descriptive phrase of the phenomenon under discussion. Both the words jetting and thermocapillarity will be used interchangeably to describe the same phenomenon.

Thermocapillarity has been observed in a variety of fluids. Trefethen²² has reported jetting, and the resulting bubble motion in freon, pentane, as well as very pure acetone (.3% water). McGrew, Rehm, and Bamford,²³ have taken motion pictures through a microscope showing flow induced by a variation in surface tension around bubbles. They obtained similar results for n-butyl alcohol, methanol, carbon tetrachloride, and distilled water. The flow was marked by suspended particles and is qualitatively the same as shown in Fig. 7b.

In the present pool boiling studies mentioned in Chapter VII, jetting similar to that of Fig. 9 could be seen. The jets were directed downward at the ends of the heated test section where the strength of the upward impinging flow was the weakest. The jets were first observed before any vapor could be seen. (Semeria²⁰ has taken Schlieren photographs of what appears to be the same phenomenon.) Slight increases in the heat flux caused the bubbles to appear with the jets coming off the tops as shown in Fig. 9. The jets, in a manner quite similar to the smoke from a cigarette, would rise several inches before they

would become turbulent. As the heat flux was increased further, the point at which transition occurred approached the bubble itself. At a slightly higher heat flux, the bubbles would depart from the heated test section agitating the liquid and preventing the further observation of the jets. Visual jets could again be observed by either immediately lowering the heat flux or by sustaining boiling for several hours and then lowering the heat flux. No detectable hysteresis was observed in these results.

C. Order of Magnitude Calculations

1. Model Formulation

The primary question concerning thermocapillarity is how much heat is removed via this mechanism. Of necessity one must resort to a simplified model which will yield only order of magnitude results. It will be surprising, however, to see just how much information such a model provides.

Consider the spherical bubble shown in Fig. 10a, which is moving quite close to the hot wall. Thermocapillarity induced forces, which are proportional to $\left(\frac{dq}{dT}\right) \Delta T_b$, cause the hot liquid at the base of the bubble to be thrown into the colder bulk stream. The total heat flux associated with jetting can be expressed as

$$(q/A)_j = (C_p)_L \left(\frac{\dot{m}}{A}\right)_L \Delta T \quad (7)$$

where ΔT is the temperature difference between the hot liquid at the base of the bubble and the temperature of the liquid it replaces, and $\left(\frac{\dot{m}}{A}\right)_L$ is the liquid mass flux away from and perpendicular to the hot wall.

$$\Delta T = C_1 (T_w - T_b) \quad (8)$$

One might expect C_1 to have a value of about 1/2. The surface tension induced force must equal the rate of change of momentum of the liquid perpendicular to the hot wall. Therefore,

$$C_2 (N/A) \left(\frac{d\sigma}{dT}\right) \Delta T_b (\pi D_b) = \frac{d}{dt} \left[\left(\frac{\dot{m}}{A_L}\right) v_j \right] = \left(\frac{\dot{m}}{A_L}\right) v_j \quad (9)$$

The constant C_2 reflects primarily the uncertainty in the length over which the surface tension variation acts. In all probability its value is between 1 and 1/2. The mass flow rate of this liquid jet can be calculated if one assumes that the jet diameter is C_3 times the bubble diameter.

$$\left(\frac{\dot{m}}{A_L}\right) = C_3 \rho_L v_j \left(\frac{\pi D_b^2}{4}\right) (N/A) \quad (10)$$

From the photographs of Figs. 8 and 9, the value of C_3 should be about equal to unity. It will be convenient to define the projected bubble area as

$$A_b \equiv A (N/A) \left(\frac{\pi D_b^2}{4}\right) \quad (11)$$

Combining Eqs. 7, 8, 9, 10, and 11 yields the desired relation

$$(q/A)_j = (C_p)_L (T_w - T_b) \left(\frac{A_b}{A}\right) \sqrt{\frac{(4 C_1^2 C_2 C_3) \Delta T_b \rho_L \left(\frac{d\sigma}{dT}\right)}{D_b}} \quad (12)$$

More insight into the jetting phenomenon can now be gained by solving Eq. 12 for ΔT_b and asking if a reasonable value for ΔT_b results if typical quantities are substituted for all other variables. For example, the following examples are selected for water.

$$\rho_L = 62.4 \frac{\text{lbm}}{\text{ft}^3}$$

$$(q/A)_j = 10^6 \frac{\text{BTU}}{\text{hr ft}^2}$$

$$T_w - T_b = 180^\circ\text{F}$$

$$D_b = .001 \text{ ft}$$

$$C_2 = 1$$

$$C_p = 1 \frac{\text{BTU}}{\text{lbm } ^\circ\text{F}}$$

$$\frac{A_b}{A} = 1/2$$

$$\frac{d\sigma}{dT} = 9 \times 10^{-6} \frac{\text{lb f}}{\text{ft } ^\circ\text{F}}$$

$$C_1 = 1/2$$

$$C_3 = 1$$

The predicted value for temperature difference across the bubble is then

$$\Delta T_b = \left[\frac{10^6}{180 \times 1/2 \times 3600} \right]^2 \frac{.001}{62.4 \times 9 \times 10^{-6} \times 32.2} = .52^\circ\text{F}$$

The question must now be asked if even such a small value of ΔT_b is reasonable.

From an engineering viewpoint, it is desirable to know what parameters determine the value of ΔT_b . Since the thermal resistance of the bubble is much less than that of the liquid, ΔT_b will be much less than the temperature gradient in the liquid multiplied by the bubble diameter. A possible explanation of the reported observations of jetting discussed previously is suggested by realizing that the temperature variation within the bubble and across the interface is composed of (1) the resistance due to evaporation at the hot side of the bubble, (2) the resistance due to condensation at the cold side of the bubble, and (3) the resistance within the bubble.

The presence in the gas phase of sufficient noncondensable gas might cause this third type of resistance to become dominant. It is quite possible that much of the jetting which has been observed is a result of a noncondensable gas being present. On the other hand, the requirement that the velocities of both the liquid and gas phases be equal at their interface would indicate that high velocities exist in the gas. There would, therefore, be a good deal of mixing and convective flow of the vapor towards the condensation interface. The effective diffusional resistance, even though it does exist, might then be small.

This third type of thermal resistance suggests that if a volatile additive were intentionally added to a pure liquid the jetting heat transfer would be modified. If an additive could be found which did not adversely effect the fluid properties, D_b , or $\frac{dg}{dT}$, then heat transfer by this mechanism would be increased. Bergles and Morton,²⁴ in a survey of the effects of additives, have found that additives give inconclusive results in their effect on the heat transfer coefficient, but usually increase the burnout heat flux. It seemed likely that the characteristics which should be looked for in an additive from a thermocapillarity standpoint are (1) a high volatility and (2) a negligible reduction in surface tension.

2. Interfacial Temperature Drop

Schrage²⁵ has arrived at the following expression for the mass flow rate across a phase boundary:

$$\left(\frac{\dot{m}}{A_v}\right) = \frac{2 \lambda}{2 - \lambda} \frac{\Delta T_p}{\sqrt{2\pi R_v T_v}} \quad (13)$$

The pressure drop across the phase boundary can be related to a

corresponding temperature drop by the Clapeyron relation

$$\frac{dp}{dT} = \frac{h_{fg}}{T (v_v - v_L)} \quad (14)$$

which can be approximated as

$$\Delta p = \frac{h_{fg}}{T_v (v_v - v_L)} \Delta T \quad (15)$$

The quantity $R_v T_v$ can be replaced by use of the perfect gas law

$$R_v T_v = p_v v_v \quad (16)$$

The minimum possible mass flux can be derived by assuming that no condensation takes place during growth and no evaporation takes place during collapse. The mean mass flux during either the growth or the collapse period would then be

$$\left(\frac{\dot{m}}{A}\right)_v = \frac{\text{maximum bubble volume}}{v_v \left[\begin{array}{l} \text{bubble} \\ \text{area} \end{array} \right] \left[\begin{array}{l} \text{growth or} \\ \text{collapse period} \end{array} \right]} = \frac{4/3 \pi r^3}{v_v (\pi r^2) \theta / 2} = \frac{8 r}{3 v_v \theta} \quad (17)$$

Combining Eqs. 13, 15, 16, and 17 gives the temperature drop across only one (condensing or evaporating) of the bubble interface. This should therefore be a lower limit on ΔT_b :

$$\Delta T_b = \frac{8/3 \sqrt{\frac{2\pi p_v}{v_v}} \left(\frac{r}{\theta}\right) (v_v - v_L) (1/\lambda - 1/2) T_v}{h_{fg}} \quad (18)$$

Sufficient data exist in the work of Gunther¹¹ to arrive at a reasonable estimate of $\frac{r}{\theta}$. It will be noticed in reference 11 that although r and θ vary from one flow situation to another, as well as statistically, their ratio remains relatively constant. A typical value for $\frac{r}{\theta}$ might be $\frac{.02 \text{ in}}{.5 \times 10^{-3} \text{ sec}}$.

Great uncertainty exists as to the value of the accommodation coefficient λ . Rohsenow and Sukhatme²⁶ suggest that $.04 < \lambda < 1.0$. The following values, pertaining to water, will be used in arriving at a bracket for ΔT_b .

$$\begin{aligned}
 .04 < \lambda < 1.0 & & T_v &= 300^\circ\text{F} = 760^\circ\text{R} \\
 \frac{r}{\theta} &= \frac{.02}{.5 \times 10^{-3}} \frac{\text{in}}{\text{sec}} & v_v - v_L &= 5.45 \frac{\text{ft}^3}{\text{lbm}} \\
 h_{fg} &= 800 \frac{\text{BTU}}{\text{lbm}} & p_v &= 70 \text{ psia}
 \end{aligned} \tag{19}$$

Below is given a sample calculation for the interfacial temperature drop when $\lambda = 1.0$.

$$\Delta T_b = \frac{8/3 \sqrt{\frac{2\pi \times 70}{5.47 \times 32.2}} \frac{.02}{.5 \times 10^{-3}} 760 \times 5.45 \times 1/2}{800 \times 778} = .56^\circ\text{F}$$

In a similar manner, if $\lambda = .04$, ΔT_b is found to be 27.4°F . Therefore, the lower limit of the temperature drop across the bubble for the conditions of Eq. 19, assuming zero diffusional resistance, is

$$.56^\circ\text{F} < \Delta T_b < 27.4^\circ\text{F}$$

The nearness of this value of $.56^\circ\text{F}$ to the previous calculation of $.52^\circ\text{F}$ suggests that λ may be quite near 1.0 for the present conditions.

We can now write an expression for $(q/A)_j$ without involving the unknown ΔT_b . From Eq. 18 with the conservative assumption that $\lambda = 1.0$ and taking $C_1^2 C_2 C_3 = 1/4$ we have

$$(q/A)_j = (C_p)_L (T_w - T_b) \left(\frac{A_b}{A}\right) \sqrt{\frac{2/3 \sqrt{2\pi \frac{p_v}{v_v}} \left(\frac{v_v}{v_L} - 1\right) \frac{d\sigma}{dT} T_v}{\theta h_{fg}}} \tag{20}$$

3. Applicability of Model

The order of magnitude reasoning which has lead to Eq. 20 should be equally valid for both pool and flow boiling. However, it will be recalled that the value of θ in pool boiling is about twenty times greater than in flow boiling.²⁷ From another point of view, the velocity gradient existing across the bubble as it flows next to the wall (Fig. 10a) adds considerably to the mass flux through the bubble and consequently the temperature drop across the bubble. A number of investigators have reported that the bubbles move at a velocity less than the mean stream velocity (for example: $V_b \approx .8V$). This velocity field as seen from a reference system fixed in the bubble (Fig. 10b) causes a hot stream of liquid to wash under the bottom of the bubble and cold liquid, flowing in the opposite direction, to wash over the top. Had this not been the case (as in pool boiling), there would of necessity be a stagnation point on the bubble with the dividing stream line surrounding the bubble with a nearly constant temperature liquid. For this reason, it is felt that thermocapillarity would play a less important role in pool boiling than in flow boiling.

This conclusion is substantiated by the **Schlieren** photographs in both the pool boiling studies of Hsu and Graham²⁸ as well as Isshiki and Tamaki.²⁹ The photographs of Hsu and Graham indicate that pumping is the primary means of heat removal for their conditions. The photographs of Isshiki and Tamaki, being significantly clearer, show both the dominance of pumping (the tail on the bottom of a bubble) and the slight, but observable, presence of thermocapillarity (the jet on the top of a bubble which is separated from the previous bubble's tail).

It is well known that θ is a strong function of velocity and subcooling. The data of Gunther¹¹ allow an approximation of θ as follows

$$\theta = \frac{(.236^\circ\text{F ft}^{\cdot 8} \text{ sec}^{\cdot 2})}{(V^{\cdot 8}) (\Delta T_{\text{sub}})} \quad (21)$$

It must be emphasized that this is valid only for the conditions of his experiment (water, $5 \text{ ft/sec} < V < 20 \text{ ft/sec}$, $p_L = 50 \text{ in Hg}$, $1 \frac{\text{BTU}}{\text{in}^2 \text{sec}} < q/A < 6 \frac{\text{BTU}}{\text{in}^2 \text{sec}}$, $60^\circ\text{F} < \Delta T_{\text{sub}} < 200^\circ\text{F}$). In addition, the surface which was fit through the data points is exact only at $V = 10 \text{ ft/sec}$ and $\Delta T_{\text{sub}} = 150^\circ\text{F}$. The relationship is indicative, however, of all reported observations concerning bubble lifetimes.

Eq. 21, along with Eq. 20, indicates that the heat flux due to thermocapillarity varies approximately as the .4 power of velocity. McAdams, et al.,³⁰ for their conditions which are similar to the above, have correlated the heat flux at burnout (corresponding to the maximum value of A_b/A). They found that it varied as the 1/3 power of velocity. Gunther,¹¹ for his conditions determined that the burnout heat flux varied as the .5 power of velocity.

Gunther's work indicates that the value of A_b/A at burnout varies typically from .1 to .4. Using these values as a bracket for A_b/A and the heat transfer measurements of McAdams, et al.,³⁰ one is able to evaluate a range for $(q/A)_j$ using Eqs. 20 and 21 and compared it with the actual $(q/A)_{BO}$. This is shown in Fig. 11 where the agreement between the jetting heat flux and the net heat flux is shown.

D. Other Proposed Mechanisms for Heat Transfer

The order of magnitude analysis, as well as visual and photographic observations, have given strong justification to suspecting that thermocapillarity may be the dominant heat transfer mechanism in flow boiling. Since conclusive evidence is not available, attention will now be focused on a few of the other possible mechanisms of heat transfer, to see if some basis for comparison exists.

The literature contains numerous explanations for the extremely high boiling heat fluxes. Several of the more reasonable explanations will now be examined from a flow boiling standpoint and compared with thermocapillarity.

1. Pumping

Pumping, or vapor-liquid exchange, in its most general sense refers to the displacement of a volume of liquid equal to the volume of a bubble. During a bubble's growth through and beyond the thermal layer, pumping is visualized as the bubble pushing the hot liquid into the cold bulk liquid. During departure it is visualized (and photographically observed in reference 29) as the sucking of hot liquid in the bubble's wake. During collapse it is visualized as the converging of liquid surrounding the bubble (both hot and cold) towards the bubble's center.

In the light of thermocapillarity, one would expect that jetting would accompany the growth and collapse of the bubble. In fact, the pool boiling photographs of Isshiki and Tamaki²⁹ show a jetting spike during the growth stage. (In pool boiling the collapse usually takes place far from the thermal layer.) An exact comparison of the growth and

collapse aspects of pumping with thermocapillarity cannot be made at low pressures. However, at high pressure Ivey and Morris³¹ have made the following observations.

"The vapour-liquid exchange mechanism has been shown to be inadequate at high pressures. The corollary of this is that the growing and collapsing bubbles, at least at high pressures, must be responsible for the circulation of more liquid than is accounted for by a simple exchange of a volume of liquid for a similar volume of vapour in the bubble as postulated by the vapour-liquid exchange mechanism. This introduces the concept of a "pocket" of liquid with which each growing and collapsing bubble is associated. Each bubble may be responsible for the circulation of a quantity of liquid far greater than the volume associated with the vapour in the bubble itself. It is quite feasible for a growing and collapsing bubble to "influence" a volume of liquid larger than the maximum volume the bubble may occupy... A visual inspection was made by the present authors [Ivey and Morris] of a horizontal wire boiling in water at atmospheric pressure when the liquid bulk is sub-cooled. Illumination was provided by either a stroboscope or a tungsten-filament point source placed to the rear of the pool. Glass observation windows were provided. It was observed, as indicated in the literature, that the bubbles growing and collapsing on the heater surface are able to project large volumes of hot liquid for some distance into the cooler surrounding liquid, the directions in which the hot "pockets" moved being random and irrespective of the direction of the gravity vector."

Ivey and Morris did not attempt to give any analytical justification for this extended influence of a bubble on adjacent liquid. However, their observations bear a close resemblance to thermocapillarity induced jetting.

The sucking action of pumping appears to be a significant, if not the dominant, mechanism in low pressure pool boiling based upon various photographic studies. This conclusion is further substantiated by the extremely high bubble departure velocities, which on the basis of Chapter VI appear to be explainable. In flow boiling, however, the bubbles move parallel and quite close to (possibly touching) the hot

wall and large quantities of heat are not removed by this means.

2. Latent Heat

Latent heat, or mass transfer through the bubble, was originally felt to be a minor mechanism in heat transfer. This conclusion was based upon the observation that in subcooled-nucleate boiling the rate of visible vapor production accounted for less than two percent of the total heat flux³². Recent experiments of Bankoff and Mayson³³ have revived this explanation. In these experiments, condensation heat transfer coefficients were calculated at the surface of single bubbles formed by injecting steam into a subcooled water stream at atmospheric pressure. The system variables were velocity (.9 to 7.2 ft/sec) and subcooling (32°F to 132°F). Depending upon these parameters, the heat transfer coefficient varied from 13,000 to 320,000 Btu/hr ft²°F. It will be interesting to now approximate the ΔT_b required to transfer 10⁶ Btu/hr ft²°F when $A_b/A = 1/2$ and the heat transfer coefficient is 320,000 Btu/hr ft²°F at both an evaporating and condensing interface.

$$\Delta T_b = \frac{10^6 \times 2}{320,000 \times 1/2} = 12.5^\circ\text{F}$$

Comparing this value with the similarly calculated value of .52°F for thermocapillarity, one can conclude that latent heat cannot be a significant mechanism of heat transfer.

3. Micro-layer

Moore and Mesler³⁴, in 1961, presented the surprising evidence indicating the existence of a micro-layer of liquid between the vapor of the bubble and the hot wall. Further evidence has confirmed

this observation beyond any reasonable doubt.^{35,36} The question which still remains to be answered is how much heat does the evaporation and subsequent condensation of the liquid in this micro-layer contribute to the total heat flux. One can view the micro-layer theory of heat transfer as being included in the more general theory of latent heat discussed above. In this context, the micro-layer theory is not able to explain the high rates of heat transfer unless the temperature drop across the bubble was on the order of 12.5°F. If such a temperature drop did exist, then thermocapillarity would be an even more reasonable explanation for boiling heat fluxes.

No attempt has been made in the above discussion to exhaust all possible mechanisms. More specifically, the mechanisms of micro-convection, quenching, and bubbles as surface roughness have been omitted since no direct comparison with thermocapillarity appears to exist.

E. "Anomalies" Explainable by Thermocapillarity

The observations of Jiji and Clark, as described in section A and Fig. 6 will now be considered in light of the existence of significant thermocapillarity effects. The existence of sub-saturation temperatures deep within the bubble boundary layer can only imply a highly efficient means of removing the superheated liquid within the laminar sublayer (Fig. 6a). It also implies an equally efficient means of injecting cold liquid down into the bubble boundary layer and pulling warmer liquid back out in such a way that the circulation through this boundary layer doesn't sweep the bubbles away from the hot wall. Jetting is

the only conceivable means for accomplishing these two apparently conflicting requirements. One can also conclude that some means exist of preventing the bubbles from collapsing in this cold liquid. Styrikovich and Nevstrueva³⁷ have suggested that either there must be a large temperature drop (from 30°F to 150°F) at the condensing interface or there must be a film of warm liquid surrounding the bubble. Such large temperature drops are highly unlikely in light of the work of Schrage²⁵ and the inequality of page 33. The concept of a warm envelope for the bubbles is in keeping with the thermocapillarity circulation around the bubble as shown in Fig. 10a.

The wide amplitude of the temperature fluctuations (Figs. 6a and 6b) obviously results from hot pockets of liquid striking the thermocouple. To attribute it to some type of instrumentation error would not explain the constant frequency and reduced amplitude at larger distances from the hot wall. It seems highly likely that the thermocapillarity jets provide these hot packets of liquid. The thermal layer at the base of the bubble (see Fig. 10a) would both supply the hot liquid for these pockets and cause the surface tension of that portion of the bubble to be reduced.

As one proceeds downstream from the point where boiling begins, this thermal layer should be reduced in thickness since a greater number of bubbles would be passing over the region. As a result, these bubbles would find their base in a colder region than bubbles further upstream and, therefore, would not be able to jet as strongly. This would be evidenced by a decrease in the amplitude of the temperature fluctuations as the distance from the leading edge (point where boiling begins) increases (Fig. 6c).

If the heat flux were increased one would expect even hotter liquid at the bubble base. This would cause an even greater circulation of the cold bulk liquid down through the bubble boundary layer. It should not be surprising, therefore, to see, as in Fig. 6d, that the temperature at the edge of the bubble boundary layer decreases as the heat flux increases.

One further anomaly which may be explained as a thermocapillarity effect (at least partially) is the vanishing of the micro-layer. Previous analyses have presumed that the microlayer vanishes by evaporation only. It is to be expected that the temperature within the thin micro-layer would be substantially higher than that at the top of the bubble because of its proximity to the wall and its being insulated by vapor over a wide area. The surface tension variation would then be strong at the outer perimeter of the micro-layer. One would, therefore, expect this layer to be pulled out from under the bubble at the same time it was evaporating. This would be consistent with the thermocouple measurements in the literature.^{35,36}

F. Conclusions

1. Bubbles, in flow boiling, are attracted toward the hot wall by thermocapillarity action.
2. The mass flux necessary to create only the visible vapor within the bubble is sufficient to account for a large ΔT_b . This ΔT_b creates a significant heat transfer via thermocapillarity. This mechanism, may, under some or all flow conditions, be the dominant mechanism.

3. Latent heat, micro-layer evaporation, and pumping by means of sucking, are not significant mechanisms of heat removal in flow boiling. Latent heat and micro-layer evaporation are not significant mechanisms of heat removal in pool boiling.

4. In general, thermocapillarity will remove more heat in flow boiling than in pool boiling.

5. Frequently the complicated problem of flow boiling has been approached by studying, in the manner of a first approximation, either pool boiling or isothermal two phase mixtures. This approach cannot be fundamentally correct since both the velocity field and the temperature gradient interact in a manner to produce a different flow pattern and a significant removal of heat by thermocapillarity.

6. The addition of suitable volatile additives could be expected to give both increased heat transfer and increased burnout by increasing ΔT_b . This would take place through either decreasing the accommodation coefficient or increasing the diffusional resistance to vapor within the bubble.

7. Under the present conditions for flow boiling of water, the accommodation coefficient appears to be very close to 1.0.

Chapter IV - The Measurement of Temperatures at the Heat
Transfer Surface for Electrically-Heated Tubes

A. Introduction

The present technique for measuring the temperature of the liquid-solid interface for flow either inside or outside of an electrically-heated tube consists of creating an adiabatic surface at the opposite wall of the tube. The temperature of this adiabatic wall is then measured by means of thermocouples which, for DC heating, must be electrically insulated from the tube itself. The temperature drop between the outer and inner wall is then found by solving the conduction equation. This equation turns out to be nonlinear because of the relatively strong dependence of the thermal conductivity and electrical resistivity upon temperature. The magnitude of the temperature drop can be as much as 500°F. Thus an accurate solution and accurate properties are required to avoid significant error in the temperature at the liquid-solid interface.

The solution of the heat-conduction equation for an electrically-heated tube with radial heat flow and constant properties (k and ρ) can be handled by standard techniques. Unfortunately, the commonly used materials have substantial variations in both k and ρ and to overlook their dependence upon temperature would introduce substantial error in many cases. This heat-conduction problem can be handled by the Kirchhoff transformation³⁸ for the special case where k is a known function of temperature and ρ is a constant.

The more exact solutions of this problem (those involving variable properties) have involved (1) series solutions, (2) finite difference solutions, and (3) analog computer solutions. The first series solution appears to have been solved in 1949 by Stewart as reported by Kreith and Summerfield.³⁹ Their solution consisted of the first three terms of a Taylor's series expansion. This non-linear solution was extended in 1958 to five terms by Dickenson and Welsh.⁴⁰ This combined solution is sufficiently accurate for most purposes, but usually requires the aid of a digital computer. Rohsenow, et al.,⁴¹ modified this solution for the case when the voltage drop across the tube was not known. The drawback to this substitution of I^2 (Res) for E lies in not knowing the temperature at which to evaluate the tubes resistance. In some cases this error is significant. Clark⁴² simplified the Kreith-Summerfield solution by showing that the series solution could be written as the sum of two functions, the first being a geometric function (solution for constant properties) and the second a function which accounted for the variable properties.

A number of investigators have employed finite difference techniques, usually in conjunction with a digital computer.^{43, 44, 45, 46} Characteristic of these solutions is the recent solution by Van Sant and Pitts.⁴⁶ They solved the nonlinear problem for several specific cases and compared it with the linearized problem. They felt that their computer results were accurate to within one percent. It was observed that the solution for their case was noticeably unstable unless the number of pivotal points exceed 50.

In 1962, Harden and Bryant,⁴⁷ using an analog computer, solved this heat-conduction equation for a number of hypothetical cases. In the present work an analog computer solution was also accomplished. Careful scaling and programming of the problem on the large and precise Philbrick computer of M.I.T.'s Engineering Projects Laboratory, yielded only about one percent error in the wall temperature drop. For most purposes this accuracy would be sufficient, however, for later work a more accurate solution was required.

A new method of solution is now presented which extends and simplifies the series approach. It has the following advantages. First, a compact and rapidly converging solution results which, if necessary, could give a numerical answer without the aid of a computer. Second, the technique employed to arrive at this nonlinear solution has application to a large class of nonlinear differential equations (see section D). Third, the accuracy of this solution and its rapid-convergence characteristic may be useful in evaluating the thermal conductivity under the same conditions found in heat transfer experiments (see section E).

B. Problem Formulation

The requirement for steady state to exist in an electrically-heated tube with radial heat flow is

$$\frac{d}{dr} \left(\frac{q}{A} r \right) - W_i r = 0 \quad (22)$$

Using the subscripts "h" and "c" to refer to the hot (adiabatic) and cold wall respectively, the boundary conditions become

$$T \Big|_{r_h} = T_h \quad \frac{dT}{dr} \Big|_{r_h} = 0 \quad (23)$$

where T is the temperature (the dependent variable).

The constitutive relations are

$$q/A = -k \frac{dT}{dr} \quad \text{and} \quad (24)$$

$$W_i = \frac{\frac{E^2}{\rho l/A} cs}{A cs} = \frac{E^2}{l^2 \rho} \quad (25)$$

Both ρ and k are assumed to be functions of temperature and can be well approximated by the form

$$\rho \equiv \rho_o (1 + \alpha T) \quad (26)$$

$$k \equiv k_o (1 + \beta T) \quad (27)$$

Equations 22, 24, and 25 combine to give

$$\frac{d}{dr} \left[k_o (1 + \beta T) r \frac{dT}{dr} \right] + \frac{E^2 r}{\rho_o (1 + \alpha T) l^2} = 0 \quad (28)$$

The problem can be put into dimensionless form by defining

$$\theta \equiv \frac{T}{T_h} \quad R \equiv \frac{r}{r_h} \quad P \equiv \frac{E^2 r_h^2}{4 l^2 \rho_h T_h k_h} \quad (29 \text{ a,b,c})$$

$$A \equiv \frac{\alpha T_h}{1 + \alpha T_h} \quad B \equiv \frac{\beta T_h}{1 + \beta T_h} \quad (30 \text{ a,b})$$

Therefore,

$$\rho = \rho_h [1 + A (\theta - 1)] \quad (31)$$

$$k = k_h [1 + B (\theta - 1)] \quad (32)$$

Equation 28, when placed into dimensionless form, becomes

$$\frac{d}{dR} \left\{ R \left[1 + B (\theta - 1) \right] \frac{d\theta}{dR} \right\} + \frac{4 P R}{1 + A (\theta - 1)} = 0 \quad (33)$$

with the boundary conditions

$$\theta = 1 \quad \text{and} \quad \frac{d\theta}{dR} = 0 \quad \text{at} \quad R = 1 \quad (34)$$

C. The Rapid-Convergence Solution

A solution of this equation will be sought of the form

$$\theta = a_0 + a_1 L + a_2 L^2 + a_3 L^3 + \dots \quad (35)$$

where a_0 , a_1 , etc. are the power series coefficients, and L is (for the present) an arbitrary function of R and the parameters of the problem.

The function form for L will be selected so as to achieve a simple and compact form for the final answer. If the functional form were simply $L = R$, the solution technique would be the conventional power series approach and would yield the same solution as Kreith-Summerfield achieved using a Taylor series expansion.

It should be observed that the nonlinearity in this problem enters by means of the constitutive relationships, as is frequently the case in practical applications. In other words, if both k and ρ were constant, the solution could be handled by straight-forward techniques. With this in mind, the functional form of L will be selected so that all terms beyond a certain point in Eq. 35 become identically zero, at least for the case where A and B are zero. In other words, L will be made the linearized solution. The coefficients a_0 and a_1 can be

determined by the boundary conditions. Deviations of A and B from zero (making the problem nonlinear) will cause the coefficients a_2 , a_3 , etc., which will be functions of A and B, to depart from zero. A rapidly converging solution results.

Setting $A = B = 0$ in Eq. 33 and solving for L gives

$$L = P (R^2 - 1 - \ln R^2) \quad (36)$$

The boundary conditions require that

$$a_0 = 1 \text{ and } a_1 = -1 \quad (37)$$

With the functional form of L now fixed, the values for a_2 , a_3 , etc. can be determined for the nonlinear problem.

Using the following relationships

$$\frac{d\theta}{dR} = \frac{d\theta}{dL} \frac{dL}{dR} \quad (38)$$

$$\frac{d^2\theta}{dR^2} = \frac{d^2\theta}{dL^2} \left(\frac{dL}{dR}\right)^2 + \frac{d\theta}{dL} \frac{d^2L}{dR^2} \quad (39)$$

$$\frac{dL}{dR} = 2 P \left(R - \frac{1}{R}\right) \quad (40)$$

$$\frac{d^2L}{dR^2} = 2 P \left(1 + \frac{1}{R^2}\right) \quad (41)$$

and substituting into Eq. 33 gives

$$\left[P \left(R - \frac{1}{R}\right)^2 \right] \left[B \left(\frac{d\theta}{dL}\right)^2 + B \left(\frac{d^2\theta}{dL^2}\right) (\theta - 1) + \frac{d^2\theta}{dL^2} \right] + \left[1 + B (\theta - 1) \right] \frac{d\theta}{dL} + \frac{1}{1 + A (\theta - 1)} = 0 \quad (42)$$

Eq. 42 will now be written in terms of the variable L . This permits the coefficients of like powers of L to be equated to zero, thereby determining the coefficients a_2, a_3 , etc. Before this can be done, the first bracket in Eq. 42 must be expressed in terms of L . Using at least squares fit, the following was found

$$P \left(R - \frac{1}{R} \right)^2 = b_0 + b_1 L + b_2 L^2 + \dots \quad (43)$$

| | b_0 | b_1 | b_2 |
|---------------------|-------|-------|-------------------|
| if $1.4 > R > 1.02$ | 0 | 1.90 | $\frac{-2.09}{P}$ |
| if $1.02 > R > .98$ | 0 | 2.00 | 0 |
| if $.98 > R > .72$ | 0 | 2.10 | $\frac{-2.09}{P}$ |

These values are sufficiently accurate for about any conceivable application, as can be verified later.

Substituting Eqs. 35 and 43 into Eq. 42 and setting the sum of the coefficients of like powers of L equal to zero, gives

$$a_2 = -1/2 \left(B + \frac{A}{1+b_1} \right) \quad (44)$$

$$a_3 = \frac{a_2 \left[3 B (1 + 2 b_1) + A (3 + 2 b_1) - 2 b_2 \right] + AB (1+b_1) - b_2 B}{3 (1 + 2 b_1)} \quad (45)$$

The accuracy of this rapid-convergence solution can be compared with that of the Taylor series expansion or conventional power series expansion in several respects:

1. As the strength of the nonlinearity approaches zero (α and β approach zero) the dimensionless temperature drop $(1 - \theta)$ approaches a one term answer. However, other techniques (with

the exception of Clark's modification of the Kreith-Summerfield solution) continue to give an infinite series answer as α and β approach zero. Therefore, the influence of the nonlinearity can be examined by comparing the first two terms of this solution.

2. By comparing the expansion variables in each method it can be shown that "n" terms of the rapid convergence solution is equivalent to more than n^2 terms of the other series solutions.

3. A typical numerical example has given the following results as a basis for comparing the rates of convergence. The various terms composing the temperature drop are:

| | rapid-convergence result via hand calculation | conventional result via digital computer |
|---|---|---|
| 1st term | 223.2016 | 199.6917 |
| 2nd term | 13.4204 | 18.5741 |
| 3rd term | 1.1509 | 14.6795 |
| 4th term | ----- | 2.6904 |
| 5th term | ----- | 1.6808 |
| temperature drop across the tube wall | 237.7729 | 237.2961 |

As can be seen in this example, the first (linear term) and second (nonlinear term) provide sufficient accuracy for most temperature measurements.

The solution then becomes

$$1 - \theta \cong L + 1/2 \left(\frac{A}{3} + B \right) L^2 \quad (46)$$

where

$$L \equiv \frac{E^2 r_h^2}{4 \ell^2 \rho_h k_h T_h} \left[\left(\frac{r_c}{r_h} \right)^2 - 1 - \ln \left(\frac{r_c}{r_h} \right)^2 \right]$$

$$\theta \equiv \frac{T}{T_h} \quad A \equiv \frac{\alpha T_h}{1 + \alpha T_h} \quad B \equiv \frac{\beta T_h}{1 + \beta T_h}$$

Two facts should be observed from Eq. 46. The first is that the influence of B on the nonlinearity is about three times as important as A. In other words, if $\alpha = \beta$ there would be about three times as much error in the wall temperature drop if the temperature dependence of k were neglected as there would be if the temperature dependence of ρ were neglected. This fact, stated qualitatively, was one of the main contributions of reference 43. The second fact to be observed in Eq. 46 is that an error of a given percent in any one of the following

$$E^2, \ell^2, \rho_h, k_h \text{ or}$$

$$r_h^2 \left[\left(\frac{r_c}{r_h} \right)^2 - 1 - \ln \left(\frac{r_c}{r_h} \right)^2 \right] \approx \frac{r_h^2}{2} \left[\left(\frac{r_c}{r_h} \right)^2 - 1 \right] = \frac{r_h^2}{2} \left[\frac{(r_c - r_h)(r_c + r_h)}{r_h^2} \right]^2 \approx \left(\frac{\Delta t_w}{r_h} \right)^2$$

will produce approximately the same percent error in the tube wall temperature drop. Of these quantities, the one which is the most difficult to measure and which contains the greatest error is k_h .

D. The Application of the Rapid-Convergence Technique to Other Problems

Computer solutions or numerical techniques certainly provide the most general means for solving nonlinear problems. However, the results of a computer or numerical solution are numbers and not relationships. In addition, the time and expense in setting up,

debugging, and running a given problem on a computer may be large. The rapid-convergence technique, although not as general as numerical techniques, is capable of solving a large class of practical nonlinear problems. Its use requires no special knowledge beyond a course in advanced calculus. Furthermore, a rapid-convergence solution, which usually requires less time than programming a numerical solution, yields functions thereby permitting insight into the problem.

A differential equation can be thought of as defining some function. In general, this function (the solution) is expressible as an infinite series. The solutions which have appeared most frequently have been tabulated.

For example:

| Differential Equation | Solution | Series |
|-----------------------------|--------------|---|
| $\frac{dy}{dx} - y = 0$ | $y = e^x$ | $y = 1 + \frac{x}{1!} + \frac{x^2}{2!} + \dots$ |
| $\frac{d^2y}{dx^2} + y = 0$ | $y = \sin x$ | $y = x - \frac{x^3}{3!} + \frac{x^5}{5!} + \dots$ |

The fact that an unsolved differential equation has a solution which is expressible only as a series should therefore be expected. Of significance, however, is the rate at which the solution converges. The technique presented here is able to accelerate this convergence by building a power series out of a linear solution which is itself a power series. In this way, each term contains itself an infinite series.

The primary requirement for using this technique to obtain the solution to a given nonlinear differential equation is the existence of some linearized solution of the problem. This linearized solution

may be arrived at by giving some parameter an appropriate value or by neglecting completely some term of the differential equation.

A characteristic of this technique is the job of fitting a power series to one or more given functions as was done in Eq. 43. Contained in appendix A is an example which fortuitously does not require this fit. This example is the classical pendulum problem which until now has ~~not been~~ solved.

E. The Measurement of Thermal Conductivity Appropriate for Electrically-Heated Tubes

As has been mentioned, the accuracy of the tube wall temperature drop in electrically-heated tubes is no better than the accuracy with which the thermal conductivity is known. It should also be noted that the values for this property, which are published, have been measured under different conditions than those that exist in electrically-heated tubes. These major differences are:

1. The electrically-heated tube may have been formed differently or may contain a different composition than the specimen from which the published conductivity was evaluated.
2. The thermal conductivity appropriate for an electrically-heated tube is perpendicular to that of standard measurements.
3. The thermal conductivity appropriate for an electrically-heated tube must be valid across a thin wall, valid at high temperature gradients (about 10,000°F/inch), and valid when a voltage gradient is perpendicular to the heat flux.

The first difference can be avoided by assuming that thermal conductivity is a function of the easily measured electrical

resistivity (the Lorenz approach states that $\frac{k\rho}{T}$ is a constant for electrical conductors). Powell⁴⁸ has published such functional relationships for a wide variety of electrical conductors which he claims will result in no more than a 7-9 percent error. Based upon the measurements of Tye,⁴⁹ the second difference will probably contribute no more than a one percent error. This was concluded by measuring the electrical resistivity on two sets of faces of a stainless steel cube and making the Lorenz assumption. The third difference remains to be resolved as a cause for erroneous thermal conductivity values for electrically-heated tubes.

These potential sources of errors, coupled with the compact temperature profile given by Eq. 46, suggest the following means for measuring the appropriate value of thermal conductivity.

The energy equation for the electrically-heated tube is

$$\frac{EI}{2\pi r_c \ell} = -k_c \frac{dT}{dr} \Big|_{r_c} \quad (47)$$

The temperature gradient as derived from Eq. 46 is expressed as

$$\frac{dT}{dr} = \frac{dT}{dr} \left[E, \ell, r_c, r_h, k(T), \rho(T), T_h \right] \quad (48)$$

Eqs. 47 and 48, together with the known tube geometry, resistivity, and sets of measured values of E, I, and T_h , will determine $k(T)$.

The derivation of $k = k(T)$ is as follows:

$$EI = 2\pi k_c R_c \ell T_h \left[\left| \frac{d\theta}{dL} \right| \left| \frac{dL}{dR} \right| \right] \quad (49)$$

$$\frac{d\theta}{dL} = -1 + 2 a_2 L + 3 a_3 L^2 + \dots \quad (50)$$

$$\frac{dL}{dR} = 2P \left(R - \frac{1}{R} \right) = \frac{E^2 r_h^2}{2\ell^2 \rho_h k_h T_h} \left(R - \frac{1}{R} \right) \quad (51)$$

substituting Eq. 50 and Eq. 51 into Eq. 49 gives

$$I/E = \left[\frac{\pi |r_c^2 - r_h^2|}{\rho_h \ell} \right] \left[\frac{k_c}{k_h} \right] \left[1 - 2 a_2 L - 3 a_3 L^2 - \dots \right] \quad (52)$$

Some insight into the problem will result by defining

$$\frac{(\text{Res})_h}{E/I} \equiv \frac{\rho_h \ell}{\pi |r_c^2 - r_h^2| E/I} \quad (53)$$

$(\text{Res})_h$ can be thought of as the tube's electrical resistance when it is at the uniform temperature T_h . Rewriting Eq. 52 by substituting Eqs. 35, 37, and 53 gives

$$\frac{(\text{Res})_h}{E/I} = \left[1 + B (-L + a_2 L^2 + \dots) \right] \left[1 - 2a_2 L - 3a_3 L^2 - \dots \right] \quad (54)$$

where $(\text{Res})_h$ is the tube's electrical resistance when it is at the uniform temperature T_h . Neglecting the L^2 term as a first approximation gives

$$\frac{(\text{Res})_h}{E/I} - 1 \approx \frac{E^2 r_h^2}{4\ell^2 \rho_h k_h T_h} (R_c^2 - 1 - \ln R_c^2) \left(\frac{A}{1 + b_1} \right) \quad (55)$$

or

$$k_h \approx \frac{E^2 r_h^2 (R_c^2 - 1 - \ln R_c^2)}{4 \ell^2 \rho_h (1 + \alpha T_h) (1 + b_1) \left[\frac{(\text{Res})_h}{E/I} - 1 \right]} \quad (56)$$

In order to best evaluate the ratio defined by Eq. 53, the identical test section (including voltage tap positions) was used to

calculate $(Res)_h$ as was to be used in the subsequent heat transfer experiments. This was done by using an electrically heated furnace in conjunction with a DC power source connected in series with a standard resistor and the test section. A value of $(Res)_h$ was then found for each temperature setting of the furnace and was evaluated as

$$(Res)_h = \left[\begin{array}{l} \text{Resistance} \\ \text{of standard} \\ \text{Resistor} \end{array} \right] \left[\frac{\text{Potential drop across test section}}{\text{Potential drop across standard resistor}} \right] \quad (57)$$

Subsequent to this measurement, the test section was connected into the boiling loop and values of E/I were also taken as a function of temperature.

The values of k_h as calculated from Eq. 56 are shown in Fig. 12. The inaccuracy in the measurement of E and I certainly contribute the majority of the scatter. The test section length was able to be measured with a high degree of accuracy from X-rays. The following are felt to be a realistic estimate of the various measurement errors.

| | | | | | | | | |
|-------------------|-----|-----|-------|-------|-------|--------|----------|-----|
| Quantity Measured | E | I | T_h | r_h | r_c | ρ | α | l |
| \pm error (%) | .3 | .2 | 4°F | .3 | .2 | .5 | .5 | .2 |

The scatter of the data, as well as the wide band of experimental uncertainty (probably about $\pm 15\%$) is disappointing. A detailed examination of the total error is not warranted here due to the subjective nature of the above individual error estimates. It does suggest, however, that the thermal conductivity appropriate to heat transfer experiments may be lower than that derived from the Lorenz assumption. The most likely causes for this discrepancy appear to be those listed under difference 3 on page 53.

Eq. 56 indicates that by doubling the value of $\left[\frac{(\text{Res})_h}{E/I} - 1 \right]$ the resulting error will be cut in half. From Eq. 55 one can see that $\left[\frac{(\text{Res})_h}{E/I} - 1 \right]$ is proportional among other things to

$$(E/l)^2 \quad \text{and} \quad \left(\frac{\Delta t_w}{r_h} \right)^2$$

Therefore, by doubling either the wall thickness or the voltage drop per unit length, the error could be cut approximately by one fourth. With this in view, it appears possible that by selecting a more appropriate test section geometry and power level the error attributed to the factor $\frac{(\text{Res})_h}{E/I} - 1$ could become negligible. This would allow the expected scatter band to be reduced to a point where the phenomenon described under difference 3 on page 53 could be more definitely isolated.

Shown also in Fig. 12 is the value of thermal conductivity as calculated using the Lorenz approach. The comparatively simple resistivity measurement which is required in that approach was measured in the laboratory and found to fit very tightly the curve

$$\rho \text{ (ohm ft)} = 2.331 \times 10^{-6} \left[1 + .569 \times 10^{-3} T \text{ (}^\circ\text{F)} \right] \quad (58)$$

over the range 100°F to 500°F the Lorenz "constants" were furnished by Tye⁴⁹ (for example, $3.16 \times 10^{-8} \frac{\text{volts}^2}{\text{degree Kelvin}^2}$ at 392°F). All calculations involving $k(T)$ used the Lorenz derived expression.

Chapter V - Experimental Equipment and Procedure

A. Boiling Apparatus

The experimental program was carried out using the low pressure heat transfer boiling loop of the Heat Transfer Laboratory. The details of the loop are shown in Fig. 13. Low-voltage direct current power was supplied by two 36-kw Chandeysson motor-generators connected in series. Distilled, degassed water was circulated at a maximum rate of 3.6 gpm. The system water was checked periodically to insure proper surface tension (>72 dynes/cm) and low volume resistivity (<1 megohm cm). A detailed description of this boiling loop and the associated instrumentation can be found in reference 50.

The initial objectives of the experimental program were (1) to obtain inception data primarily at low heat fluxes and thereby assess the validity of various inception theories, and (2) to control the cavity size distribution of a boiling surface, as discussed in Chapter II, in order to determine the resulting heat transfer effects. To achieve these ends the test section design aimed at:

1. observing visually the onset of vapor formation and comparing it with the first significant increase in heat transfer due to boiling
2. achieving the greatest possible accuracy in measuring the temperature of the boiling surface
3. insuring that inception could be made to occur in a low heat flux region ($q/A < 10^4$ BTU/hr ft²) still maintaining turbulent flow

4. preventing flow disturbances from taking place at the entrance to the heated length of the test section
5. reaching the maximum heat flux consistent with the loop limitations and the above design considerations
6. controlling and systematically varying the heat transfer surfaces with regard to the scratch orientation and roughness while at the same time holding all other variables constant

The first design consideration clearly required that the test section be an annulus. The annulus geometry with inner tube heated further simplified the achievement of the second consideration by automatically providing an adiabatic wall required to solve the associated conduction problem. To further reduce inaccuracy in this difficult measurement, a very thin tube wall was selected (.019 in) and a special thermocouple bundle was designed which will be discussed in section B. The material selected for the heat transfer surface was 304 stainless steel. This was based on its resistance to corrosion, a relative abundance of published property values for this material and a history of successful usage in previous heat transfer work. To meet design consideration three, the hydraulic diameter was made purposely large (.25 in) in order to give a low velocity (.4 ft/sec) but still maintain turbulent Reynolds number. At this low velocity the heat flux at inception was expected to be less than 10^4 BTU/hr ft². This diameter still allowed velocities in excess of 5 ft/sec corresponding to nucleate boiling heat fluxes in excess of 10^6 BTU/hr ft². Flow disturbances at the inlet of heated test sections (consideration four) resulting from the joining of the low resistance current carrying

member to the high resistance heated boiling surface were felt to seriously hinder the analysis of boiling data. To avoid this problem (see Fig. 14) the inlet low resistance element (copper) was inserted five inches inside the high resistance element (steel). This allowed the flow to proceed undisturbed along the outside of the steel element for five inches (or twenty diameters) before reaching the heated portion of that element. Such care was less important at the exit end of the heated length and therefore the low resistance element was joined on the outside of the steel tube. The thermocouple bundle could then be inserted at the downstream side of the test section and the size of this bundle was therefore limited only by the ID of the heated tube. The length of the heated surface (five inches) was arrived at primarily based upon achieving the optimum independence match for the 36 kw - 3000 ampere power source.

Teflon o ring sealants were used to support the conductor and to allow for thermal expansions. The pyrex was supported by neoprene o ring sealants. Both types of o rings were sealed by Veeco Couplings. The voltage taps consisted of 30-gauge teflon coated wire and were soldered directly to the copper at the ends of the heated surface insuring an accurate reading. The bulk liquid thermocouples (30-gauge copper-constantan) were placed at such a location as to insure that the liquid was completely mixed. The pyrex tubing was 0.5 inch precision bore made by Corning.

To meet the sixth design consideration, four identical test section conductors were made. Each surface was then prepared with one of the following finishes: axial scratches - smooth finish (AS), axial scratches - rough finish (AR), circumferentially scratches smooth

finish (CS), circumferentially scratches - rough finish (CR). The same test section assembly and thermocouple bundle could be used for each of the four surfaces. The test surfaces could also be reused at a later date with assurance that all test section variables would be unchanged.

The finishing procedure consisted of turning each test section conductor on a lathe while polishing with 360 grit silicon carbide paper. Following this, the polishing was done axially until all circumferential grooves were removed. This polishing sequence was then repeated using 400 grit silicon carbide paper along with an oil lubricant. The two surfaces which were to receive a rough finish were then hand polished with an 180 grit aluminum oxide clothe. The two smooth surfaces resulted from lapping with lap A valve grinding compound.

The surfaces were cleaned with acetone several minutes prior to the test section being filled with the loop water. An alternate cleaning procedure consisted of using trichlorethylene instead of acetone. No boiling differences were observed as a result of using the alternate solvent.

X-rays were taken of each test section conductor to insure the absence of flaws both within the steel wall and in the soldered joints. From the X-rays it was also possible to very accurately measure the length of the heated surface and to insure that the dimensions of each conductor were identical.

B. Thermocouple Design

The original thermocouple bundle consisted of six-30-gauge copper-constantan, glass insulated thermocouples with the junctions spaced 1/2 inch apart. Each thermocouple was placed parallel to the bundle axis and rigidity was achieved by tightly wrapping them with Scotch Electrical Tape No. 27.

Initial fully developed boiling data indicated that the temperatures measured by the tube thermocouples were decreasing in the downstream direction. On closer examination of the cause of this effect, it was found that axial heat conduction was taking place down the thermocouples. This deduction was made both analytically and experimentally. Analytically the thermocouple was modeled as a thin fin in stagnant air with the tip temperature and base temperature known. Experimentally the thermocouple bundle was placed in air at room temperature while the base was placed in an ice bath. This temperature difference of about 40°F was found to cause a significant thermocouple error. For example, when the thermocouple bead was two inches away from the ice bath, the temperature error was 10°F. This error, as predicted from the fin model, was

$$(\Delta T)_{\text{error}} \approx \frac{(T_{\text{air}} - 32) Dk}{2l^2 h} \quad (59)$$

The other variables were verified within the uncertainty of the effective values of k and h . Experimentally the length effect of Eq. 59 was substantiated.

The problem was remedied by first replacing the 30-gauge copper-constantan thermocouple wire with 36-gauge teflon coated wire of the same material. This reduced the fin diameter and consequently the error

by a factor of two. The teflon coating instead of the glass insulation also increased h significantly. The effective length was increased by a factor of four by wrapping the wire in a spiral around a solid rod which was electrically and thermally insulated. This in itself reduced the error by a factor of about sixteen. Additional improvement could have been made by selecting a less conductive thermocouple material; for example, iron-constantan. This further measure was not felt to be necessary. The ice bath test was again performed on the redesigned thermocouple bundle with the result being an error reduction by a factor of between twenty and one hundred. This final bundle design consisted of seven thermocouples spaced $5/7$ inches apart.

Further fully developed boiling data showed that the wall temperature no longer decreased in the downstream direction, but instead remained constant. This is in agreement with the reported observations of Kennel.⁵¹ Elrod, et al.,⁵² have recently reported conflicting results, stating that the wall temperatures dropped in the downstream direction. Their geometry, from a thermocouple standpoint, was quite similar to the original thermocouple bundle of the present work. Although other factors may be involved, one suspects that axial thermocouple conduction could account for their observations.

C. Bubble Detector

A number of attempts have been made by past investigators to detect with instruments the presence of first vapor when boiling begins. These attempts have employed high speed photography⁵³ and sound.⁵⁴ Others have tried to precisely relate an increase in pressure drop to

first vapor⁵¹ or to relate a change in thermocouple fluctuations with the first vapor.⁵⁵ None of these approaches have yielded sufficient precision to enable first vapor to be defined by the technique.

Visual approaches, even with the aid of a magnifying glass, suffer from the lack of sufficient resolution. At elevated pressures, velocities and subcoolings, one does not know if the apparent absence of bubbles is because boiling is truly not taking place or if the human eye is insensitive to the very small bubbles.

The approach which was taken in the present work employed light as shown in Fig. 15a. A DC light source was directed nearly parallel to the heated surface. The only light to reach the light detector was that which was continually scattered from various stationary surfaces. The presence of the first bubble, even though it was well below the resolving level of the eye, reflected light from its meniscus into the detector. The wires leading from the bud box (Fig. 15b) were shielded from stray voltages and the box itself was grounded. The detector itself consisted of less than \$10.00 worth of subcomponents, the most expensive of which was a \$4.00 light dependent resistor. The particular resistor, made by Clairex (CL 703L), was selected because of its high sensitivity in the visual region, fast decay and fast response. To give some idea of the sensitivity, one was able to cover the light aperture with the finger of one hand while wiggling the fingers of the other hand somewhere in front of the detector. Even with no direct light source this motion would cause the oscilloscope trace to oscillate on and off the scope.

The initiation of bubbles was seen on the oscilloscope as a sharp jump in the trace accompanied by high frequency, random oscillations.

As the intensity of boiling further increased, both the level and amplitude of oscillations increased. It was not possible to associate these effects with any particular bubble or bubble frequency. A result of having such a distinct threshold was that one could conclude that the unaided eye was able to see first vapor at conditions below 60 psia, 150°F subcooling, and 5 ft/sec. Once this fact had been firmly established only visual observations were made of first vapor when conditions were below those listed above. However, at higher pressures, velocities and subcoolings the detector was used giving a sharp indication of first vapor at low heat fluxes than that seen by the eye. In this region the detector was heavily relied upon.

D. Measurement of Gas Concentration

Since the concentration of dissolved gas is an important variable in boiling, the experimental procedure in boiling must either measure and control this concentration or else reduce the variable to an insignificant amount. To approximate the strength of this variable one has only to realize from Henry's Law that the ratio of the gas concentration at saturation equals the ratio of partial pressure of the gas within a nucleation site to the local pressure. For example, at atmospheric pressure, a concentration of 1 cc of air per liter (the saturation concentration equals 21 cc air/l) will increase the pressure within all nuclei by 0.7 psi. This would correspond to a reduction in incipient nucleation superheat of about 2.5°F. Fig. 16 shows the qualitative results of a variation of gas concentration as measured by the amount of dissolved oxygen in the liquid. From an examination of the boiling literature, it is safe to say that most boiling liquids contain more

than 1/20th of saturation and therefore discrepancies should be expected when one attempts to compare data in the incipient region.

Unfortunately there is no developed technique for measuring the concentration (or more importantly, the partial pressure at the boiling temperature and pressure) of the gas within the liquid. Often in the literature, investigators, using the well known Winkler technique for measuring the dissolved oxygen concentration, claim to be able to infer the air concentration from the oxygen concentration. The error in this approach lies in the fact that the dissolved air and oxygen only bear a fixed ratio when they are in equilibrium with atmospheric air. At concentration less than saturation they are not in equilibrium. However, from the data compiled by Dorsey⁵⁶, one can conclude that this error results in the erroneous air concentration being no more than 300% high.

For these reasons, the approach to the dissolved gas problem in this experimental program was to reduce the gas concentration to the lowest level possible, consistent with the boiling loop and time. The Winkler test was then performed both at the beginning and at the end of each day of data collecting. Data were not taken or were rejected if the oxygen concentration was greater than 0.1 cc/l. This would correspond to about 0.3 cc air/l if the liquid were in contact with a standard atmosphere.

E. Experimental Procedure

The experimental procedure consisted of first assembling a specific boiling surface inside the test section assembly. All electrical connections were cleaned to insure good contact and the test section was installed vertically in the boiling loop. Loop water was then allowed to slowly enter the test section from the bottom, which constrained the direction of liquid advance relative to the scratches on the heat transfer surface. The trapped gas in the loop itself was bled at several points. All degassing heaters were then turned on, bringing the liquid in the degassing tank to boiling. The loop water was circulated by the pump, a portion of it going upwards through the test section as well as through the degassing tank. This was continued for the duration of the degassing, which usually lasted five hours. To increase the ability of the loop water to absorb small pockets of trapped air on surfaces and in the pumping, the heat exchanger was operated continuously maintaining the water at the coldest possible temperature. For this reason also, the pressure level of the loop was held at a minimum of 30 psia. The steam and air mixture was continually bled from the top of the degassing tank. At the end of about one and a half hours, the liquid level in the degassing tank would be depleted, requiring a refill and continued degassing. When the gas content was felt to be sufficiently low, a Winkler test was performed which gave some indication of the dissolved air. If the dissolved oxygen was sufficiently low, the data collection commenced; otherwise, the degassing was continued.

The pattern of collecting data was to hold pressure, velocity, and subcooling (evaluated at the center of the test section) constant while varying the heat flux. In order to detect any hysteresis, the power level was first increased from well within the nonboiling region to a predetermined level of nucleate boiling followed by a decrease back to the nonboiling region. In general, no hysteresis tendency was observed except as discussed in Chapter VII. During both the increase and decrease in heat flux, inception was carefully noted both visually and by the bubble detector. Vapor was always detected at slightly lower heat fluxes than the sharp change from forced convection to boiling heat transfer. This sharp transition in the boiling curve is certainly due to a large extent on the low gas concentration in the liquid since a gradual transition would always occur in those cases where gas inadvertently entered the system (Fig. 16). However, other factors may also account for the effect such as the characteristic low velocities or the annulus geometry.

The raw data was processed at the M.I.T. Computation Center using an IBM 7094 computer. The data reduction program, written by R. F. Lopina,⁵⁷ produced the following output quantities for each of the seven tube thermocouples:

- | | |
|--------------------------------------|----------------|
| 1. heat flux | 4. $T_w - T_b$ |
| 2. wall temperature (T_w) | 5. $T_w - T_s$ |
| 3. Bulk liquid temperature (T_b) | 6. subcooling |

- | | |
|----------------------------------|-----------------------------|
| 7. heat transfer coefficient (h) | 11. Prandtl Number (Pr) |
| 8. Grashof Number | 12. Fanning Friction Factor |
| 9. Nusselt Number (Nu) | 13. $\frac{Nu}{Pr^{.4}}$ |
| 10. Reynolds Number (Re) | |

Reference 57 contains further details on the data reduction program.

Chapter VI - The Inception of First Significant Boiling

A. Introduction

During the past ten years there has been a great deal of interest in determining, in a general manner, the point at which boiling begins. This interest is motivated by the following:

1. The accurate prediction of the incipience of boiling, or of first vapor, in a liquid-moderated nuclear reactor is important from a safety standpoint. The replacement of the liquid by its vapor reduces the moderating ability of the liquid and thereby acts as an inherent shut-down mechanism.
2. The accurate prediction of the transition from natural convection or forced convection to boiling is important in enabling the designer to determine when significant increases in heat transfer will begin.
3. The prediction of the onset of nucleation within the liquid film in two-phase annular flow has been shown, under certain conditions, to be equivalent to the prediction of the critical heat flux under those same conditions.⁵⁸
4. The prediction of boiling inception bears a very close analogy to the prediction of the onset of cavitation. Although there has been no determined effort to use this analogy, the two fields have frequently (and independently) arrived at the same conclusions regarding their respective phenomena.

B. Literature Survey

The analyses which have lead to a prediction of the inception of boiling from a solid surface can best be compared by pointing out the structural similarity between the various models. The four structural elements which comprise all of the inception models are shown in Fig. 17.

The first element is the specification of a physical model for the liquid such that a temperature distribution within the liquid can be analytically derived. Practically all of the published models treat the liquid as a semi-finite slab in which solid body conduction is the only mechanism of heat transfer. As a rule, a transient temperature distribution is employed for pool boiling situations and a steady-state temperature distribution is used in a flow situation. With the liquid temperature known, it is then possible, using some criteria for growth, to determine the equilibrium vapor pressure within the nuclei. This is practically always done by using the Clapeyron relation of Eq. 14. However, it is equally valid to determine this equilibrium vapor pressure from tabulated values of the saturation state properties of the particular fluid or to utilize some form of the equation of state of the fluid.

In the event there is a gas dissolved in the liquid, there will exist a partial pressure of that gas within the nuclei according to Henry's Law

$$p_g = \frac{C}{K(T)} \quad (60)$$

A knowledge of the total pressure ($p_v + p_g$) within the bubble can then be related to the radius of curvature of the bubble itself as

$$p_v + p_g - p_L = \sigma \left(\frac{1}{R_1} + \frac{1}{R_2} \right) \quad (61)$$

Adams has pointed out that where the bubble is uninfluenced by gravity the sum $1/R_1 + 1/R_2$ is constant even though the surface is not symmetrical.⁵⁹ Therefore, in the interest of generality this constant will be selected by defining r as the effective radius of curvature such that

$$p_v + p_g - p_L \equiv \frac{2\sigma}{r} \quad (62)$$

This relationship (with $p_g = 0$) is common to all inception models and is referred to in the literature by any one of the following names: Rayleigh, Helmholtz, Gauss, Young, Laplace, Poisson, and Gibbs.

The major distinctions between the models reviewed in this survey are in the statements of the criteria for growth. In all cases, this criteria "feeds back" sufficient information to make the problem determinant. That is, some function r is related to the liquid temperature profile necessary to cause inception. Often this criteria implies the definition of what is meant by boiling inception. For example:

1. Michiyoshi and Schrock⁶⁰ using a transient temperature profile said that nucleation would take place when the superheat contained in the liquid slab of variable thickness r is a maximum [a maximum must be reached since r decreases as $T_L(y,t)$ increases].
2. Lienhard,⁶¹ using a transient temperature profile, gave a criterion for growth which said that the nondimensional rates of change of availability and thermodynamic potential are comparable

at a distance r away from the wall. Fabric⁶² observed that the mathematical formulation of this criteria can be reduced to that of Michiyoshi and Schrock.

3. Hsu,⁶³ using a transient temperature profile, stated that inception would occur when $T_L (2r) \geq T_v$.

4. Bergles and Rohsenow,⁶⁴ using a steady state (linear) temperature profile, stated that inception would occur when $T_L (r) \geq T_v$.

5. Sato and Matsumura,⁶⁵ two years later, arrived at the same mathematical formulation as Bergles and Rohsenow.

6. Han and Griffith,⁶⁶ using a transient temperature profile said that inception would occur when $T_L (3/2 r) \geq T_v$.

7. Davis and Anderson,⁶⁷ using a steady state temperature profile, which accounted for turbulent effects beyond the laminar sublayer, stated that inception would occur when $T_L (r) \geq T_v$.

8. Faneuff, McLean, and Scherrer⁶⁸ used a transient temperature profile which was found by fitting Plesset and Zwick's bubble growth equation (asymptotic form) to his bubble growth data. They postulated inception when $T_L (2/3 r) \geq T_s$.

9. Zuber,⁶⁹ assumed a transient exponential temperature distribution and suggested that inception would take place when $T_L (r) \geq T_v$.

10. Kenning and Cooper,⁷⁰ using a steady state (linear) temperature profile, suggested that two different criteria for growth were possible. If $(Re) (Pr) \gg 1$, then inception would occur when

$$T_L \left[.54 H (1 - \epsilon^{Re/45}) \right] \geq T_v$$

If $(Re) (Pr) \ll 1$, then inception would occur when

$$T_L (H) \geq T_V$$

11. Howell and Seigel⁷¹ developed a model which required numerous assumptions. Their model is equivalent to assuming a steady state (linear) temperature profile with inception occurring when

$$T_L (1/2 r) \geq T_V \quad \text{if } r < \delta$$

If $r > \delta$ then inception occurs when

$$T_L \left[(\delta/r) - 1/2 (\delta/r)^2 \right] \geq T_V$$

One can conclude on the basis of the differences in the above models that the weakness element of our knowledge of boiling inception is the criteria for growth. These criteria generally have taken the form

$$T_L (n r) \geq T_V \quad (63)$$

where the value of n has been based at best on one's physical intuition of the complicated interactions of three phases (a solid wall, a fluid, and a gas of one or more species) containing strong temperature and velocity gradients.

C. Analytical Solution

In what follows, the solution to the inception problem will be attempted by letting the value of n be an unknown parameter whose value hopefully can be determined experimentally. Since flow surface boiling is of primary interest for this work, the temperature distribution

within the liquid, for the present, will be assumed to be linear, i.e.

$$T_L = T_w - \left(\frac{q}{Ak_L}\right) y \quad (64)$$

This assumption will only be correct if solid body conduction predominates in the vicinity of the bubble and if a sufficient portion of the bubble's growth takes place in the laminar sublayer. Appendix B contains the justification for this latter assumption.

To arrive at the vapor temperature within the nuclei, several approaches are possible. The first, as well as the most common, relies upon an integration of the Clapeyron relation given by Eq. 14 which is repeated below:

$$\frac{dp}{dT} = \frac{h_{fg}}{T(v_v - v_L)} \quad (14)$$

Perhaps the simplest method of integrating Eq. 14 is to assume that the right side is constant. It is then possible to integrate this directly as T varies from T_s (known) to T_v (unknown) while p varies from p_L (corresponding to T_s) to p_v (known from Eq. 62). This would immediately yield the vapor temperature of the nuclei as

$$T_v = T_s + \frac{(p_v - p_L)(v_v - v_L) T}{h_{fg}} \quad (65)$$

where the properties are evaluated as some temperature between T_v and T_s . Using Eq. 62 with the further assumption that $p_g = 0$ gives

$$T_v = T_s \frac{2\sigma(v_v - v_L) T}{r h_{fg}} \quad (66)$$

A second method for integrating the Clapeyron equation is to assume that $\frac{h_{fg}}{(v_v - v_L)}$ is a constant. Integrating between the same limits

as above would give

$$T_v = T_s \epsilon \frac{(p_v - p_L)(v_v - v_L)}{h_{fg}} \quad (67)$$

If, as before $p_g = 0$, this would become

$$T_v = T_s \epsilon \frac{2\sigma(v_v - v_L)}{h_{fg}} \quad (68)$$

A third integral results by neglecting v_L with respect to v_v , evaluating the temperature of Eq. 14 at the vapor temperature (for the present unknown) and making the assumption of a perfect gas in order to eliminate v_v . The integration can be carried out as follows by assuming the $\frac{h_{fg}}{R_v}$ to be constant.

$$\int_{p_L}^{p_v} \frac{dp}{p} = \frac{h_{fg}}{R_v} \int_{T_s}^{T_v} \frac{dT_v}{T_v^2} \quad \text{or} \quad (69)$$

$$\ln \frac{p_v}{p_L} = \frac{h_{fg}}{R_v} \left(\frac{1}{T_s} - \frac{1}{T_v} \right) \quad (70)$$

Substituting Eq. 62 into Eq. 69 with the temporary assumption that $p_g = 0$ gives

$$\ln \left(1 + \frac{2\sigma}{p_L r} \right) = \frac{h_{fg}}{R_v} \left(\frac{1}{T_s} - \frac{1}{T_v} \right) \quad (71)$$

$$T_v = \frac{T_s}{1 - \frac{T_s R_v}{h_{fg}} \ln \left(1 + \frac{2\sigma}{p_L r} \right)} \quad (72)$$

To best evaluate the various assumptions leading to Eqs. 66, 68, and 72, Table 1 has been prepared. Values of the predicted vapor temperature are given for each of the three integrals over a wide range of pressures. These calculated values can then be compared with the true values as taken from Steam Tables.⁷² In order to make the three integrals comparable, the nuclei was assumed to have a radius of .0001 in., which on the basis of Chapter II is reasonable.

From Table 1 it can be concluded that only Eq. 72 gives accurate results at low pressures (in the neighborhood of atmospheric pressures or less) and all three integrals produce sufficient accuracy at higher pressures. For this reason, all further work will be based upon Eq. 72.

Another approach which yields the vapor temperature and which is valid at all pressures is to use tabulated properties and a trial and error solution as outlined in Fig. 17. Unfortunately, this is laborious. In addition, only a few fluids have sufficiently accurate tabulated properties. However, for those fluids which have tabulated properties, this method will yield the most accurate value for T_v .

A third approach, which also requires tabulated properties and is valid at all pressures is given by Shai.⁷³ It has the advantage of not requiring a trial and error solution. Shai has suggested fitting tabulated saturation pressure and temperature data to the form

$$\ln p = c - \frac{d}{T} \quad (73)$$

and evaluating the constant d . It has been pointed out by Bonilla, Sawhney, and Makansi⁷⁴ that Eq. 73 is a suitable form for an equation of state. It follows then that

$$\ln \frac{P_v}{P_L} = d \left(\frac{1}{T_s} - \frac{1}{T_v} \right) \quad (74)$$

Table 1

Comparison of Various Integrals of the Clapeyron Equation
(Eq. 14)

The comparison is based upon water with a bubble whose radius of curvature is .0001 inch. All properties are evaluated at T_s .

| Assumptions | Expression for T_v | $P_L = 1$ psia $T_s = 101.74^\circ\text{F}$ | $P_L = 14.7$ psia $T_s = 212.0^\circ\text{F}$ | $P_L = 100$ psia $T_s = 327.8^\circ\text{F}$ | $P_L = 500$ psia $T_s = 467.0^\circ\text{F}$ |
|---|---|--|--|---|---|
| | tabulated | 185.64°F | 231.45°F | 331.59°F | 467.69°F |
| $\frac{h_{fg}}{T(v-v_L)} = \text{constant}$ | $T_v = T_s + \frac{2\sigma(v-v_L)T}{r h_{fg}}$ | 353.0°F | 234.7°F | 331.68°F | 467.69°F |
| $\frac{h_{fg}}{v-v_L} = \text{constant}$ | $T_v = T_s \epsilon \frac{2\sigma(v-v_L)}{r h_{fg}}$ | 419.0°F | 235.0°F | 331.68°F | 467.69°F |
| $v_L = 0$ | | | | | |
| $\frac{p_v}{v} = R_v T$ | | | | | |
| $\frac{h_{fg}}{R_v} = \text{constant}$ | $T_v = \frac{T_s}{1 - \frac{T_s R_v}{h_{fg}} \ln(1 + \frac{2\sigma}{r p_L})}$ | 188.8°F | 231.7°F | 331.82°F | 467.86°F |

This equation is identical with Eq. 70 if one replaces d by $\frac{h_{fg}}{R_v}$.

The graphical description of boiling inception (Fig. 18) as given by Bergles and Rohsenow⁶⁴ provides the clearest description of the effects of the relevant heat transfer variables. They postulate that the nucleus of a hemispherical shape with radius r will grow if the liquid temperature at a distance $y = r$ from the wall is greater than the critical vapor temperature defined by Eq. 72. For their model then, $n = 1$, and the criterion for growth is satisfied when the straight line representing the temperature profile (Eq. 64) becomes tangent to Eq. 72. This criterion can be generalized in terms of the parameter n , as in Eq. 63, by replacing y by y/n . It will now be shown that based upon the above assumptions, two dimensionless variables (a dimensionless heat flux and a dimensionless superheat) determine whether inception will take place.

The two conditions which insure a tangency as shown in Fig. 18 are

$$T_L(nr) = T_v \quad (75)$$

and

$$\left. \frac{\partial T_L}{\partial y} \right|_{y=nr} = \left. \frac{\partial T_v}{\partial r} \right|_r \quad (76)$$

Performing these operations on Eq. 64 and 72 gives

$$T_w - \left(\frac{qn}{Ak_L} \right) r = \frac{T_s}{1 - \frac{T_s R_v}{h_{fg}} \ln \left(1 + \frac{2\sigma}{p_L r} \right)} \quad (77)$$

$$\frac{q}{Ak_L} = \frac{T_s \left[\frac{R_v T_s}{h_{fg}} \left(\frac{2\sigma/p_L r^2}{1 + 2\sigma/p_L r} \right) \right]}{\left[1 - \frac{T_s R_v}{h_{fg}} \ln(1 + 2\sigma/p_L r) \right]^2} \quad (78)$$

Substituting the denominator of the right hand side of Eq. 77 into Eq. 78 gives

$$\frac{q}{Ak_L} = \frac{R_v}{h_{fg}} \left(\frac{2\sigma}{p_L r^2} \right) \left(T_w - \frac{q n r}{Ak} \right) \quad (79)$$

By defining the following dimensionless variables

$$q/A^* \equiv \left(\frac{R_v \sigma n}{h_{fg} p_L k_L} \right) q/A \quad \text{and} \quad r^* \equiv \frac{r p_L}{\sigma} \quad (80 \text{ a,b})$$

$$T_s^* \equiv \frac{T_s R_v n}{h_{fg}} \quad \text{and} \quad T_w^* \equiv \frac{T_w R_v n}{h_{fg}} \quad (81 \text{ a,b})$$

Eq. 79 can be rewritten as

$$q/A^* = \frac{2}{r^* (r^* + 2)} \left[(T_w^*)^2 - 2 (r^*) (T_w^*) (q/A^*) + (r^*) (q/A^*) \right] \quad (82)$$

Solving this quadratic equation for r^* gives

$$r^* = \frac{\sqrt{1 + 4 \frac{T_w^*}{q/A^*} + \frac{2 T_w^*}{q/A^*}} - (1 + 2 T_w^*)}{1 - 2 (q/A^*)} \quad (83)$$

The problem which will now be solved is that of determining the heat flux necessary for inception. The implicit solution will involve the following variables:

$$(q/A)_i = (q/A)_i \left[T_w, T_s, R_v, h_{fg}, \sigma, k_L, r, p_g, n \right] \quad (84)$$

Rearranging Eq. 77 in terms of the dimensionless variables of Eqs. 80 and 81 and solving for q/A^* gives

$$q/A^* = \frac{1}{r^*} \left[T_w^* - \frac{T_s^*}{1 - \frac{T_s^*}{n} \ln(1 + 2/r^*)} \right] \quad (85)$$

From Eq. 83 and 85, r^* may be eliminated, yielding the relation

$$\frac{1}{T_s^*} = \frac{1}{n} \ln \left[1 + \frac{2 - 4(q/A^*)}{\gamma} \right] + \frac{1 - 2(q/A^*)}{T_w^* [1 - 2(q/A^*) - \gamma(q/A^*)]} \quad (86)$$

where

$$\gamma \equiv \sqrt{1 + 4 T_w^* + \frac{2(T_w^*)^2}{q/A^*} - (2 T_w^* + 1)}$$

Eq. 86 with T_w^* as a parameter is plotted in Fig. 19 by making, as a first approximation, $n = 1$. This is accomplished by selecting some value for q/A^* and T_w^* . From Eq. 86 a corresponding value of T_s^* is calculated and consequently the abscissa $(T_w^* - T_s^*)$ can be formed. In this way, $(q/A)^*$ can be plotted vs. $(T_w^* - T_s^*)$ with T_w^* as a parameter.

Eq. 83 is also shown in Fig. 19 by drawing lines of constant r^* . It should be noted that knowing any two of the inception quantities T_w^* , $T_w^* - T_s^*$, or q/A^* will allow one to approximate the effective radius of the mouth of a nucleation site.

The importance of this figure lies in being able to observe that the lines of constant T_w^* are essentially parallel. This suggests that either one or both of the coordinates could be defined by including some suitable function of T_w^* such that the lines of constant T_w^* would

all collapse upon a specific line ($T_w^* = .1$ for example). This is done most simply by defining a dimensionless superheat as follows:

$$\Delta T_s^* = \frac{T_w^* - T_s^*}{T_w^*} = \frac{T_w - T_s}{T_w} \quad (87)$$

The result of this collapse is given in Fig. 20 as the solid line labeled $n = 1$.

An alternate approach to collapsing the nearly parallel lines of constant T_w^* is to redefine the ordinate and abscissa of Fig. 19 as $\frac{q/A^*}{(T_w^*)^2}$ and $\frac{T_w^* - T_s^*}{(T_w^*)^2}$ respectively. This definition of coordinates is slightly more complicated and does not result in the lines of constant T_w^* falling as nearly coincident upon each other as that previously described. It does have the advantage in that the collapse takes place along lines of constant r^* , and therefore, the lines of constant r^* are compressed into points. This coordinate system is shown, for $n = 1$, as the solid line of Fig. 24. The former approach and coordinate system has been arbitrarily selected as the basis for comparing theory with data.

To include the effect of gas, one can visualize a pure vapor bubble ($p_g = 0$) in its stable state just prior to inception. By injecting into this bubble a mass of gas whose partial pressure is p_g we can simultaneously reduce the partial pressure of the vapor by the amount p_g (and still maintain the pressure balance required for this stable state). However, the entire liquid temperature profile must be lowered by the amount necessary to maintain thermal equilibrium. From Eq. 14 this would imply that

$$(T_w)_{\text{with gas}} \approx (T_w)_{\text{without gas}} - \frac{(T_w)_{\text{without gas}} (v_v - v_L) p_g}{h_{fg}} \quad (88)$$

The error resulting from this reasoning will in all probability be less than the error resulting from the measurement of p_g .

The problem as stated in Eq. 84 has been reduced from nine variables and the parameter n down to two dimensionless variables and the parameter n . An attempt will now be made to evaluate the parameter n . This will be possible if the assumptions leading to Fig. 19 are valid. The fluid pressures will be evaluated at the wall temperature.

D. Experimental Results of Other Investigators

For the remainder of this work, inception will be defined as the state existing when significant heat removal due to boiling begins. That is, it will be the state in which the total heat flux exceeds that which would be expected in nonboiling flow or forced convection.

The data of McAdams, et al.,³⁰ as contained in the thesis of Kennel,⁵¹ was examined from the standpoint of boiling inception. This data was felt to be especially good from the standpoint of having a low gas content as discussed in Chapter V. In addition, dissolved gas content measurements were taken for almost all of their data runs. As a first step in the analysis of their data, the boiling curves (q/A vs. ΔT_g) were plotted for all of their data, consisting of over fifty runs. The inception point was then selected based upon the first significant increase in heat flux due to boiling. These points were reduced (see Fig. 20) to the dimensionless coordinates given by Eqs. 80a and 87. The details of this procedure are described in Appendix C. It should first be noted that based upon these results

a value of $n = 3$ would seem appropriate. Secondly, the scatter of the data, which is appreciable, was examined and found to be unaffected by the pressure level. On the other hand, the higher velocities lie closer to the $n = 1$ line.

Additional data, which is available in the literature for water, is shown in Fig. 21. In Fig. 22 is shown the data available for flow boiling of other fluids. It should be pointed out that the lack of precision (as compared with water) in determining the properties σ and k_L for the fluids of Fig. 22 reduce the accuracy of q/A^* .

The existence of the data of Figs. 20, 21, and 22, which apparently were very carefully taken, raised the question as to why such high inception superheats were achieved relative to a growth criterion of $n = 1$. Madejski⁷⁵ has proposed that the occurrence of inceptions at higher wall superheats than the models of previous investigators would predict is attributable to a flattened bubble. He states that this flattening of the bubble results from the large temperature gradient across the bubble as it grows into colder liquid. A key assumption that he makes is that the temperature gradient resulting from only solid body conduction in the liquid is the temperature gradient (perpendicular to the wall) at the liquid-vapor interface of the bubble. In light of the comments made concerning thermocapillarity (Chapter III), it should be apparent that bubbles cannot support temperature gradients which even remotely approach those assumed by Madejski.

Early in this present work it was known that if the surface lacked sufficiently large cavities, inception would be delayed. This delay

can be visualized as shown in Fig. 23. It seemed possible that if the largest cavities present are of size r_{\max} , then that portion of Eq. 72 pertaining to radii of curvatures in excess of r_{\max} would have no meaning. That is, a tangency which took place (see temperature profile A) at r_1 would be able to activate cavities whose mouth radii were r_1 , if they existed. Since only cavities smaller than r_1 exist, nucleation would not take place. Temperature profile B, having a higher superheat than that of A, would be able to activate cavities of size r_{\max} . This possibility is mathematically described as follows:

$$T_L = T_v \text{ at } r = r_{\max} = y \quad (89)$$

From Eqs. 77 and 85 the dimensionless heat flux at inception becomes

$$\frac{q^*}{A} = \frac{1}{r_{\max}^*} \left[T_w^* - \frac{T_s^*}{1 - \frac{T_s^*}{n} \ln \left(1 + \frac{2}{r_{\max}^*} \right)} \right] \quad (90)$$

This equation is shown plotted as a dashed line in Fig. 24 for various values of the dimensionless maximum radius. The solid line of Fig. 24 is the predicted inception (for $n = 1$) if sufficient cavities are present. It will be noted that the coordinate system of Fig. 24 has $\frac{q/A^*}{(T_w^*)^2}$ vs. $\frac{T_w^* - T_s^*}{(T_w^*)^2}$ instead of that given in Figs. 20, 21, and 22. This was arrived at as discussed earlier by having the collapse of the lines of constant T_w^* in Fig. 19 take place along lines of constant r^* .

To explain the data of Figs. 20, 21, and 22 (showing inception delayed relative to criterion, $n = 1$) by there being a lack of large

large cavities, requires cavities of about 10^{-6} feet or less. It will be recalled, from the measurements which were made of natural cavities (Chapter II), that a hundred nucleation sites per square inch might reasonably be expected which are greater than 10^{-6} feet.

Despite this evidence that a large cross section of cavity sites are available on commercial surfaces, it was decided to investigate inception at low values of q/A^* to see if delayed nucleation took place because of a lack of large cavities. Fig. 25 shows the results of this present investigation. From this work and that of the other investigators it can be concluded that:

1. No lack of large nucleation sites is observed.
2. Inception is delayed relative to the $n = 1$ criterion.
3. A more accurate criterion for inception, based upon all data considered, appears to be stated, not in terms of n , but in terms of the best fit line. Admittedly, the scatter about this line is wide and indicates the presence of other important variables. This best fit line is expressed as

$$q/A^* = .13 (\Delta T_s^*)^3 \quad (91)$$

4. The $n = 1$ line appears to be approached as velocity and (or) subcooling is increased.

E. A Reexamination of the Model's Assumptions

The questions which now present themselves are the following: Why, at inception, must the liquid temperature, evaluated at one bubble radius from the hot wall, appear to be significantly higher than the equilibrium temperature for the same size bubble in an isothermal system? Why is there such a wide scatter in the inception data?

It seems obvious that the answer to these questions is either one or both of the following:

1. the data are very inaccurate
2. the basic assumptions of the model are incorrect.

The first possibility seems quite unlikely in light of the large number of different data sources. One further suspects the presence of important variables not previously considered. For this reason, an examination will be made of the fundamental assumptions.

To assist the answering the above questions reference will be made to Fig. 26 and to the assumptions implied by Eqs. 75 and 76. It will be assumed in Fig. 26 that the temperature felt by the bubble corresponds to that of the liquid at the top of the bubble. This assumption is not germane to the reasoning which follows, but merely simplifies the graphical explanation. The bubble shown in Fig. 26a is in a hemispherical shape which guarantees that its radius of curvature will increase regardless of whether its volume increases or decreases. If the liquid temperature profile is $(T_L)_A$, this bubble must collapse. Consider now this bubble with negligible inertia in a liquid whose temperature profile is $(T_L)_B$. If the bubble height is either greater than or less than \hat{y} , its volume must decrease, since the vapor temperature required for equilibrium is greater than the liquid temperature. This decrease in the bubble's size would both bring the bubble into a region of warmer liquid and increase its radius of curvature. This is shown for the case where $\hat{y} > \hat{y}$ by the successive states 1, 2, and 3, with state 3 being an equilibrium state since $T_L(y) = T_v(r)$. Likewise for $\hat{y} < \hat{y}$, the successive states might be 4, 5, and 6, with state 6 also being an equilibrium state. One

can then conclude that many equilibrium states exist for the case where the temperature profile is tangent to Eq. 72. By similar reasoning, equilibrium states exist when the temperature profile intersects Eq. 72. However, the argument must then take into consideration the consequence of the bubble's inertia.

It should now be observed (Fig. 26b) that Eq. 72 simply expresses the vapor temperature required for equilibrium in a bubble of a given size. If that vapor temperature is suddenly exceeded, the bubble will become unstable and accelerate. The region within which this condition will hold is cross-hatched and is designated as the acceleration region. The converse holds for the deceleration region.

All of the bubbles shown in Fig. 26b will increase their radius of curvature by growing and decrease it by shrinking. In order to have grown beyond the state as shown by the bubble in Fig. 26a, the temperature profile must have intersected Eq. 72, that is, $y_1 < y$. If either of these bubbles have a height, $y_1 < y < y_2$, then the bubble will accelerate and conversely if $y < y_2$, the bubble will decelerate. Whether or not either of these bubbles achieves sufficient acceleration to enable them to detach from the surface (and therefore remove heat), depends in part on the amount by which the liquid temperature profile penetrates into Eq. 72. If insufficient penetration takes place, the bubble will oscillate in the neighborhood of $y = y_2$.

These oscillations do in fact occur. They can easily be seen in a pan of water which is beginning to boil on a stove. The accelerated growth of the bubble carries it into cold liquid causing it to condense and fall back into hot liquid where evaporation begins to take place.

The cycle then continues to repeat itself. Heat transfer measurements, taken in the laboratory during the time when this phenomena occurs, have shown that negligible heat is removed via this mechanism. (See Fig. 33.)

The mere fact that these bubbles can be easily seen (either in the laboratory or on the stove) is a good indication that the radius of curvature of the bubble at the time of departure is much greater than the cavity mouth radius from which it grew. In fact, it could easily be two orders of magnitude greater than the cavity mouth radius. In regard to Fig. 26, this would imply both that $\frac{y_2}{y}$ could be as much as two orders of magnitude and that the penetrations of Eq. 72 by $(T_L)_C$ is even greater than shown in Fig. 26b.

The tangency assumption of the inception model (Eqs. 75 and 76) now appears to have no basis. In fact, one would expect that inception would occur after some penetration of Eq. 72 has taken place. This would be seen experimentally as higher wall superheats at inception.

The next assumption to be examined concerns the liquid temperature profile as given in Eq. 64. It has been pointed out in Chapter III that thermocapillarity effects act to transfer heat from the solid surface into the cold liquid stream. However, Eq. 64 clearly assumes solid body conduction only. The presence of convection away from the wall would make the temperature profile near the wall steeper. Therefore, the amount of wall superheat would have to be increased if this convection were present, in order to bring the liquid temperature profile into the proper position relative to Eq. 72. The assumption of a temperature profile of Eq. 64 is not valid in the region of the bubble itself.

This assumption may not be valid at any location along the wall, even far from a bubble. Both visual observations in this work and Schliern photographs of Semeria²⁰ have indicated that jets appear from surfaces just before bubbles appear. Apparently they originate from the nuclei, which as shown in Chapter II, are just below the resolution of the eye. Chapter II also showed that there could be very large numbers of the smaller nuclei. The steepening of the liquid temperature profile caused by nuclei alone may be significant.

F. The Existence of Metastable States at Inception

Some insight can now be gained as to why sharp transitions are often (if not always) observed when boiling commences in a degassed liquid. The state described in Fig. 26b by the rightmost intersection of $T_L(y)$ and $T_V(r)$ is a state of metastable equilibrium. That is, if a sufficient disturbance exists, a bubble will become unstable and depart. Such disturbances might be variations, in time, of the liquid pressure and temperature surrounding the bubble; or it could be a high wall shear stress which would tend to shear the bubbles from the wall. A third possibility involves the chemical nature of the surface as regards the contact angle. If insufficient disturbances are present, then the bubble will grow in a stable manner as the wall temperature is increased. It follows that as the wall temperature is increased in Fig. 27 from A to B to C, that an increasing number of nuclei arrive at the same metastable state.

Consider the first nuclei on a heated surface which has grown through a number of successive metastable states and has just become sufficiently disturbed to cause departure. Assuming that its cavity

is not deactivated by the incoming fluid, it will create a second generation nuclei which will be immediately unstable. The succeeding generations of nuclei will then be accelerated to the point of departure as a bubble. They, in turn, will cause disturbances in their vicinity which may cause more bubble departures. It is not surprising, therefore, to see a sharp increase in the heat flux following inception. On the other hand, if there were large disturbances when the nuclei first reached a metastable condition, one might expect to see a more gradual transition (a knee) from the forced-convection region to the fully developed region.

Two interesting possibilities are immediately suggested by the previous paragraphs. The first concerns the observation of Rohsenow and Clark⁷⁶ that changing both the velocity and subcooling in flow surface boiling does not alter the position of the nucleate boiling curve. These variations only effect the position of the forced convection curve. The lack of a large transition region between forced convection and nucleate boiling for degassed systems implies that the inception locus is quite near the fully developed boiling curve. In other words, Eq. 91 could be a first approximation to the fully developed boiling curve.

Another consequence of the existence of metastable states relates to a surprising observation of the present experimental work that was made at the higher velocities and subcoolings for all surface finishes. Bubbles were first observed toward the downstream end of the heated surface. Instead of these bubbles being randomly scattered, on the surface they formed a sharp "vee" shape. The angle formed by this "vee" was about 30° and its apex pointed in the upstream direction.

As the flux was increased in very small increments, the "vee" would jump upstream in small increments and gradually cover the entire heated surface. This jumping would take place faster than the eye could follow. It appears, in light of the metastable nature of nuclei, that the sudden departure of one bubble upstream of an inactive heated area would cause disturbances in a wedge shaped region downstream. This may well explain the boiling "vee."

It may also explain several other frequently reported observations concerning pool boiling. Patch boiling, or the tendency of bubbles to become active in clusters, could also be a consequence of the metastable states. Likewise, the hysteresis, as described by Corty⁷⁷, seems to have all of the same characteristics. One example of the many reports in the literature describing decreases in wall superheat with increases in boiling heat flux is that by Tang and Rotem⁷⁸. From their description of their experimental procedure, it seems that dissolved gas and surface contamination cannot explain this behavior. Again, one now suspects that the sudden presence of new active nucleation sites resulting from an increase in heat flux will, by their disturbances, activate even more metastable nuclei and, therefore, lower the wall temperature.

G. Conclusions

1. Previous models of boiling inception (eleven were considered in Section A) have all been based on the same fundamental assumptions. They differ slightly in the criterion determining the distance into the liquid where $T_L = T_v$.

2. Using these assumptions and allowing the distance criterion to be arbitrary, a prediction of inception can be made without resorting to simplifying, but erroneous, mathematical operations.
3. Inception data taken by numerous investigators for several fluids indicates that either the data are quite bad and/or the fundamental assumptions are wrong.
4. The assumption that only solid body conduction takes place in the liquid next to the wall is seen to be incorrect in light of thermocapillarity induced heat transfer. The assumption of Fig. 18 that the point of tangency describes the nuclei equilibrium state just prior to inception is incorrect.
5. Many states of equilibrium exist as described by the intersection occurring at y_2 in Fig. 26b. These states are metastable.
6. The observations of (1) the boiling "vee," (2) patch boiling, (3) hysteresis as described by Corty, and (4) decreasing wall temperatures with increasing heat flux may be explained by metastable nuclei.

Chapter VII - The Effect of the Surface on Boiling

A. Introduction

It will be recalled from Chapter II that the cavity size distribution is strongly dependent on scratch orientation and roughness. The effect of roughness has been well established by Jakob⁵⁰ and Berenson² for the special case of pool boiling. It seems reasonable to now ask the question, what is the effect of both roughness and scratch orientation in both pool boiling and flow boiling.

B. Pool Boiling

1. Apparatus

One of the primary requirements to enable one to compare surface effects in pool boiling and flow boiling is to use the identical boiling surface in each situation. Therefore, a 2' x 1' x 1/2" plexiglass tank was constructed which supported the same electrical conductors that were used in the flow boiling work (see Fig. 14). The same power source, buss connections, and thermocouple bundle were used as described in Chapter V. The main variables which were not able to be matched to the flow boiling situation were pressure and gas concentration, since the tank was open to the atmosphere. Prior to taking data with a new surface, vigorous boiling was maintained for about two hours.

2. Results

Fig. 28 shows the results of the pool boiling tests with the four different surface finishes. The direction of liquid advance was determined shortly after "first vapor" was observed. The bubbles would form at low heat fluxes (about 10^4 BTU/hr ft²) and would slowly grow until buoyant forces would drag the bubble circumferentially around the horizontal tube until it arrived at top. A further increase in heat flux would cause more bubbles to slide circumferentially around the tube. At the same time, the bubbles on the top of the tube would depart. Therefore, more nuclei were formed on the tubes with axial scratches than with circumferential scratches since the advance of the liquid-gas interface would be perpendicular to the scratches (see Fig. 5). As the heat flux was increased further, the wall temperature became superheated and some bubbles could be seen not to slide away from their regions of growth, but rather eject themselves from the tube. At these heat fluxes (generally below 4×10^4 BTU/hr ft²), the surfaces with axial scratches required lower wall temperatures than those with circumferential scratches. This substantiates the previously found evidence (Chapter II) that there are more and larger cavities on surfaces where the liquid-gas interface advanced perpendicular to scratches.

Fig. 28 further shows that at higher heat fluxes the effect of scratch orientation was washed-out. The results at these higher heat fluxes are consistent, both quantitatively and qualitatively, with the results of Berenson.² In other words, the rough surfaces required less superheat than the smooth surfaces at a given heat flux.

As the heat flux increased to about 8×10^4 BTU/hr ft², all bubbles were ejected from the tube's surface. Those bubbles growing from the bottom of the tube would be propelled several inches downward before drag and buoyant forces would reverse their direction. The initial phase of this growth was obviously taking place within the accelerating region of Fig. 26b. It is felt that this sudden departure of the bubble from the surface allowed the liquid-gas interface to advance back over the cavity in either a random or radial direction. Since this advance was no longer controlled, as before, the effect of scratch orientation disappeared. The boiling curve of any of the four surfaces could be repeated and there was no hysteresis effect.

C. Flow Boiling

1. General Results

The apparatus and experimental procedure used in the flow boiling work have been described in Chapter V. The results of this testing, using the four main surfaces at the same flow conditions are shown in Figs. 29, 30, and 31. The very surprising, but simple, conclusion, based upon these figures, is that there is no detectable surface effect under these flow conditions. This is in direct contrast to the strong surface effect in pool boiling.

To attempt to gain an understanding of this result, one must first compare the temperature gradients at the wall for both pool and flow boiling. Marcus and Dropkin⁷⁹ have measured the temperature of the superheated liquid layer in pool boiling as near to the wall as .001 inches. Characteristic of these measurements is the fact

that the mean temperature gradient evaluated at the wall is very nearly that which would be predicted by natural convection heat transfer. No additional mechanism of heat transfer is evident.

In flow boiling, however, there is an additional mechanism (thermocapillarity) which acts to steepen the temperature gradient. One would therefore expect, for the same heat flux, pressure, bulk temperature and fluid, that flow boiling would produce steeper temperature gradients than would pool boiling. The significance of this can now be examined from the viewpoint of a nucleus attempting to grow on a heated surface.

Fig. 32 depicts the number of nucleation sites which would be activated on both a rough and a smooth surface in pool boiling (Fig. 32a) and flow boiling (Fig. 32b). To simplify the reasoning involved, it will be assumed (as stated in reference 64) that a cavity of size r will only be activated in $T_L(y) > T_V(r)$. In other words, the intersection of the temperature profile line with the line of Eq. 72 (on the top of each figure) will determine the size of the cavities activated. The number of cavities which are activated are represented by the shaded areas in the bottom half of Fig. 32. As a basis for comparing the pool boiling and flow boiling situation, the following question will be asked:

What increase in wall superheat is required to activate the same number of nuclei on a smooth surface as would be activated on a rough surface?

For pool boiling, the answer to this question can be found by first constructing Eq. 72 as shown in the top part of Fig. 32a.

Then, qualitatively, a rough and smooth nuclei size distribution, as determined in Chapter II, is constructed on the bottom set of coordinates of Fig. 32a. If the liquid temperature profile were $(T_L)_r$ when pool boiling was taking place on a rough surface, then the number of active nucleation sites would be as indicated in the triangular shaded area on the right of the bottom set of coordinates. To activate the same number of nucleation sites on a smooth surface (shown by the triangular area on the left) the temperature profile, $(T_L)_s$, must intersect Eq. 72 as shown. This produces a substantial increase in the liquid temperature at the wall.

For flow boiling (Fig. 32b) the same construction can be made. The major distinction between the temperature profiles in the flow and pool situations is in their slope, as discussed above. Comparing the quantity $[(T_w)_s - (T_w)_r]$ for the flow case with that for pool boiling, one sees that the surface plays a minor role in flow boiling.

2. Hysteresis

An unusual phenomenon was observed in these experiments which constitutes an exception to the general conclusion that surface effects are small in flow boiling. It was observed, under certain conditions, that by slightly increasing the heat flux shortly after vapor was visually observed, there would be a sharp drop in wall temperature. Following this slight increase in heat flux, the temperature drop could also be observed in the wall temperature measurements down the length of the heated surface. That is, as one proceeded along the surface in the downstream direction, the temperature would suddenly drop by as much as 7.5°F in less than $5/7$ of an inch. The length temperature

upstream of this transition was flat, as characterized by fully developed flow boiling (see Chapter V, section B). When this phenomenon was viewed as shown in Fig. 33, one could see that the transition took place from forced-convection heat transfer to fully developed nucleate boiling. The same results could be repeated on succeeding days under the same test conditions. This phenomenon can be described as a hysteresis since decreasing the heat flux produced no sudden increase in wall temperatures.

The main clue to the understanding of this type of hysteresis is the fact that of the six tests in which it was observed, five of them were using the axial rough surface finish. It will be recalled (Chapters II and V) that with this finish and the controlled direction of liquid advance when liquid first came in contact with the surface, a minimum number of nuclei would be created. Visual observations of the test surface before this sudden temperature drop occurred, showed the presence of vapor bubbles fixed to the surface, but oscillating in a manner described in Fig. 26 and Chapter VI. Following this sudden temperature drop, most of the bubbles were seen to be departing from the surface and flowing adjacent to the wall. This hysteresis and these observations were most noticeable at extremely low subcoolings (11°F) and velocities (.4 ft/sec). The definite existence of turbulent flow heat transfer prior to the transition rules out the possibility that this effect is caused by the tripping of the laminar flow boundary layer as described by Bergles and Rohsenow.⁶⁴

The cause for this type of hysteresis is felt to be related to the disturbance which causes the oscillating bubbles to depart from the boiling surface. Following departure of the metastable nuclei

there would be a continuous stream of unstable bubbles growing and departing from these same sites. Furthermore, the inrush of liquid following departure of a bubble from an AR surface would produce many more sites since the liquid direction is no longer controlled. The net result would be a lowering of the wall temperature.

D. Conclusions

1. In pool boiling, at low heat fluxes, the surface characteristic which has the most influence on the heat transfer is scratch orientation. At moderate to high heat fluxes roughness has the most influence.
2. In the flow boiling experiments of this present work, there was no detectable influence of the surface on boiling (with the exception of hysteresis). This is felt to be a consequence of the steepness of the liquid temperature profile in flow boiling and the steep negative slope of the cavity size distribution curve.
3. A hysteresis type phenomenon exists in flow boiling. It is most noticeable on surfaces with axial scratches and a rough finish, at low velocities and subcoolings. It is felt to be a consequence of the large metastable nuclei and the artificially small cavity size distributions of AR surfaces.

REFERENCES

1. Rohsenow, W. M., "A Method of Correlating Heat Transfer Data for Surface Boiling of Liquids," ASME Trans., No. 48, July, 1952.
2. Berenson, P., "Transition Boiling Heat Transfer From a Horizontal Surface," Sc.D. Thesis, Mech. Eng. Dept., M. I. T., Feb., 1960.
3. Clark, H. B., Strenge, P. S. and Westwater, J. W., "Active Sites for Nucleate Boiling," Chemical Engineering Progress Symposium Series, No. 29, Vol. 55, pp. 103-110.
4. Gaertner, R. F., "Photographic Study of Nucleate Pool Boiling on a Horizontal Surface," J. Heat Transfer, February, 1965.
5. Griffith, P. and Wallis, J. D., "The Role of Surface Conditions in Nucleate Boiling," Chemical Engineering Progress Symposium Series, No. 30, Vol. 56, pp. 49-63.
6. Corty, C. and Foust, A. S., "Surface Variables in Nucleate Boiling," Chemical Engineering Progress Symposium Series, No. 17, Vol. 51, pp. 1-12.
7. Gaertner, R. F. and Westwater, J. W., "Propulsion of Active Sites in Nucleate Boiling Heat Transfer," Chemical Engineering Progress Symposium Series, No. 30, Vol. 56, pp. 39-48.
8. Gaertner, R. F., "Distribution of Active Sites in the Nucleate Boiling of Liquids," Chemical Engineering Progress Symposium Series, No. 41, Vol. 59, pp. 52-61.
9. Kurihara, H. M. and Myers, J. E., "The Effects of Superheat and Surface Roughness on Boiling Coefficients," A.I.Ch.E. J., No. 1, Vol. 6, pp. 83-91.
10. Bankoff, S. G., "Entrapment of Gas in the Spreading of A Liquid Over a Rough Surface," A.I.Ch.E. J., pp. 24-26, March, 1958.
11. Gunther, F. C., "Photographic Study of Surface Boiling Heat Transfer to Water with Forced Convection," ASME Trans., No. 73, pp. 115-123, 1951.
12. Jiji, L. M. and Clark, J. Al, "Bubble Boundary Layer and Temperature Profiles for Forced Convection Boiling in Channel Flow," ASME Paper 62-WA-141, 1962.
13. Kirby, G. J., Staniforth, R. and Kinneir, J. H., "A Visual Study of Forced Convection Boiling, Part I: Results for a Flat Vertical Heater," AEEW-R 281, 1965.

14. Marangoni, C. S. M., Nuovo Cimento, Series 2.516, pp. 239-273, 1872.
15. Scriven, L. E., and Sternling, C. V., J. Fluid Mech., Vol. 19, p. 321, 1964.
16. Sugden, S. J., J. Chem. Soc. (London), 125, pp. 1177-1189, 1924.
17. Young, N. O., Goldstein, J. S., and Block, M. J., "The Motion of Bubbles in a Vertical Temperature Gradient," J. Fluid Mech., Vol. 6, part 3, pp. 350-356, 1959.
18. Trefethen, Lloyd, Surface Tension in Fluid Mechanics, film produced by Educational Services Inc., Watertown, Mass.
19. Farello, E., C. S. N. Casaccia, C. N. E. N., Rome, Italy, personal communication.
20. Semeria, R., "Analyse Fine de l'ebullition a l'echelle locale," C.R. Acad. Sc. Paris, pp. 471-476.
21. Behar, M., Courtaud, M., Ricque, R. and Semeria, R., "Fundamental Aspects of Subcooled Boiling with and without Dissolved Gasses," Proceedings of Third International Heat Transfer Conf., Vol. IV, pp. 1-11, 1966.
22. Trefethen, Lloyd, "On the Jet Propulsion of Bubbles in a Heated Liquid," Tufts Univ. Mech. Eng. Report No. 61-S-1, August, 1961.
23. McGrew, J. L., Rehm, T. R., and Bamford, F. L., "Marangoni Flow: An Additional Mechanism in Boiling Heat Transfer," Science, Vol. 153,
24. Bergles, A. E., and Morton, H. L., "Survey and Evaluation of Techniques to Augment Convective Heat Transfer," Mech. Eng. Dept., M. I. T. Report No. 5382-34, Feb., 1965.
25. Schrage, R. W., A Theoretical Study of Interphase Mass Transfer, Columbia University Press, New York, 1953.
26. Rohsenow, W. M. and Sukhatme, S. P., "Condensation" in Developments In Heat Transfer, edited by W. M. Rohsenow, The M. I. T. Press, Cambridge, Mass., 1964.
27. Han, C. Y. and Griffith, P., "The Mechanism of Heat Transfer in Nucleate Pool Boiling," Tech. Report 19, M. I. T., 1962.
28. Hsu, Y. and Graham, W., "An Analytical and Experimental Study of the Thermal Boundary Layer and Ebullition Cycle in Nucleate Boiling," NASA TN D-594, May, 1961.

29. Isshiki, N. and Tamaki, H., "Photographic Study of Boiling Heat Transfer Mechanism," Bulletin of the Japan Society of Mech. Eng., Vol. 6, No. 23, pp. 505-513, 1963.
30. McAdams, W. H., et al., "Heat Transfer at High Rates to Water with Surface Boiling," Ind. Eng. Chem., 41, pp. 1945-1955, 1949.
31. Ivey, H. J., and Morris, D. J., "On the Relevance of the Vapor-Liquid Exchange Mechanism for Sub-Cooled Boiling Heat Transfer at High Pressures," AEEW-R 137, January, 1962.
32. Rohsenow, W. M., and Clark, J. A., Trans. Am. Soc. Mech. Eng., 73, pp. 609-620, 1951.
33. Bankoff, S. G. and Mayson, J. P., "Heat Transfer from the Surface of a Steam Bubble in Turbulent Subcooled Liquid Stream," A.I.Ch.E. J., pp. 30-33, March, 1962.
34. Moore, F. D., and Mesler, R. B., "The Measurement of Rapid Surface Temperature Fluctuations During Nucleate Boiling of Water," A.I.Ch.E. J., pp. 620-624, 1961.
35. Hospeti, N. B., and Mesler, R. B., "Deposits Formed Beneath Bubbles During Nucleate Boiling of Radioactive Calcium Sulfate Solutions," A.I.Ch.E. J., p. 662, July, 1965.
36. Cooper, M. G. and Lloyd A. J. P., "Transient Local Heat Flux in Nucleate Boiling," I. Mech. E., pp. 193-203, 1965.
37. Styrikovich, M. A. and Nevstrueva, E. I., "An Approximate Estimation of Circulation and Temperature Characteristics of Two-Phase Pulsation Flows with Surface Boiling," Proceedings of Third International Heat Transfer Conf., Vol. IV, pp. 207-215, 1966.
38. Schneider, P. J., Conduction Heat Transfer, Addison-Wesley Publishing Company, Inc., Reading, Mass., Sept., 1957.
39. Kreith, F. and Summerfield, M., "Investigation of Heat Transfer at High Heat Flux Densities: Experimental Study with Water of Friction Drop with and without Surface Boiling in Tubes," Jet Propulsion Lab., C. I. T., Progress Report No. 4-68, 1948.
40. Dickinson, N. L. and Welch, C. P., "Heat Transfer to Supercritical Water," ASME Trans., Vol. 80, No. 3, April, 1958.
41. Rohsenow, W. M., Somma, E. H., and Osborn, P. V., "Construction and Operation of Apparatus for Study of Heat Transfer with Surface Boiling," M. I. T. Heat Transfer Lab. Technical Report No. 2, D.I.C. 6627, July 1, 1950.

42. Clark, J. A., Discussion in ASME Trans. Vol. 80, pp. 1402-1403, 1958.
43. Stein, R. P. and Gutstein, M. U., "Temperature Distribution in Solids with Electrical Heat-Generation and Temperature Dependent Properties, Chem. Eng. Prog. 56, No. 30, pp. 167-176, 1960.
44. Leppert, C. P., Costello, C. P. and Høglund, B. M., "Boiling Heat Transfer to Water Containing a Volatile Additive," ASME Trans., 80, pp. 1395-1402, 1958.
45. Daleas, R. S., term project for course 2.56, M. I. T., 1964.
46. Van Sant, J. H. and Pitts, J. H., "Variable Property Effects on the Inside Surface Temperature of a Heated Tube," ASME Trans., August, 1966.
47. Harden, D. G. and Bryant, L. T., "Analog Computation of Temperature Distribution in Solids with Electrical Heat-Generation and Temperature-Dependent Properties," ANL, Report No. 6645, November, 1962.
48. Powell, R. W., "Correlation of Metallic Thermal and Electrical Conductivities for Both Solid and Liquid Phases," Int. J. Heat Mass Transfer, Vol. 8, pp. 1033-1045, 1965.
49. Tye, R. P., Dynatech Corporation, Cambridge, Mass., personal communication.
50. Bergles, A. E. and Rohsenow, W. M., "Forced-Convection Surface-Boiling Heat Transfer and Burnout in Tubes of Small Diameter," M. I. T. Heat Transfer Lab Report No. 8767-21, May 25, 1962.
51. Kennel, W. E., "Local Boiling of Water and Superheating of High Pressure Steam in Annuli," Sc.D. Thesis in Chemical Engineering, M. I. T., 1948.
52. Elrod, W. C., Clark, J. A., Lady, E. R., and Merte, H., "Boiling Heat-Transfer Data at Low Heat Flux," ASME Paper 66-WA/HT-19, 1966.
53. Jiji, L. M. and Clark, J. A., "Incipient Boiling in Forced Convection Channel Flow, ASME Paper 62-WA-202, 1962.
54. Marto, P. J. and Rohsenow, W. M., "The Effect of Surface Conditions on Nucleate Pool Boiling Heat Transfer to Sodium," M. I. T. Heat Transfer Lab Report No. 5219-33, January, 1955.

55. Buchberg, H., et al., "Studies in Boiling Heat Transfer," Final Report AEC Research Contract No. AT-11-1-Gen 9, Dept. of Eng., University of Calif., March, 1951.
56. Dorsey, N. E., Properties of Ordinary Water-Substance, Reinhold, 1953.
57. Lopina, R. F., "Swirl Flow Heat Transfer and Pressure Drop," Ph.D. Thesis, Mech. Eng. Dept., M. I. T., (in progress - to be completed in June, 1967).
58. Todreas, N. E. and Rohsenow, W. M., "The Effect of Nonuniform Axial Heat Flux Distribution," Contract NSG-496, Report No. 9843-37, Mech. Eng. Dept., M. I. T., September 20, 1965.
59. Adams, N. K., The Physics and Chemistry of Surfaces, Oxford University Press, 1941.
60. Michiyoshi, I., "Some Discussion on Burnout of Fuel Element Cooled by Natural Circulation," Mech. Reports of the Eng. Res. Instit. Kyoto University, No. 74, Vol. X, Dec., 1960.
61. Lienhard, J. H., "Thermodynamic and Macroscopic Aspects of Boiling," Ph.D. Thesis, Univ. of Calif., July, 1961.
62. Fabric, S., "Vapor Nucleation of Surfaces Subjected to Transient Heating," Report No. NE-64-1 Institute of Engineering Research, University of California, August, 1964.
63. Hsu, Y. Y., "On the Size Range of Active Nucleation Cavities on a Heating Surface," J. of Heat Transfer, p. 207, August, 1962.
64. Bergles, A. E. and Rohsenow, W. M., "The Determination of Forced-Convection Surface-Boiling Heat Transfer," J. of Heat Transfer Paper No. 63-HT-22, April, 1963.
65. Sato, T. and Matsumura, H., "On the Conditions of Incipient Sub-cooled-Boiling with Forced Convection," Bulletin of JSME, Vol. 7, No. 26, pp. 392-398, 1964.
66. Han, C. Y. and Griffith, P., "The Mechanism of Heat Transfer in Nucleate Pool Boiling," Engineering Projects Laboratory Report No. 7673-19, M. I. T., March 30, 1962.
67. Davis, E. J. and Anderson, G. H., "The Incipience of Nucleate Boiling in Forced Convection Flow," Annual Meeting of A.I.Ch.E., Fall, 1965.

68. Faneuff, C. E., McLean, E. A. and Scherrer, V. E., "Some Aspects of Surface Boiling," J. Appl. Phys., Vol. 29, No. 1, pp. 80-84, Jan., 1958.
69. "Proceedings of the 1960 Idaho Conference in Reactor Kinetics," USAEC, IDO-16791, October, 1960.
70. Kenning, D. B. R. and Cooper, M. G., "Flow Patterns Near Nuclei and the Initiation of Boiling During Forced Convection Heat Transfer," Proceedings of the Institution of Mechanical Engineers, Paper 11, Manchester, England, Sept 1, 1965.
71. Howell, J. R., and Siegel, R., "Incipience Growth, and Detachment of Boiling Bubbles in Saturated Water from Artificial Sites of Known Geometry and Size," Proceedings of Third International Heat Transfer Conf., pp. 12-23, August, 1966.
72. Keenan, J. H. and Keyes, F. G., Thermodynamic Properties of Steam, John Wiley and Sons, 1936.
73. Shai, I., "The Mechanism of Nucleate Pool Boiling Heat Transfer to Sodium and the Criterion for Stable Boiling," Ph.D. Thesis, Mech. Eng. Dept., M. I. T., 1967.
74. Bonilla, C. F., Sawhney, D. L. and Makanski, M. M., "Vapor Pressure of Alkali Metals, III Rubidium, Cesium, and Sodium-Potassium Alloy up to 100 Pounds per Square Inch," Proceedings of 1962 High-Temperature Liquid-Metal Heat Transfer Technology Meeting, ENL 756, 1962.
75. Madejski, J., "Activation of Nucleation Cavities on a Heating Surface With Temperature Gradients in Superheated Liquid," Int. J. Heat Mass Transfer, Vol. 9, pp. 295-300, 1966.
76. Rohsenow, W. M. and Clark, J. A., "Heat Transfer and Pressure Drop Data for High Heat Flux Densities to Water at High Sub-Critical Pressures," Heat Transfer Fluid Mech. Inst., Stanford, Calif., 1951.
77. Corty, C., Ph.D. Thesis, Chem Eng. Dept., Univ. Mich., Ann Arbor, 1951.
78. Tang, S. and Rotem, Z., "A Secondary Boiling Instability?" The Canadian J. of Chem. Eng., pp. 355-356, Dec., 1965.
79. Marcus, B. D. and Dropkin, D., "Measured Temperature Profiles Within the Superheated Boundary Layer Above a Horizontal Surface in Saturated Nucleate Pool Boiling of Water," ASME Paper 64-WA/HT-4, 1965.
80. Rohsenow, W. M. and Choi, H. Y., Heat, Mass and Momentum Transfer. Prentice-Hall, Inc., 1963.

81. Jeglic, F. A., Stone, J. A., and Gray, V., "Experimental Study of Subcooled Nucleate Boiling of Water Flowing in 1/4 Inch-Diameter Tubes at Low Pressures," NASA Technical Note, NASA TN D-2626, Jan. 1965.
82. Rohsenow, W. M. and Clark, J. A., "Heat Transfer and Pressure Drop Data for High Heat Flux Densities to Water at High Subcritical Pressure," 1951 Heat Transfer and Fluid Mechanics Institute Preprints, Stanford University Press, 1951.
83. Gouse, S. W., and Coumou, K. G., "Heat Transfer and Fluid Inside a Horizontal Tube Evaporator, Phase I", Engineering Projects Laboratory Report No. 9649-1, M.I.T., June, 1964.
84. Noel, M. B., "Experimental Investigation of the Forced-Convection and Nucleate-Boiling Heat-Transfer Characteristics of Liquid Ammonia," Technical Report No. 32-125, JPL, July 19, 1961.

Appendix A

Application of the Rapid-Convergence Technique to the
Solution of the Gravity Pendulum

The problem to be solved is

$$\frac{d^2\theta}{dt^2} + \frac{g}{l} \sin \theta = 0 \tag{1A}$$

$$\text{at } t = 0 \quad \theta = \theta_0 \quad \text{and} \quad \frac{d\theta}{dt} = 0$$

It will be convenient to define

$$\omega^2 = g/l \tag{2A}$$

A solution will be sought in the form

$$\theta = a_0 + a_1 L + a_2 L^2 + a_3 L^3 + \dots \tag{3A}$$

where L is some solution to the linearized problem. For this case there are two possibilities.

$$L = \sin \omega t \quad \text{or} \quad L = \cos \omega t$$

The selection of the most desirable expression for L will be decided later.

$$\frac{d\theta}{dt} = \frac{d\theta}{dL} \frac{dL}{dt} \tag{4A}$$

$$\frac{d^2\theta}{dt^2} = \frac{d\theta}{dL} \frac{d^2L}{dt^2} + \frac{d^2\theta}{dL^2} \left(\frac{dL}{dt}\right)^2 \quad (5A)$$

$$= [a_1 + 2a_2 L + 3a_3 L^2 + \dots + na_n L^{n-1}] [-\omega^2 L]$$

$$+ [2a_2 + 6a_3 L + \dots + n(n-1) a_n L^{n-2}] [\omega^2 (1 - L^2)]$$

$$\sin \theta = \theta - \frac{\theta^3}{3!} + \frac{\theta^5}{5!} - \dots$$

$$= [a_0 + a_1 L + a_2 L^2 + \dots] - 1/3! [a_0^3 + 3a_0^2 a_1 L +$$

$$3(a_0 a_1^2 + a_0^2 a_2) L^2 + \dots] - \dots$$

Adding Eqs. 5A and 6A dividing by ω^2 , equating the coefficients of like powers of L to zero, and letting a_0 and a_1 be arbitrary, gives

$$a_2 = -1/2 \sin a_0$$

$$a_3 = \frac{a_1}{6} (1 - \cos a_0)$$

$$a_4 = -\frac{\sin a_0 (4 - \cos a_0)}{24}$$

$$\cdot$$

$$\cdot$$

$$\cdot$$

$$a_{n+2} \approx \frac{(n-1)}{(n+2)} a_n$$

Using a ratio test to examine convergence shows that

$$\frac{\text{term } (n+2)}{\text{term } n} \approx \frac{(n-1)}{(n+2)} L^2$$

and therefore, L must be restricted to values less than one. It is convenient therefore to let

$$L = \sin \omega t \quad \text{if } -(\pi/4\omega) \leq t \leq (\pi/4\omega), \text{ etc.}$$

$$L = \cos \omega t \quad \text{if } -(\pi/4\omega) \leq t \leq (\frac{3\pi}{4\omega}), \text{ etc.}$$

If it is required to find the trajectory of the pendulum across the boundaries

$$\pi/4 \omega, 3\pi/4 \omega, 5\pi/4 \omega, \text{ etc.}$$

then a new set of initial conditions must be found and the solution continued for the new variable L.

Example 1

As an example, consider the case where $\theta = \pi$ and $\frac{d\theta}{dt} = 0$ at $t = 0$.

The appropriate value for L is

$$L = \sin \omega t$$

and from Eqs. 3A and 7A we find

$$a_0 = \pi \quad a_1 = 0 \quad a_2 = a_3 = a_4 = \dots = 0$$

The required solution is simply $\theta = \pi$, which from physical reasoning we knew already.

Example 2

Assume that $\theta = \frac{\pi}{2}$ and $\frac{d\theta}{dt} = 0$ at $t = 0$, and let us compare the rapid convergence solution with both the linear solution and the elliptical integral solution.

for $t \leq \pi/4 \omega$

$$\theta = \pi/2 - 1/2 \sin^2 \omega t - 1/6 \sin^4 \omega t - \dots \quad (8A)$$

for $t = \pi/4 \omega$

$$\theta = \pi/2 - 1/4 - 1/24 - \dots = 1.26355 \quad (9A)$$

$$\omega \times \frac{d\theta}{dt} = 1/2 - 1/6 - 1/16 - \dots = -.77639 \quad (10A)$$

for $\frac{\pi}{4\omega} \leq t \leq (3\pi/4)\omega$

$$\theta = a_0 + a_1 \cos \omega t - 1/2 \sin a_0 \cos^2 \omega t + \dots \quad (11A)$$

again at $t = (\pi/4 \omega)$

$$\theta = a_0 + \frac{a_1}{\sqrt{2}} - 1/4 \sin a_0 + \dots \quad (12A)$$

$$\omega \frac{d\theta}{dt} = \frac{a_1}{\sqrt{2}} - \frac{\sin a_0}{2} + a_1 \frac{(1 - \cos a_0)}{4\sqrt{2}} \quad (13A)$$

The new values for a_0 and a_1 , found by equating Eqs. 9A and 11A, and 10A and 13A respectively, are

$$a_0 = .372$$

$$a_1 = 1.3977$$

Substitution of these "initial condition constants" into Eq. 11A gives

for $(\pi/4\omega) \leq t \leq \frac{3\pi}{4\omega}$

$$\theta = .372 + 1.3977 \cos \omega t - .1819 \cos^2 \omega t + \dots \quad (14A)$$

Eqs. 8A and 14A are shown in Fig. 34 along with the linear solution. It will be recalled that the elliptical integral solution does not give the pendulum's angle as a function of time, but instead gives only the period, i.e., far less information than is contained in Eqs. 3A and 7A.

Appendix B

Thickness of Laminar Sublayer

It still remains to be determined in what flow conditions the linear temperature profile will be valid. If one assumes that such a temperature profile, under boiling conditions, exists within the laminar sublayer, the problem can be stated as follows:

For what flow conditions will the laminar sublayer extend more than two cavity radii away from the heated wall?

From Rohsenow and Choi⁸⁰ it is shown that the thickness of the laminar sublayer is

$$y = \frac{5}{v} \sqrt{\frac{\tau_o}{\rho}} \quad (1B)$$

The wall shear stress can be expressed in terms of the friction factor as

$$\frac{\tau_o}{\rho} \equiv \frac{V^2 f}{2} \quad \text{and} \quad (2B)$$

the friction factor can be approximated for reasonably smooth surfaces as

$$f = \frac{.046}{Re^{.2}} \quad (3B)$$

Substitution of Eqs. 2B and 3B into Eq. 1B yields

$$y = \frac{31.25 D}{Re^{.9}} \quad (4B)$$

Therefore, the laminar sublayer extends more than two cavity radii into the liquid when

$$r^* \leq \frac{15.75 D p_L}{Re^{.9} \sigma} \quad (5B)$$

By examining Fig. 19, Eq. 5B is seen to be valid for the experimental conditions of this investigation as well as the great majority of other flow situations.

Appendix C

Sample Calculations of

Inception for Data of McAdams et al.

The values of $(q/A)_i$ and $(\Delta T_s)_i$ are taken from Fig. 35

| Run | P_L psia | T_{sub} °F | V ft/sec | $(q/A)_i \times 10^{-5}$ BTU/hr ft ² | $(\Delta T_s)_i$ °F | $(T_w)_i$ °R | T_w^* | $\frac{R_v \times 10^{-9}}{h_{fg} p_{L,L} k_L}$ hr ft ² /BTU | $(q/A) \times 10^{-4}$ |
|------|---------------|-----------------|---------------|--|------------------------|-----------------|---------|--|------------------------|
| 11 M | 60 | 50 | 1 | .38 | 16.7 | 764.2 | .0219 | 8.4 | 4.53 |
| 20 M | 60 | 50 | 12 | 3.4 | 34.0 | 787.9 | .0432 | " | 4.76 |
| 5 CP | 60 | 50 | 4 | 3.3 | 33.0 | 790.6 | .0418 | " | 1.82 |
| 6 CP | 100 | 100 | 4 | 2.9 | 29.0 | 798.3 | .0363 | " | 2.62 |

Appendix D
Original
Inception Data

| P_L psia | T_{sub} °F | V ft/sec | Surface Finish | $(q/A) \times 10^{-5}$ BTU/hr ft ² | $(\Delta T)_i$ °F | $(T_w)_i$ °F | (T_w) °R | T_w^* | $\frac{R \times 10^{-9}}{h_{fg} P_{L,k}^k}$ hr ft ² /BTU | $(q/A)^* \times 10^{-4}$ |
|---------------|-----------------|-------------|-------------------|--|----------------------|-----------------|---------------|---------|--|--------------------------|
| 30 | 125 | 1.0 | AS | .90 | 10.5 | 260.5 | 720.2 | .0146 | 3.8 | .237 |
| 30 | 25 | 1.0 | AS | .225 | 8.9 | 258.9 | 718.6 | .0124 | 3.8 | .0591 |
| 90 | 25 | 1.0 | AS | .225 | 6.2 | 326.0 | 785.7 | .0079 | 13.2 | .0170 |
| 60 | 50 | 1.0 | CR | .45 | 12.8 | 305.5 | 765.2 | .0167 | 8.4 | .0536 |
| 60 | 50 | 1.0 | AS | .45 | 12.8 | 305.5 | 765.2 | .0167 | " | .0536 |
| 60 | 50 | 1.0 | CR | .45 | 12.8 | 305.5 | 765.2 | .0167 | " | .0536 |
| 60 | 50 | 1.0 | AR | .43 | 9.0 | 301.7 | 761.4 | .0118 | " | .0511 |
| 60 | 11 | .4 | AR | .080 | 6.0 | 298.7 | 758.4 | .00792 | " | .00953 |
| 60 | 11 | .4 | AR | .080 | 6.0 | 298.7 | 758.4 | .00792 | " | .00953 |
| 60 | 18 | .5 | AR | .156 | 9.0 | 301.7 | 761.4 | .0118 | " | .0186 |
| 60 | 18 | .5 | CS | .156 | 13.0 | 305.7 | 765.4 | .0170 | " | .0186 |
| 60 | 150 | 4.3 | CR | 3.3 | 20.2 | 312.9 | 772.6 | .0262 | " | .393 |

Appendix D

(continued)

| P _L | T _{sub} | V | Surface | (q/A)x10 ⁻⁵ | (ΔT _s) _i | (T _w) _i | (T _w) | T _w * | $\frac{R_v \times 10^{-9}}{h_{fg} p_L k_L}$ | (q/A)* x10 ⁻⁴ |
|----------------|------------------|--------|---------|------------------------|---------------------------------|--------------------------------|-------------------|------------------|---|--------------------------|
| psia | °F | ft/sec | Finish | BTU/hr ft ² | °F | °F | °R | | hr/ft ² BTU | |
| 60 | 150 | 4.3 | CR | 3.3 | 20.2 | 312.9 | 772.6 | .0262 | 8.4 | .393 |
| 60 | 50 | 1.0 | CR | .52 | 20.0 | 312.7 | 772.4 | .0259 | " | .0619 |
| 60 | 20 | .5 | CR | .15 | 15.0 | 307.7 | 767.4 | .0196 | " | .01788 |
| 60 | 150 | 4.3 | AR | 3.3 | 16.0 | 308.7 | 768.4 | .0283 | " | .393 |
| 60 | 180 | 5.5 | AR | 5.0 | 20.0 | 312.7 | 772.4 | .0259 | " | .595 |
| 60 | 150 | 4.3 | CS | 3.3 | 25.0 | 317.7 | 777.4 | .0322 | " | .393 |
| 60 | 150 | 4.3 | CR | 3.5 | 17.5 | 310.2 | 769.9 | .0228 | " | .417 |
| 60 | 150 | 4.3 | AS | 3.65 | 24.5 | 317.2 | 776.9 | .0316 | " | .435 |
| 60 | 150 | 4.3 | CS | 3.65 | 24.5 | 317.2 | 776.9 | .0316 | " | .435 |
| 60 | 18 | .5 | AS | .156 | 13 | 305.7 | 765.4 | .0170 | " | .0186 |

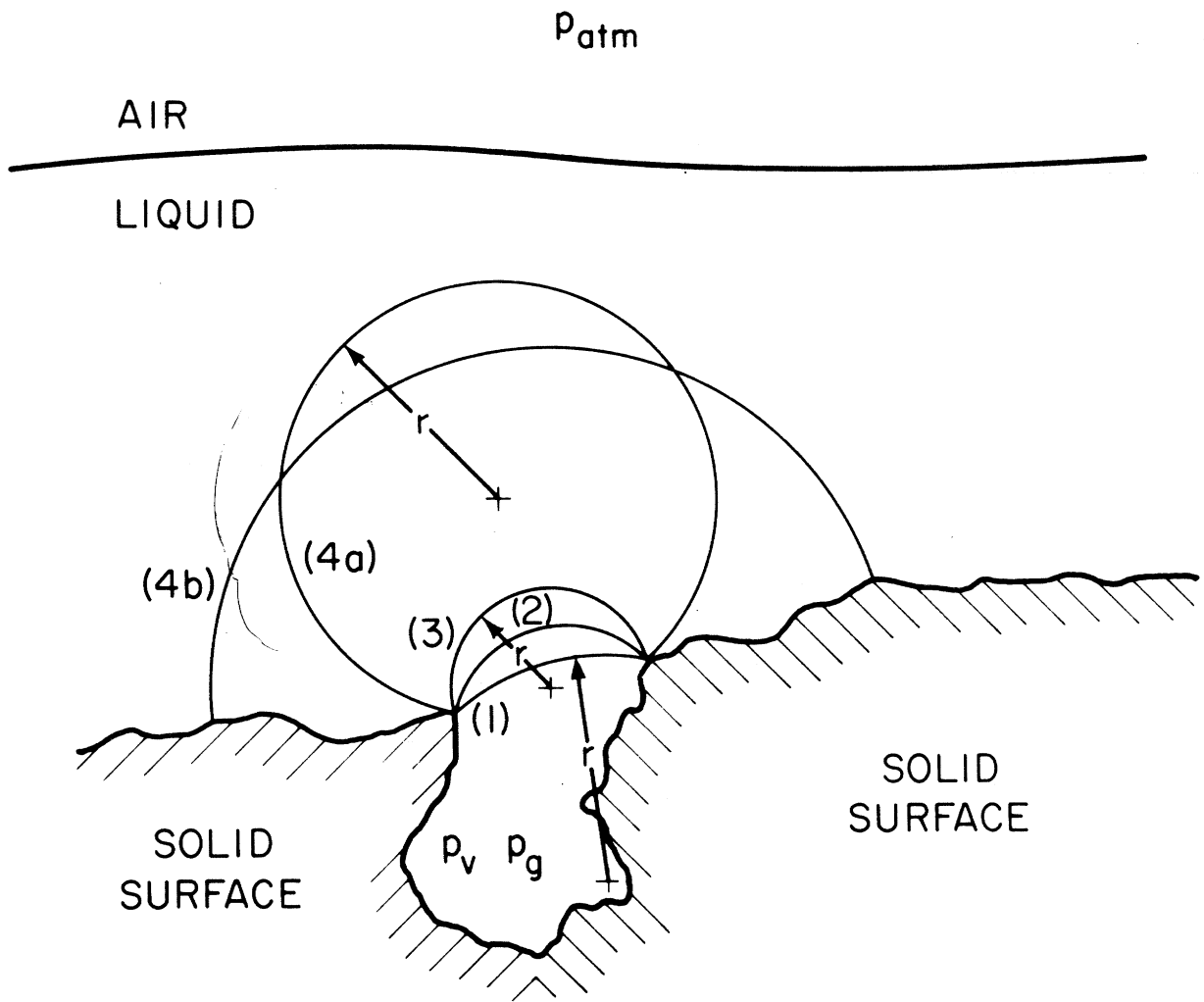


FIG. 1 VARIOUS STATES DURING THE GROWTH OF A BUBBLE

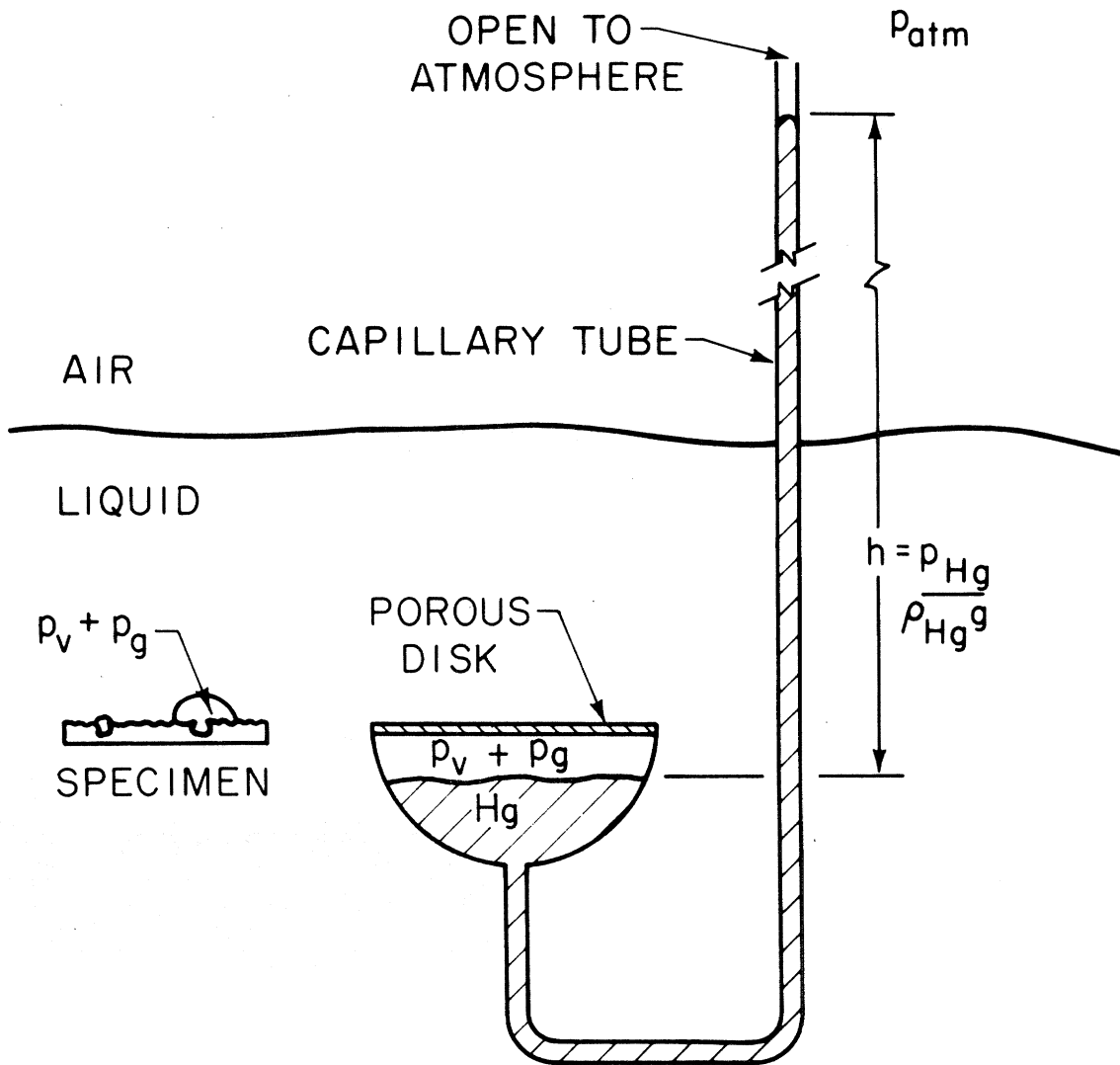


FIG. 2 BUBBLE METER FOR USE IN MEASURING THE CAVITY SIZE DISTRIBUTION

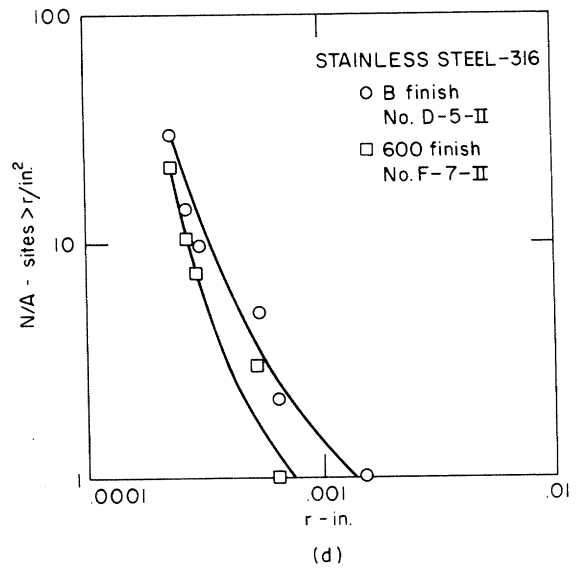
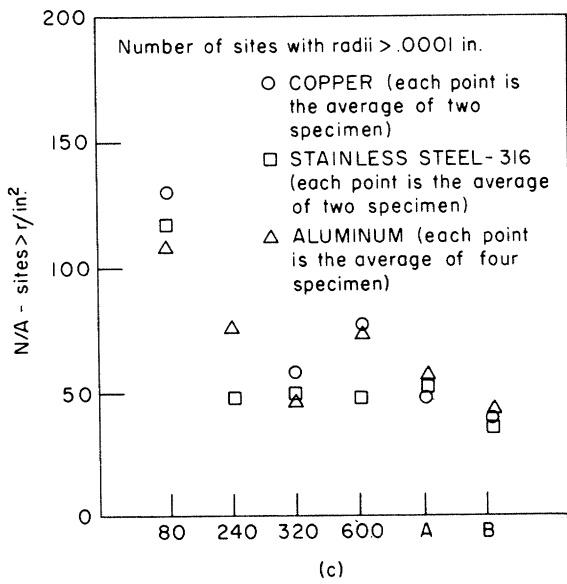
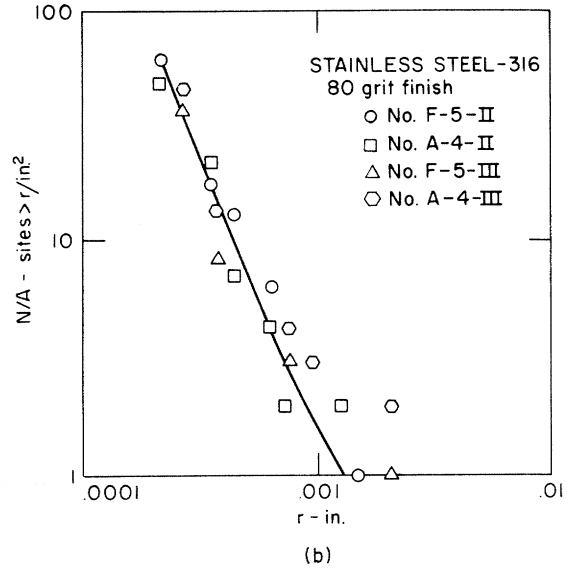
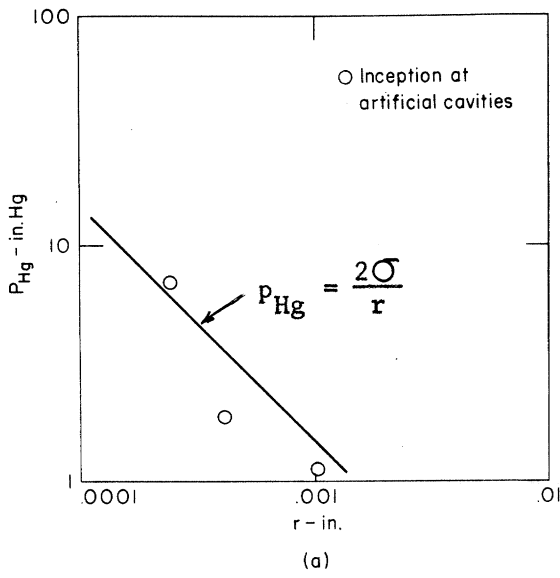


FIG. 3 SOME QUANTITATIVE RESULTS FROM MEASUREMENTS OF CAVITY SIZES

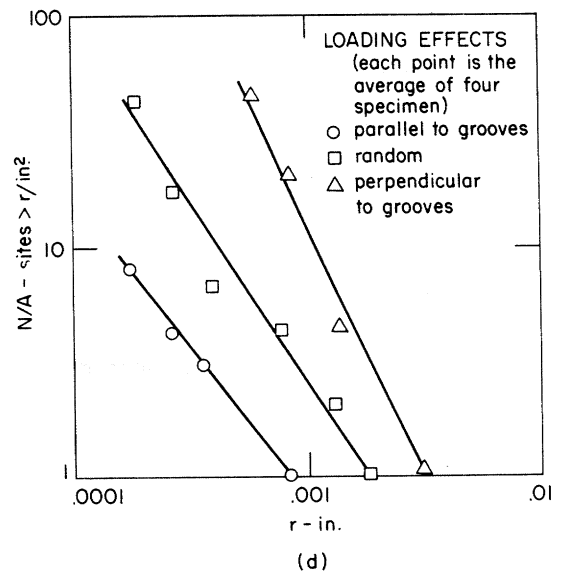
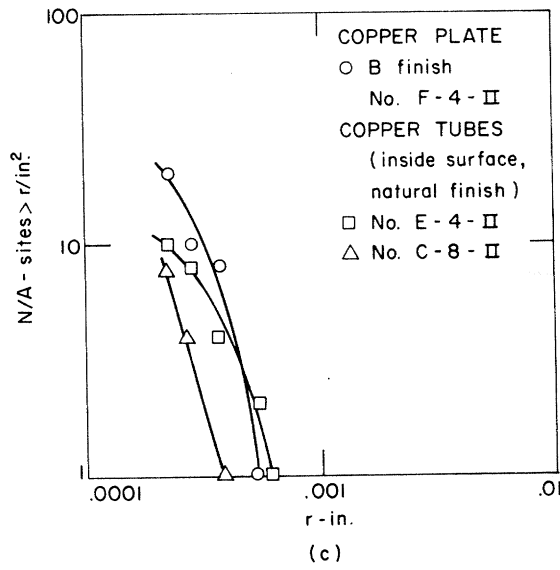
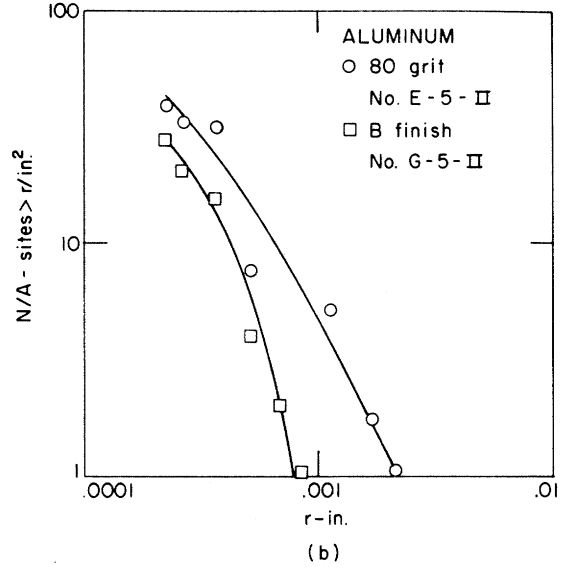
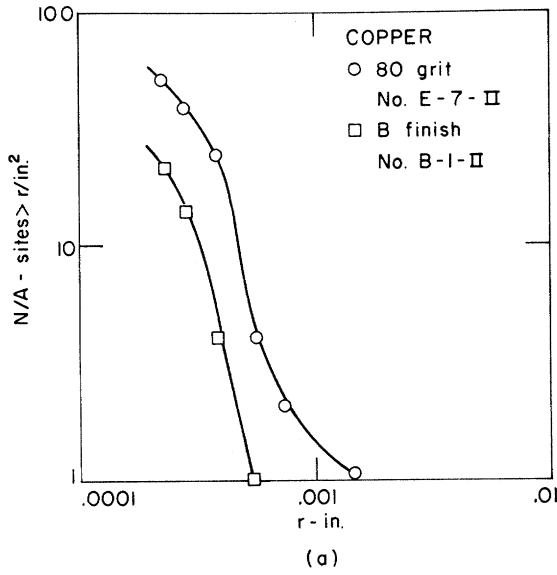


FIG. 4 CAVITY SIZE DISTRIBUTIONS FOR VARIOUS FINISHES

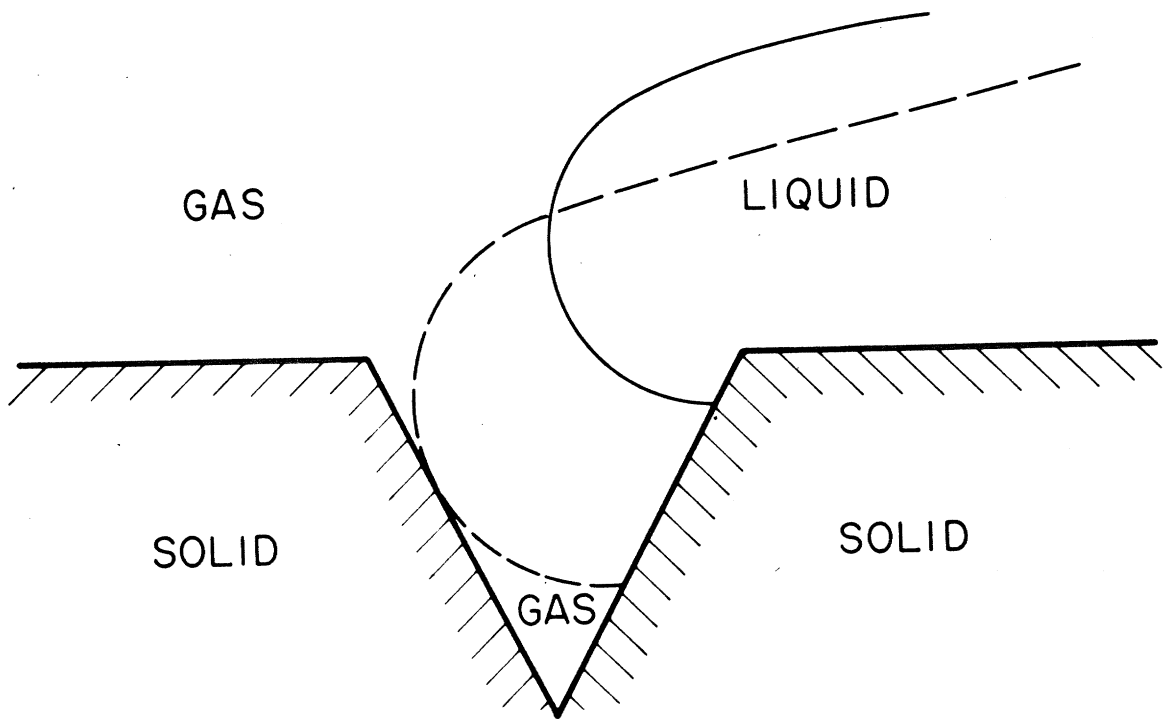


FIG. 5 BANKOFF'S MECHANISM OF NUCLEI FORMATION

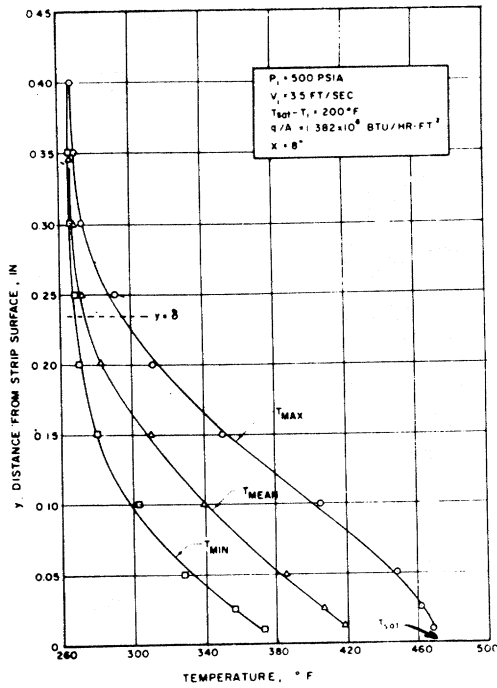


Fig. 6a Maximum, minimum, and mean temperature profiles

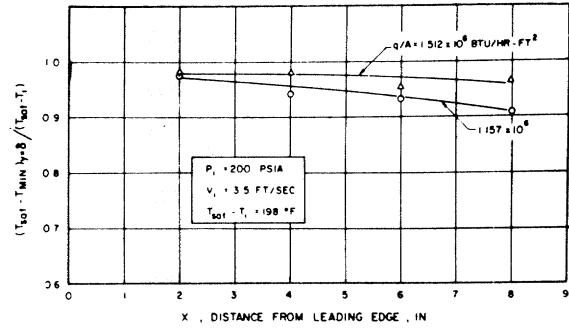


Fig. 6d Minimum temperature distribution at the single-phase core-bubble boundary interface

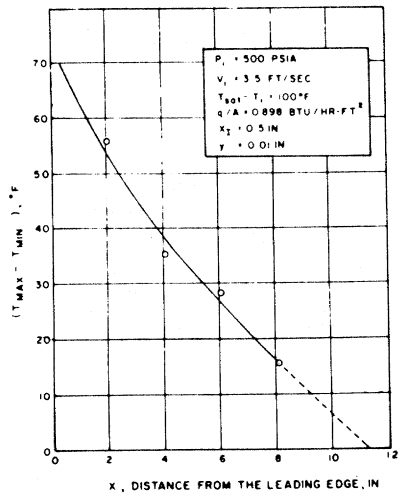


Fig. 6c Temperature fluctuations versus distance from the leading edge

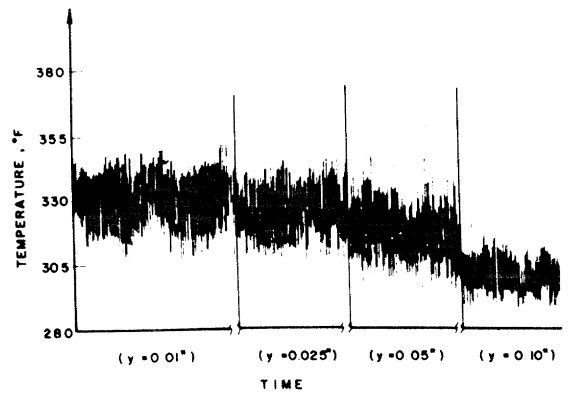
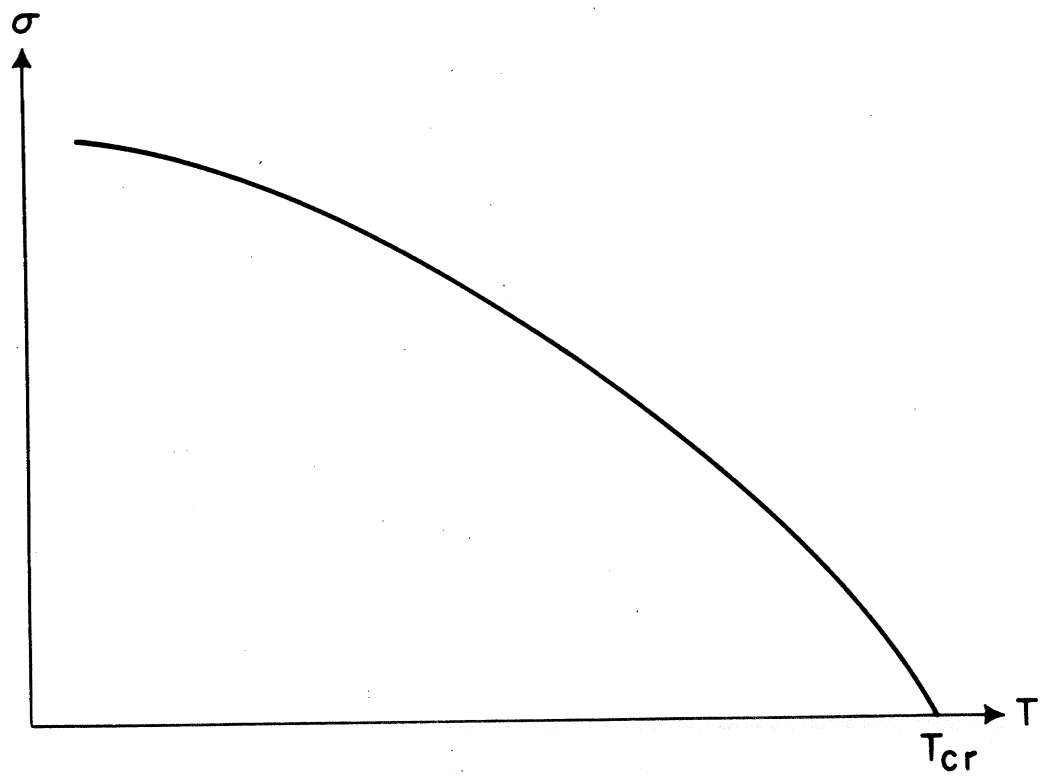
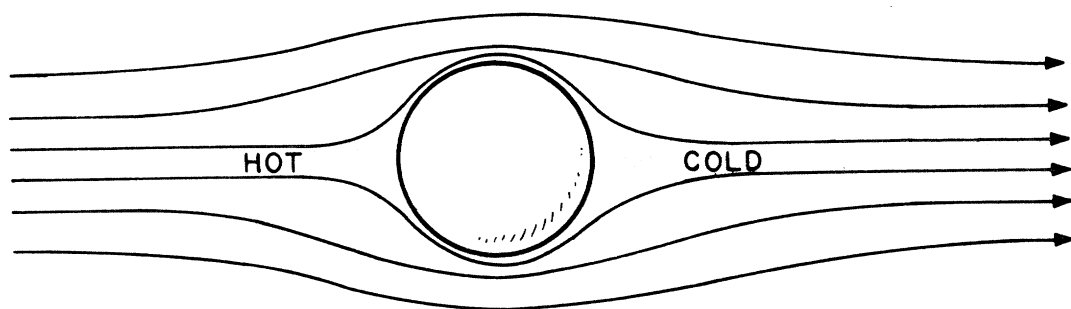


Fig. 6b Typical oscillograph trace of temperature fluctuations



(a)



(b)

FIG. 7 THE MECHANISM OF THERMOCAPILLARITY

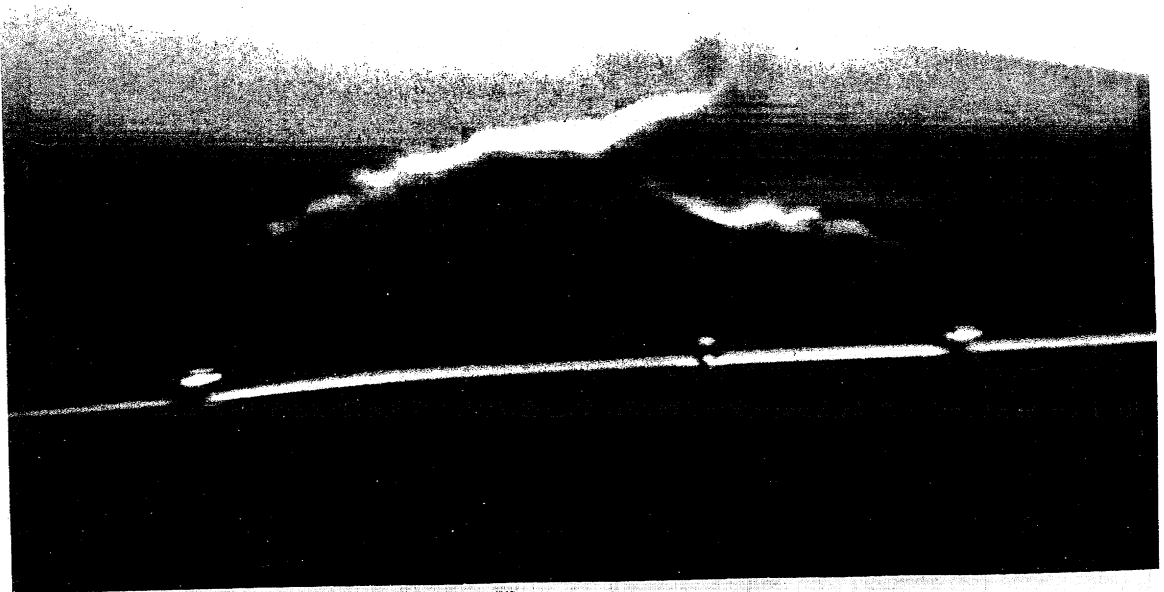
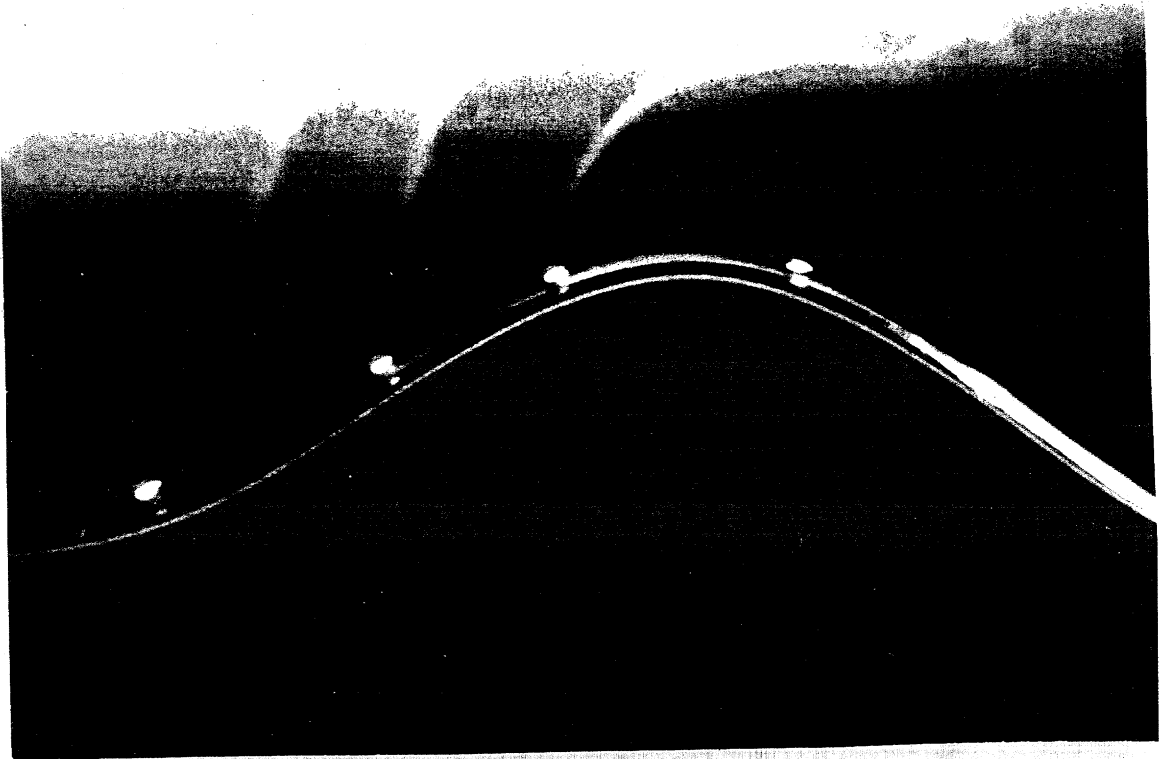


FIG. 8 JETTING IN ACETONE - TREFETHEN¹⁸

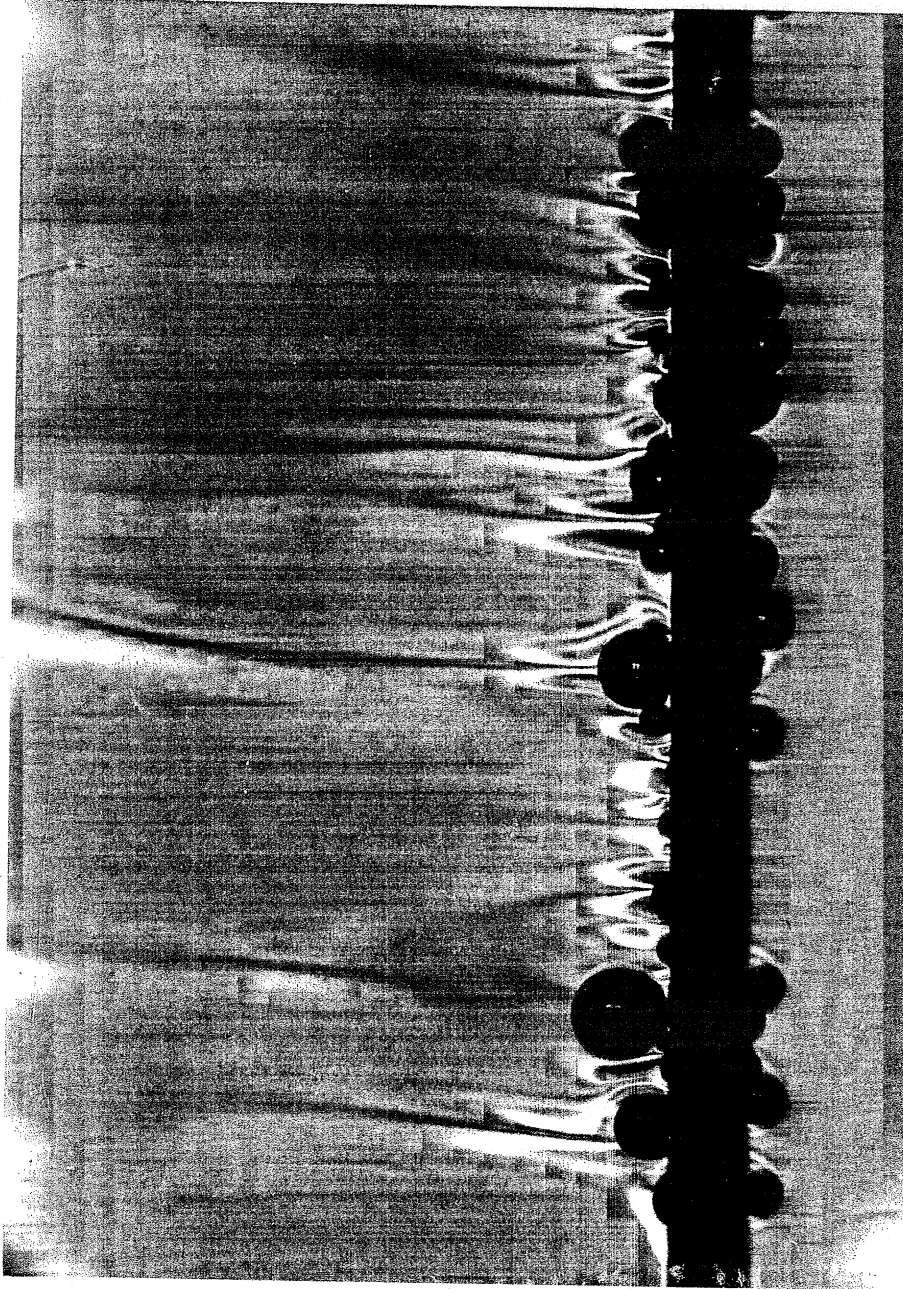


FIG. 9 JETTING IN WATER - FARELLO¹⁹

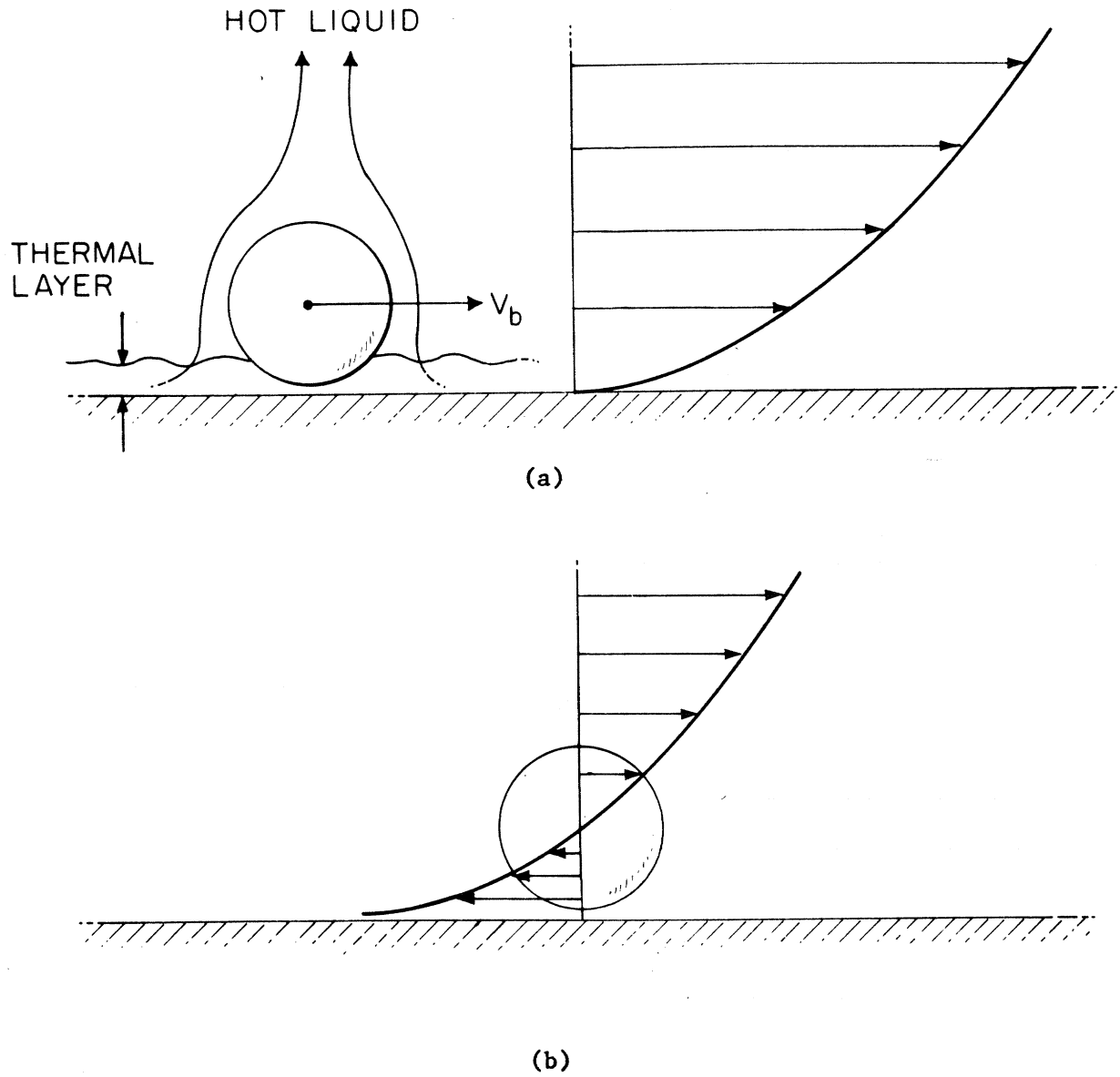


FIG. 10 THE INFLUENCE OF FLOW VELOCITY ON THERMOCAPILLARITY

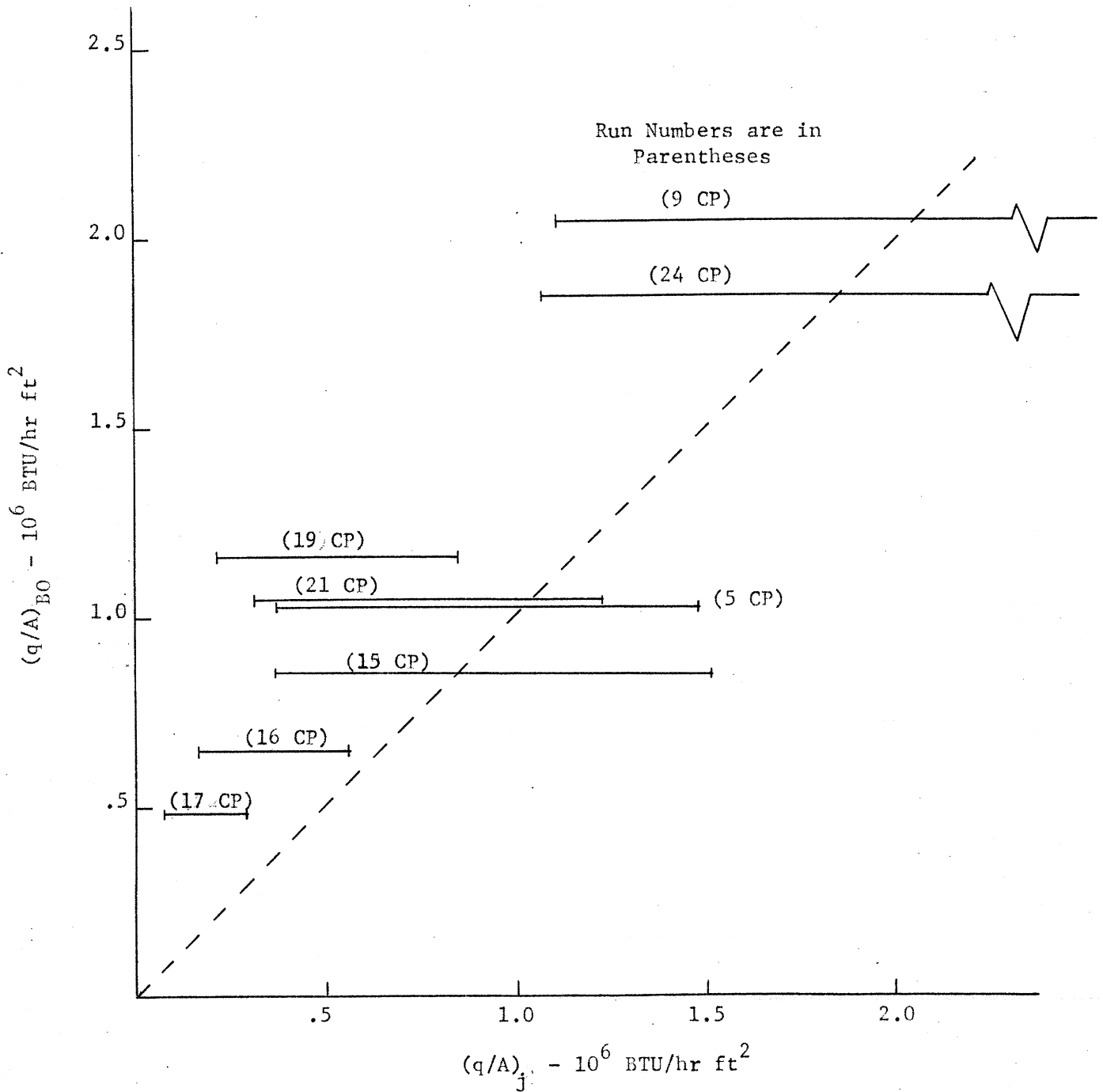


FIG. 11 COMPARISON OF BURNOUT HEAT FLUX WITH THE
EXPECTED THERMOCAPILLARITY HEAT FLUX

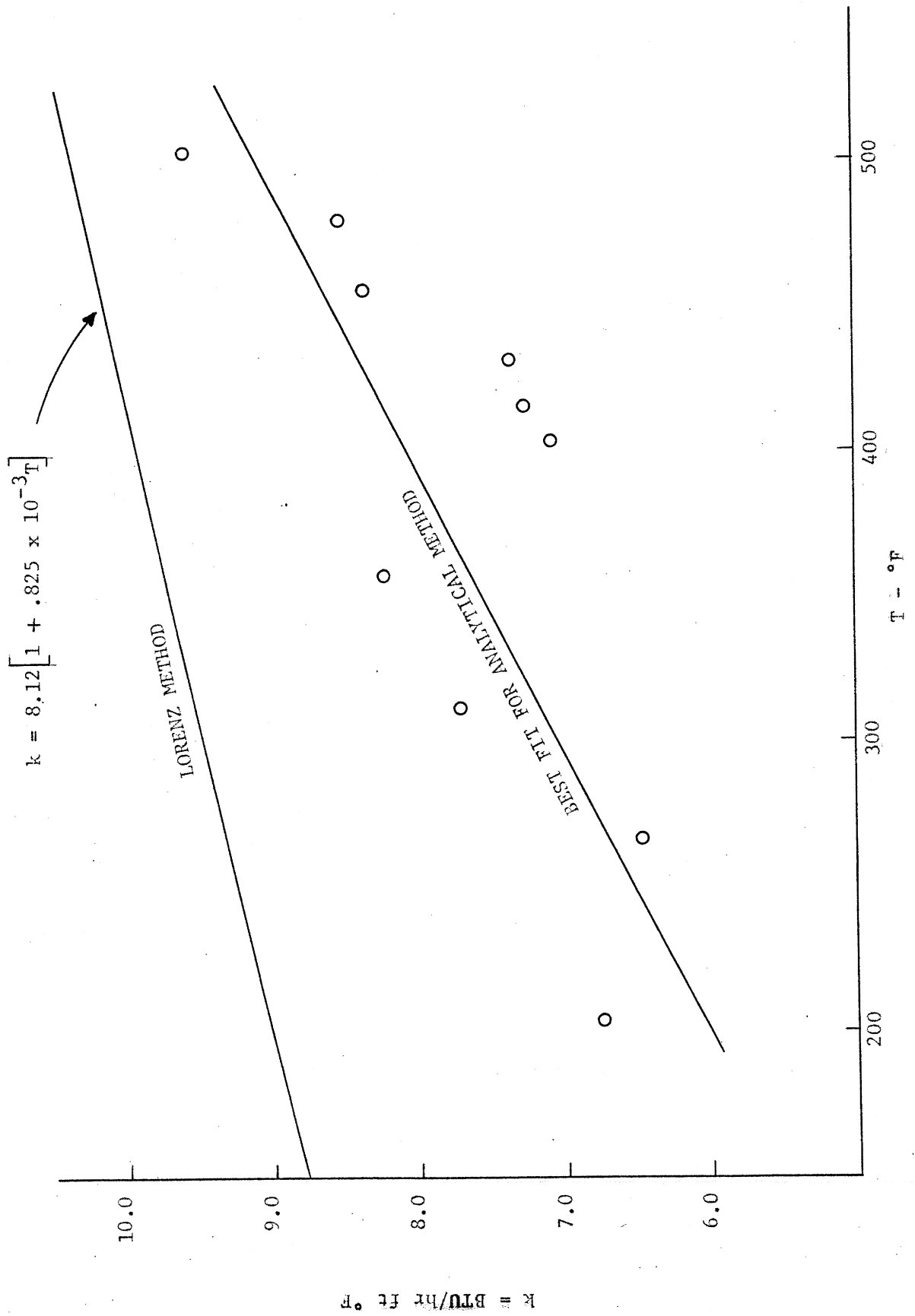


FIG. 12 TEMPERATURE DEPENDENCE OF THERMAL CONDUCTIVITY FOR 304 STAINLESS STEEL

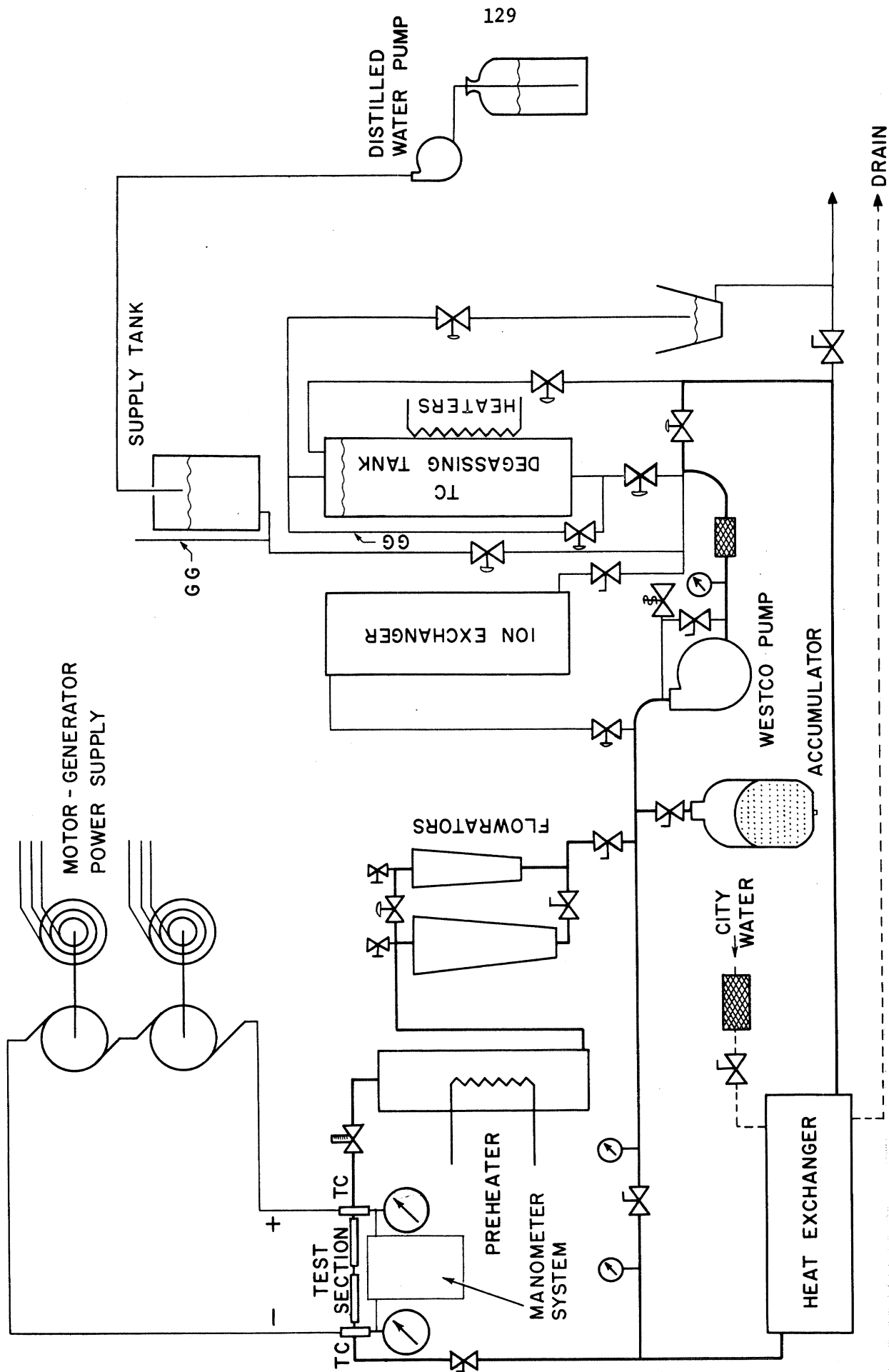


FIG. 13 SCHEMATIC LAYOUT OF EXPERIMENTAL FACILITY

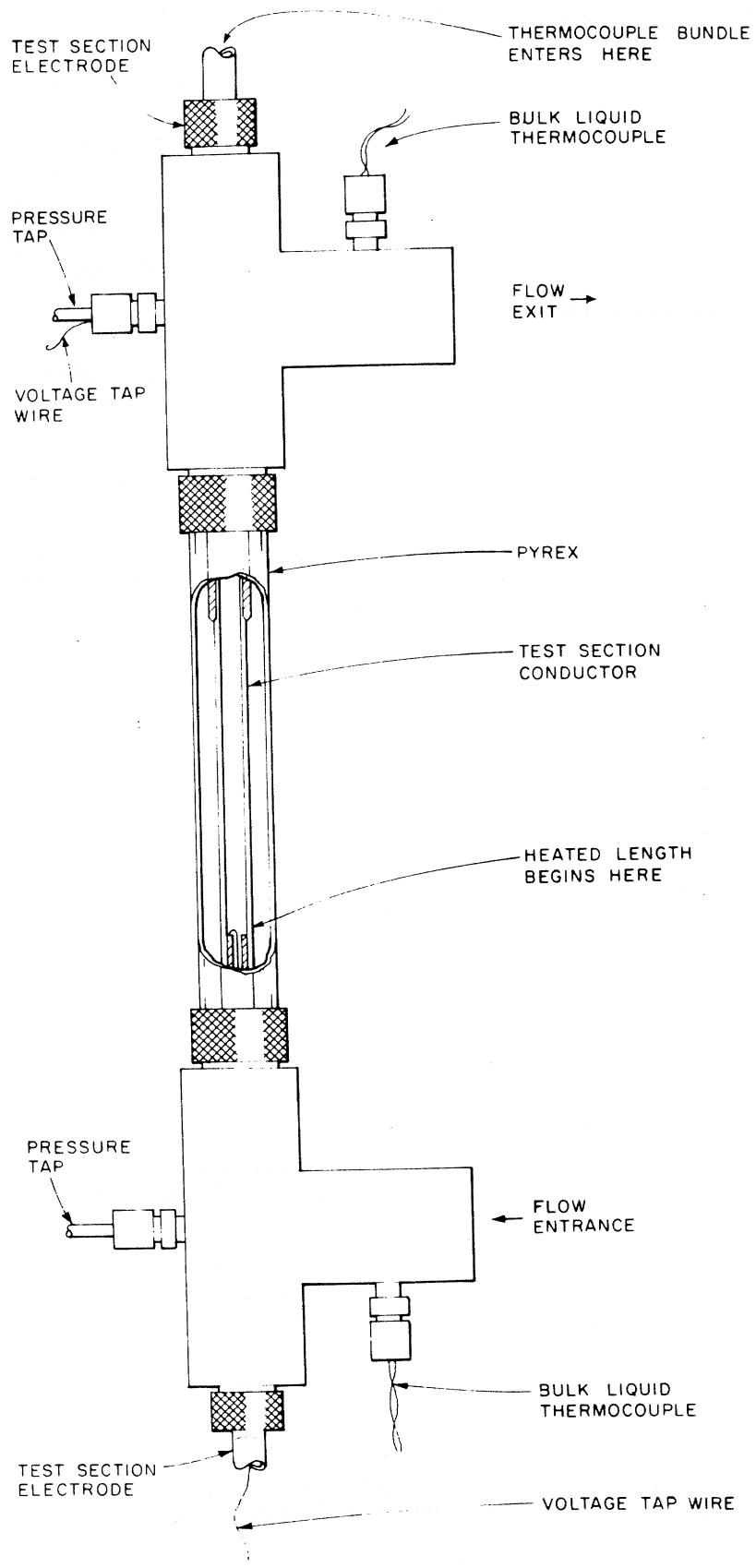


FIG. 14 TEST SECTION ASSEMBLY

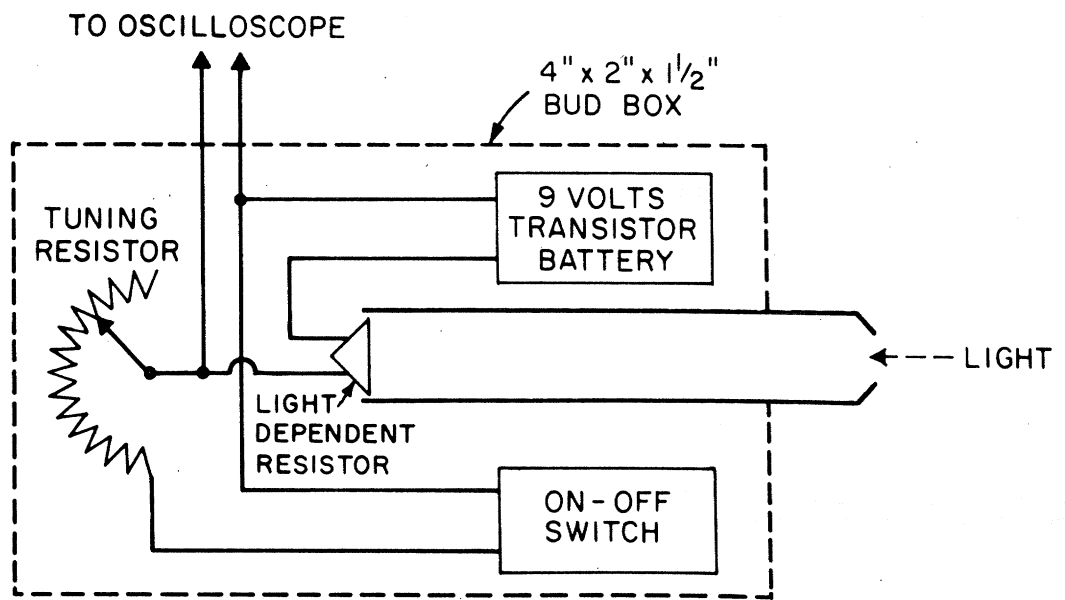
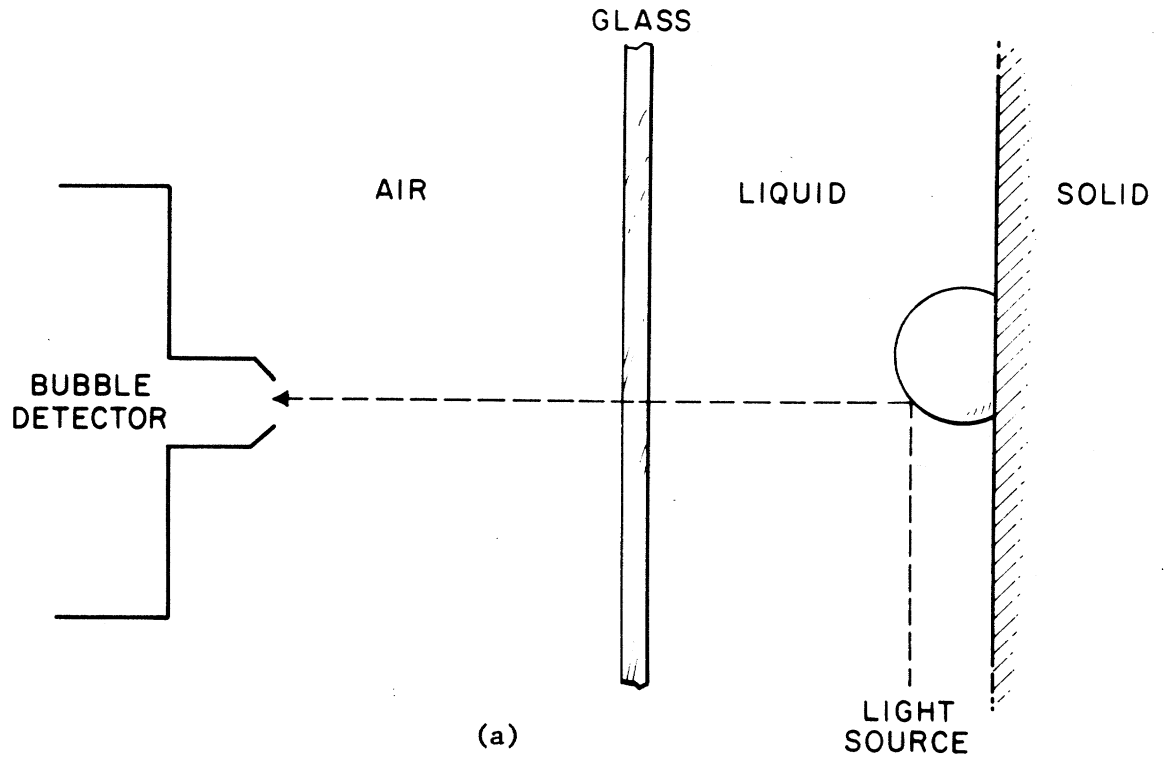


FIG. 15 SCHEMATIC OF BUBBLE DETECTOR

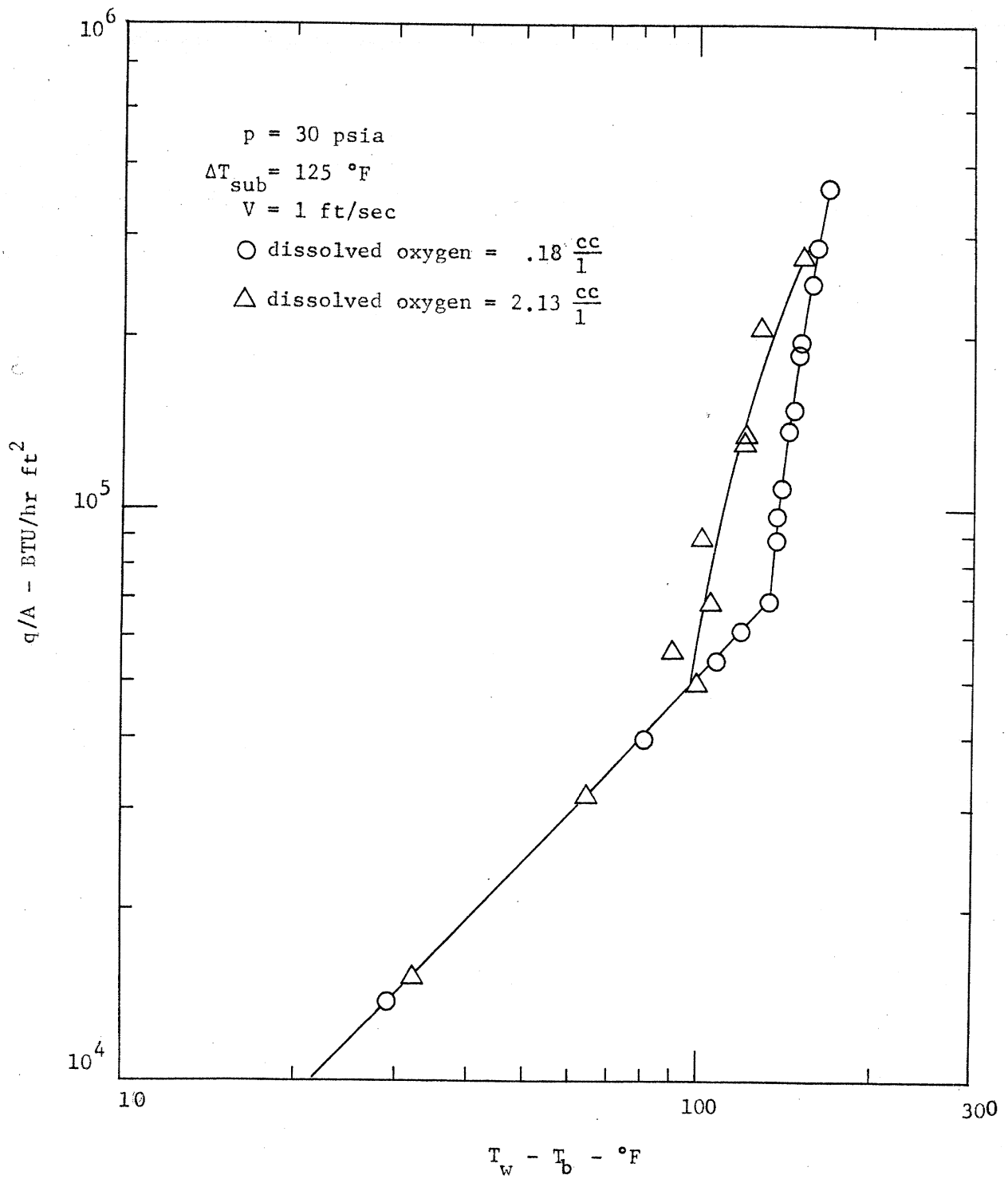


FIG. 16 INFLUENCE OF DISSOLVED GAS ON INCEPTION OF FLOW SURFACE BOILING

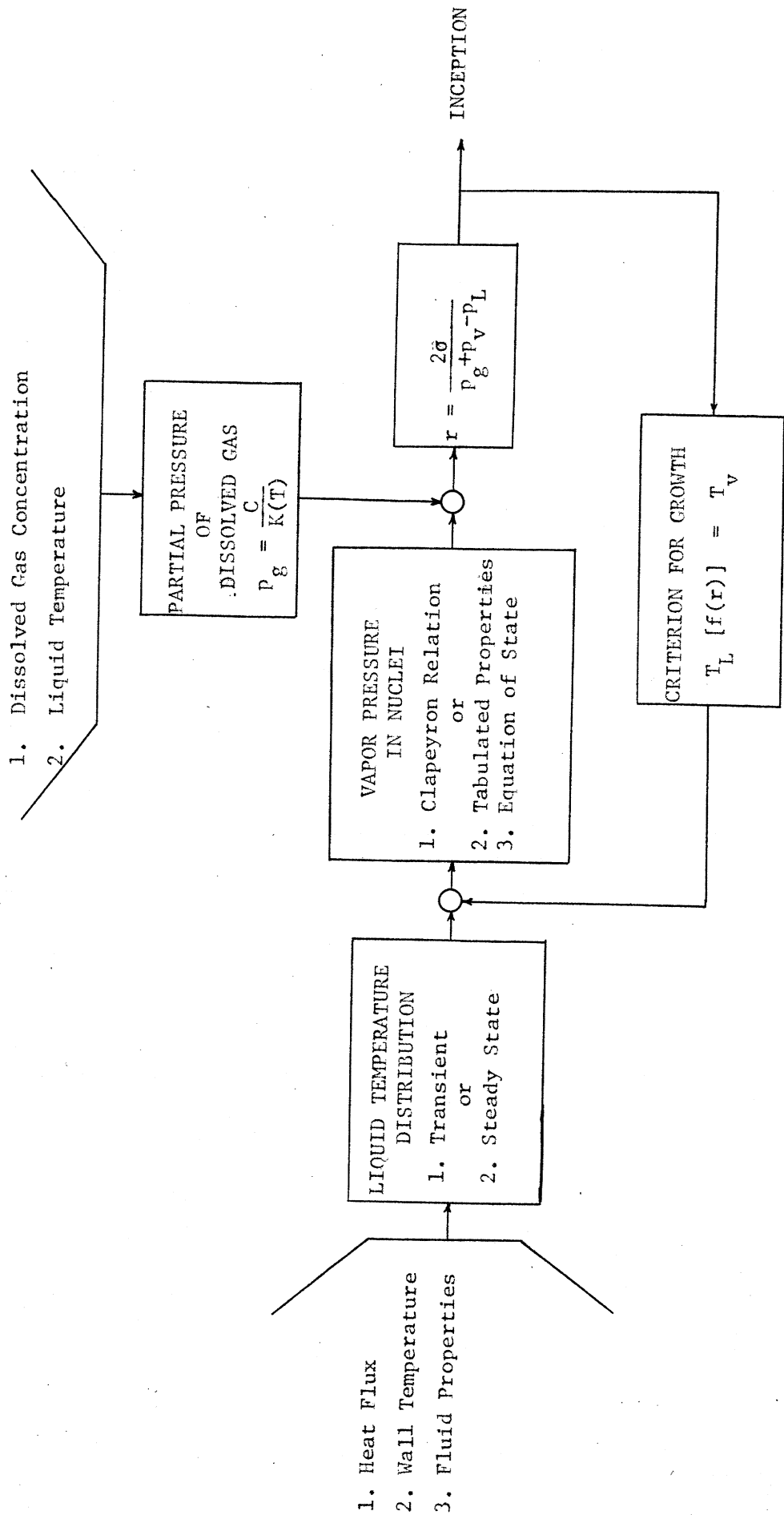


FIG. 17 GENERALIZED FLOW DIAGRAM FOR BOILING INCEPTION

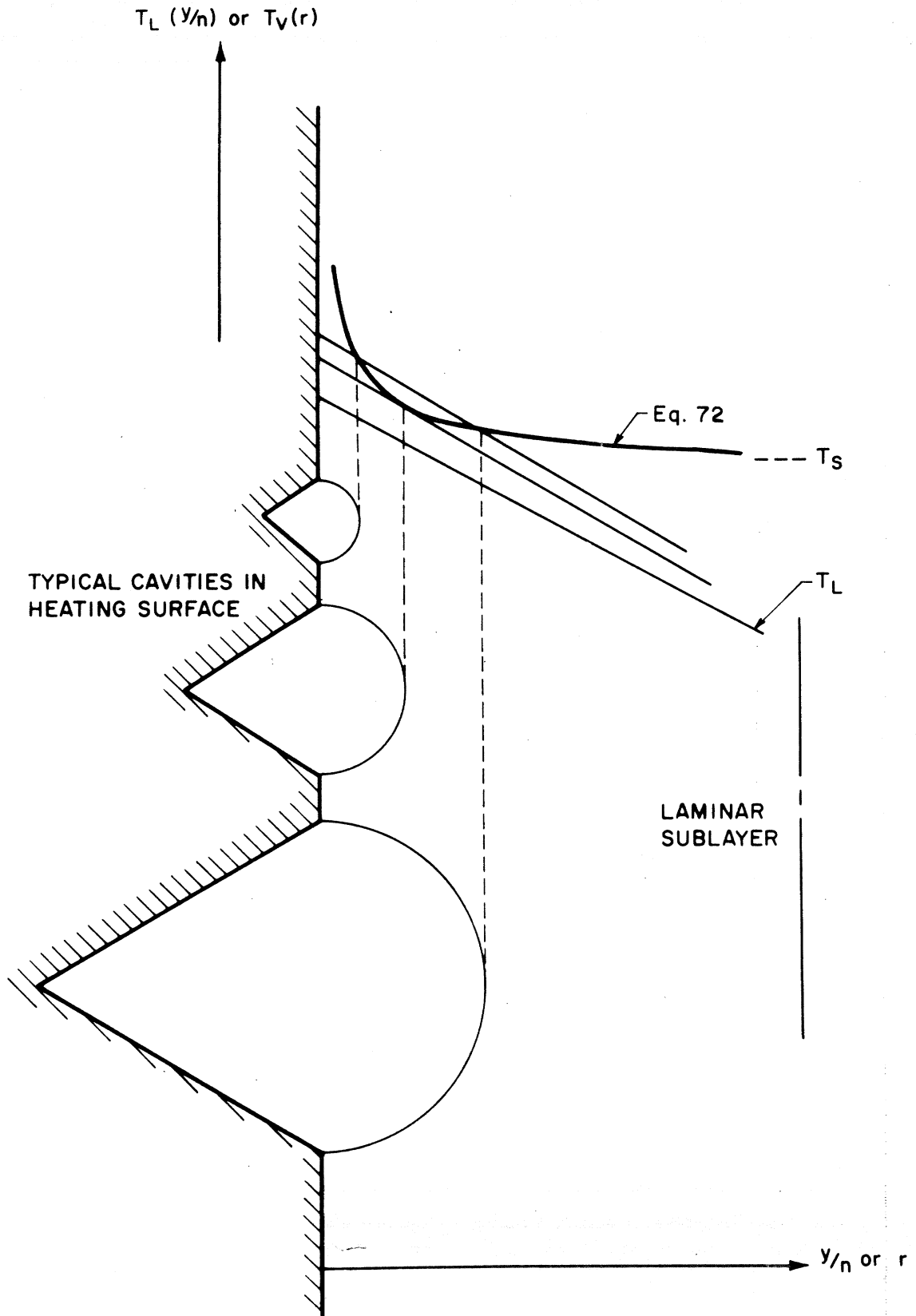


FIG. 18 SCHEMATIC REPRESENTATION OF BUBBLE GROWTH IN FLOW SURFACE BOILING

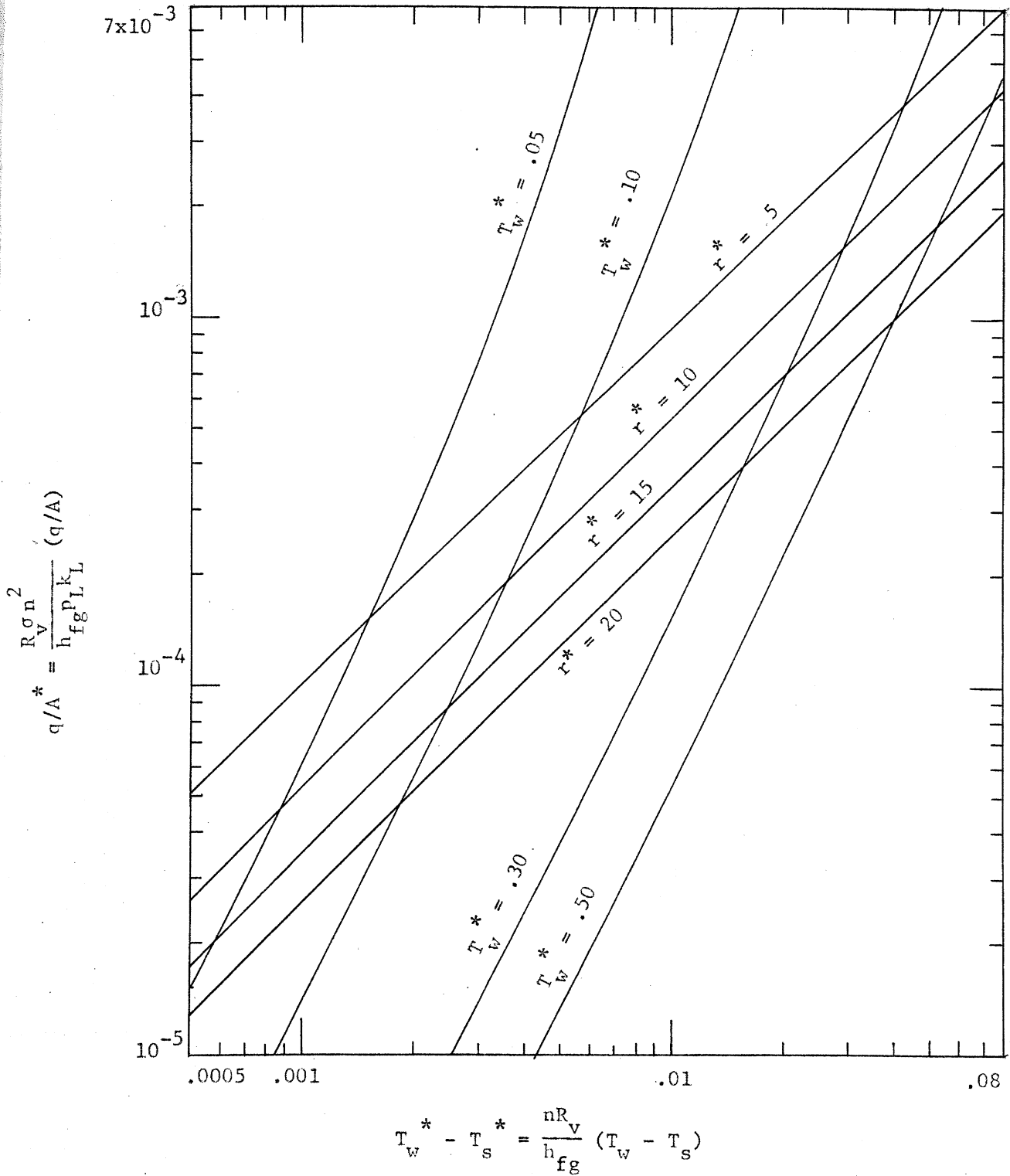


FIG. 19 DIMENSIONLESS REPRESENTATION OF INCEPTION

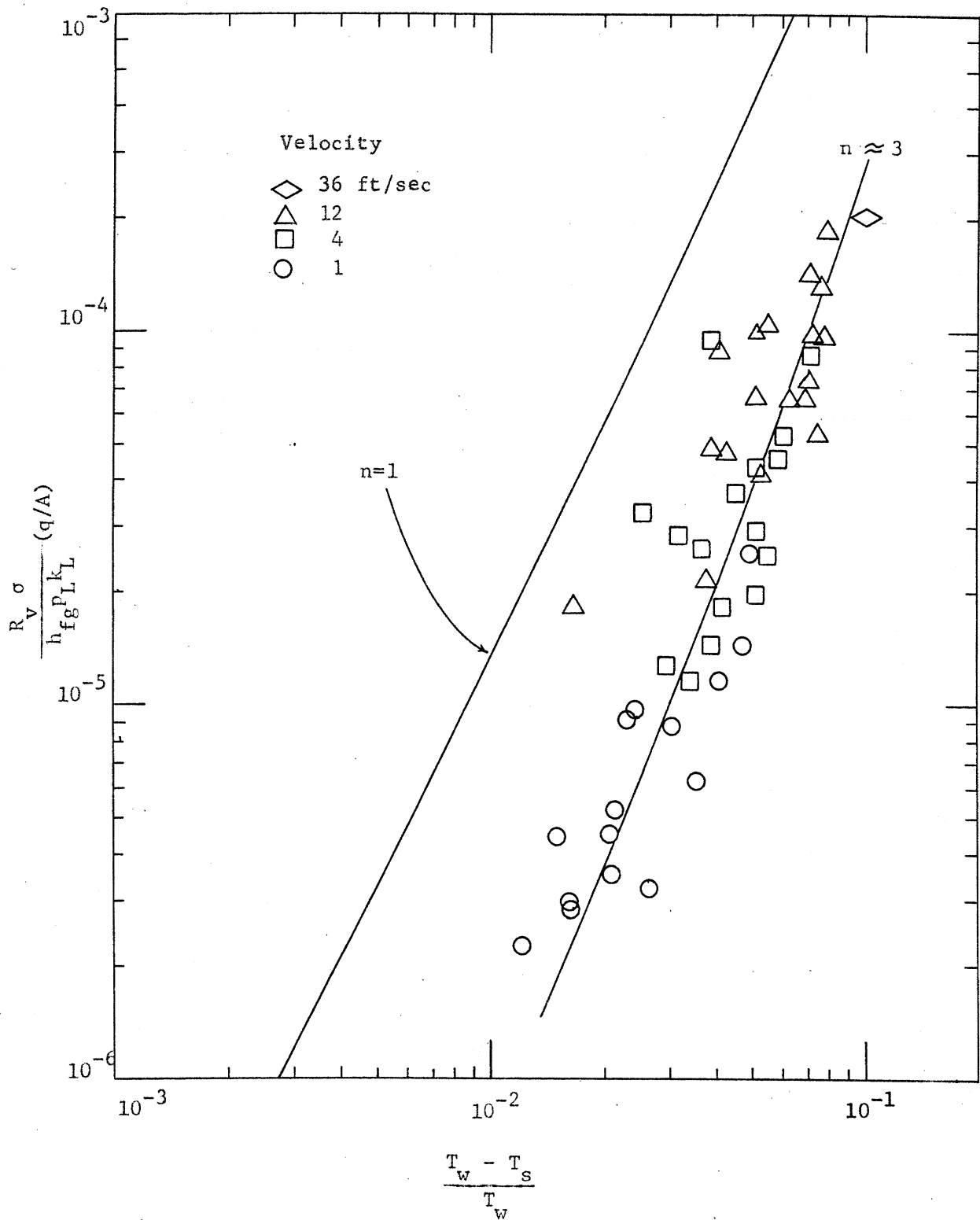


FIG. 20 FLOW BOILING INCEPTION DATA OF MCADAMS' PROJECT⁵¹

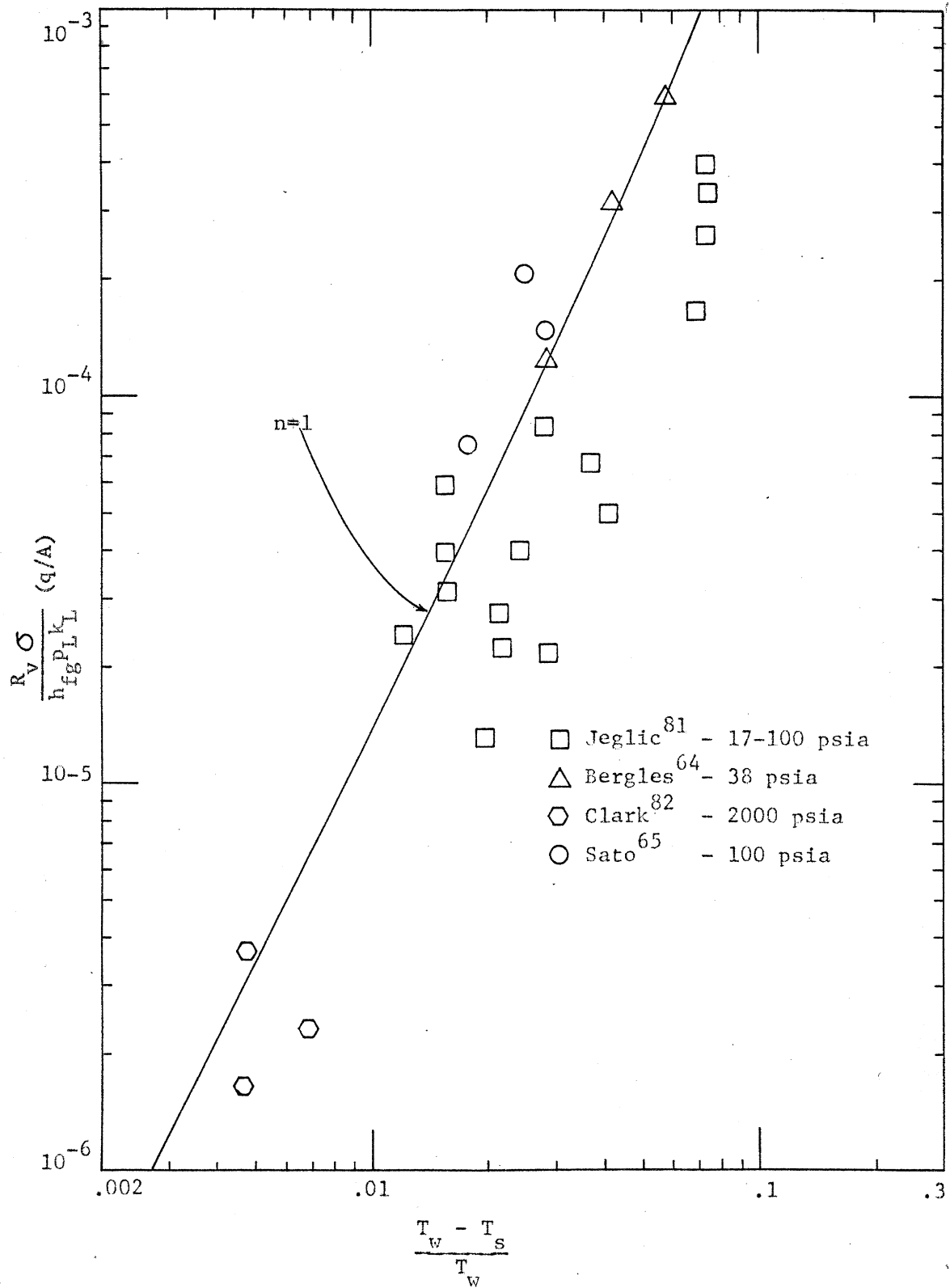


FIG. 21 FLOW BOILING INCEPTION DATA OF VARIOUS INVESTIGATORS FOR WATER

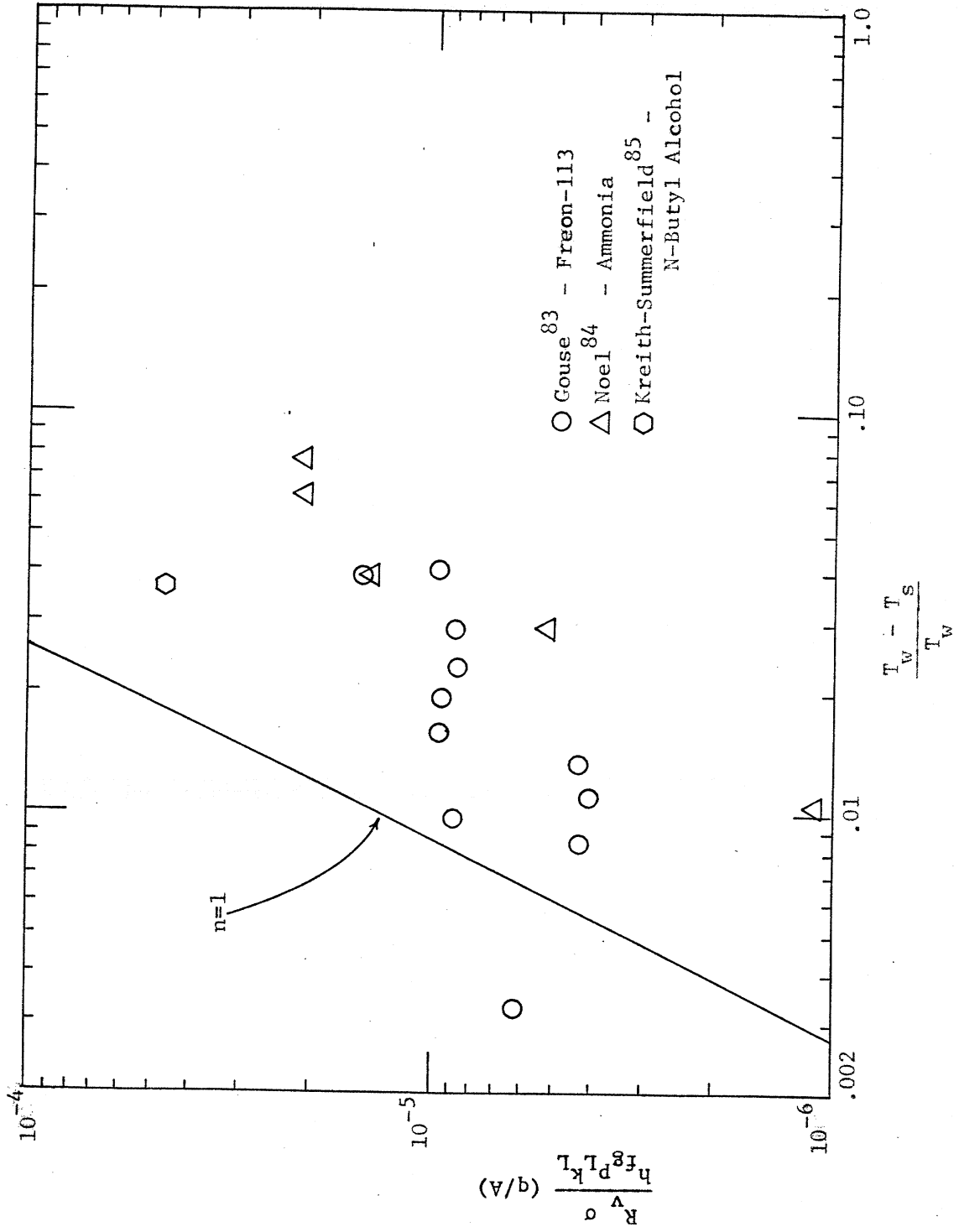


FIG. 22 INCEPTION DATA OF VARIOUS INVESTIGATORS FOR FLUIDS OTHER THAN WATER

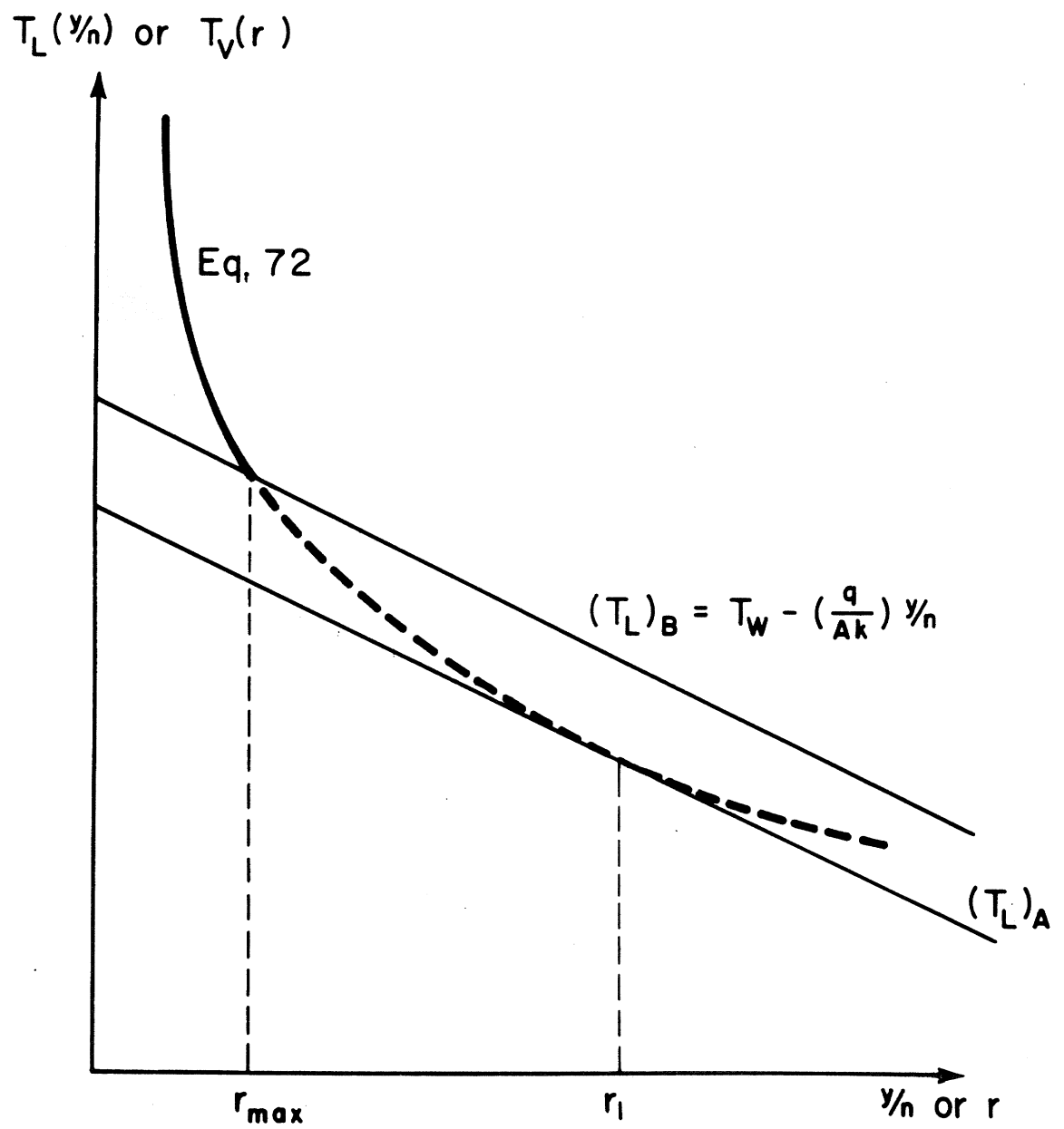


FIG. 23 INCEPTION OF FLOW SURFACE BOILING

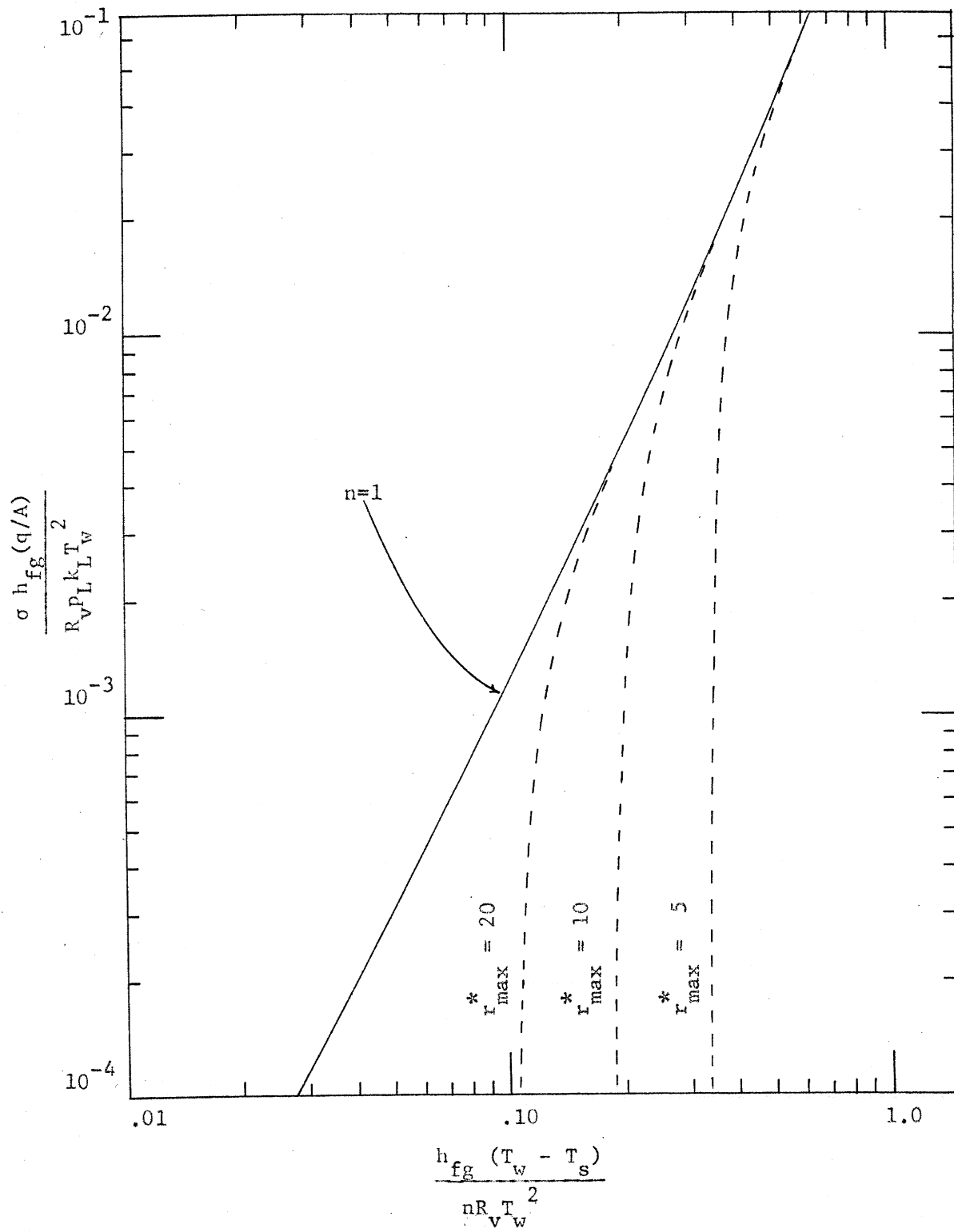


FIG. 24 DIMENSIONLESS INCEPTION LOCI WHEN THE LARGEST CAVITY IS r_{max}

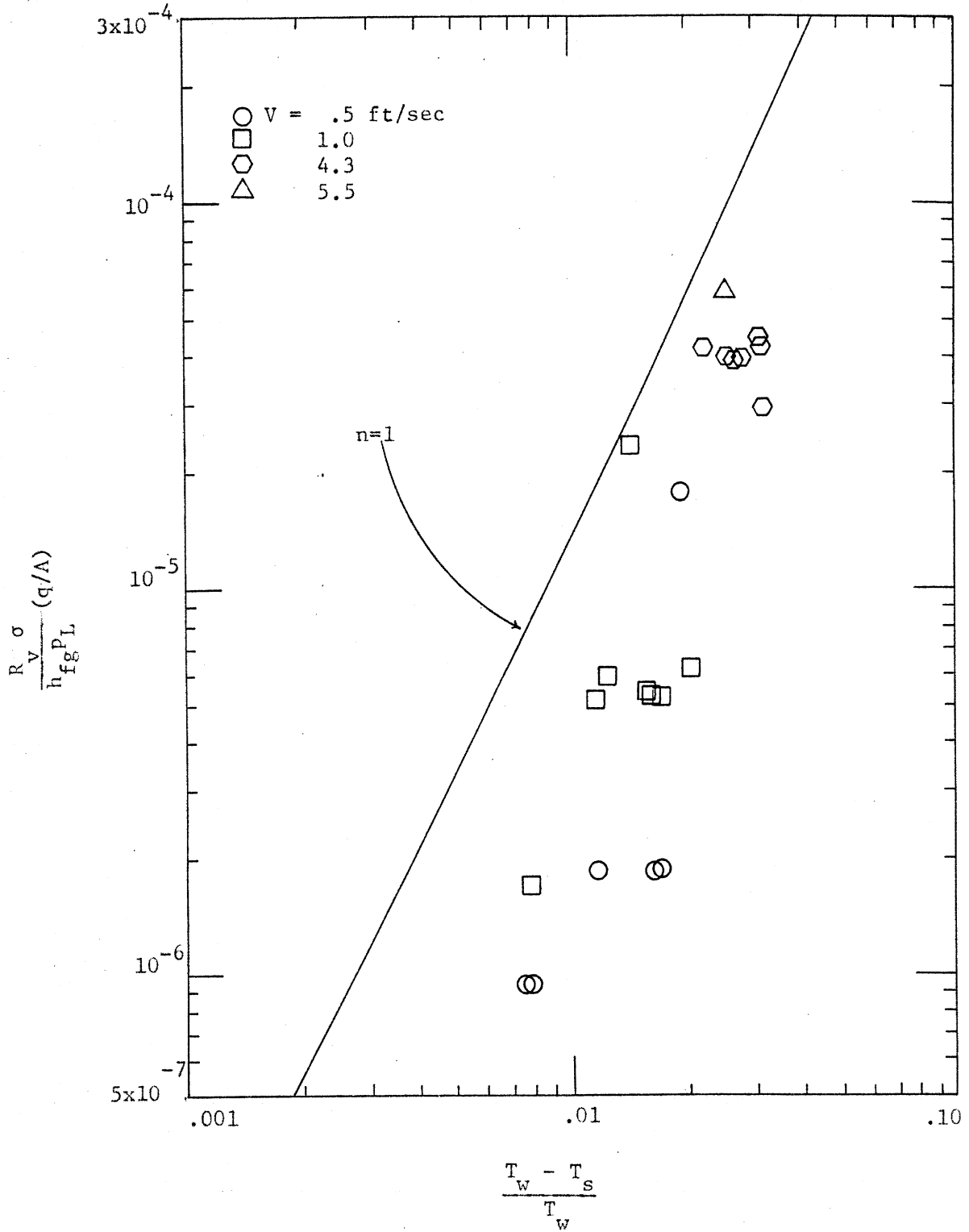


FIG. 25 FLOW BOILING INCEPTION DATA FOR WATER FROM PRESENT INVESTIGATION

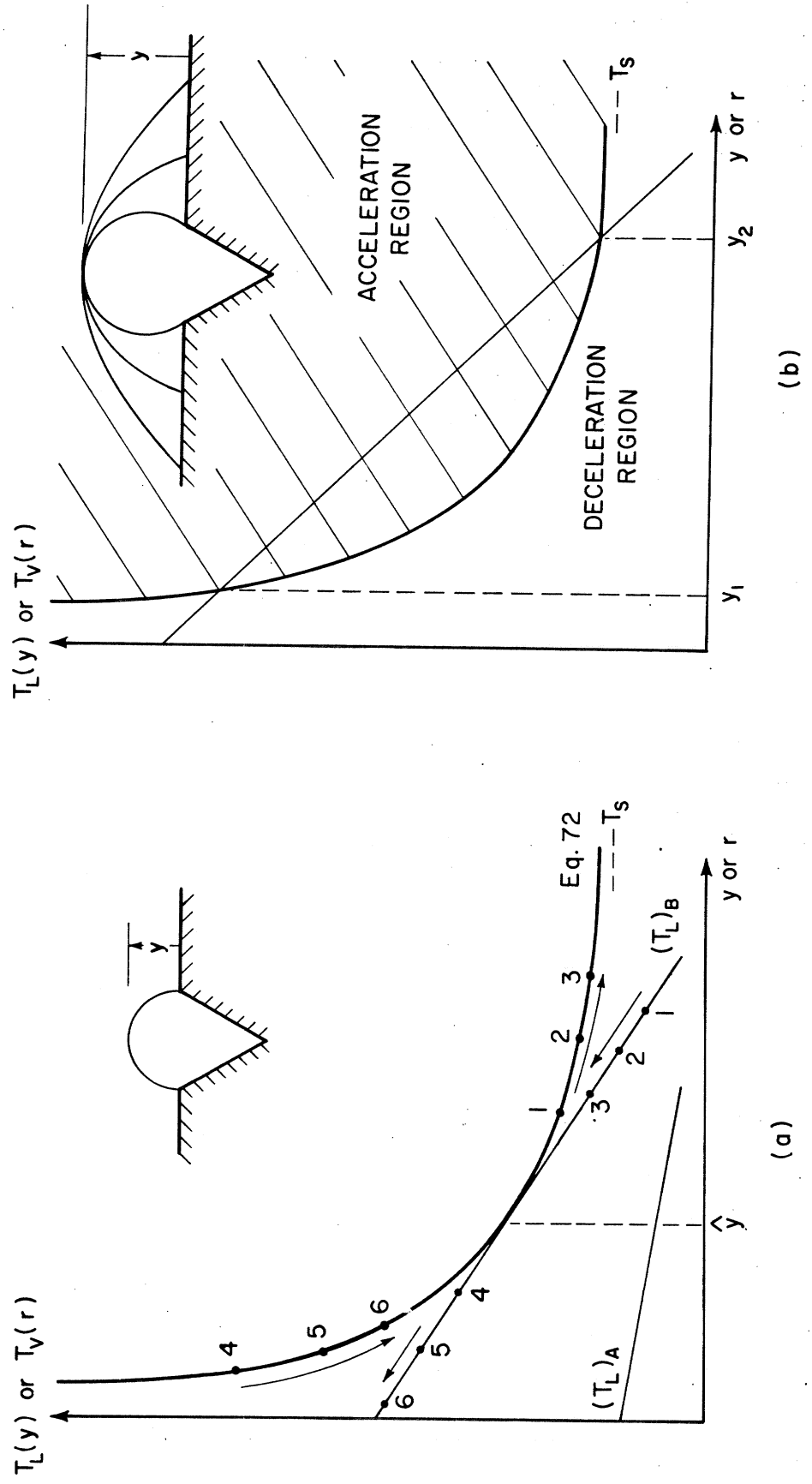


FIG. 26 SOME CONDITIONS OF BUBBLE GROWTH AND COLLAPSE

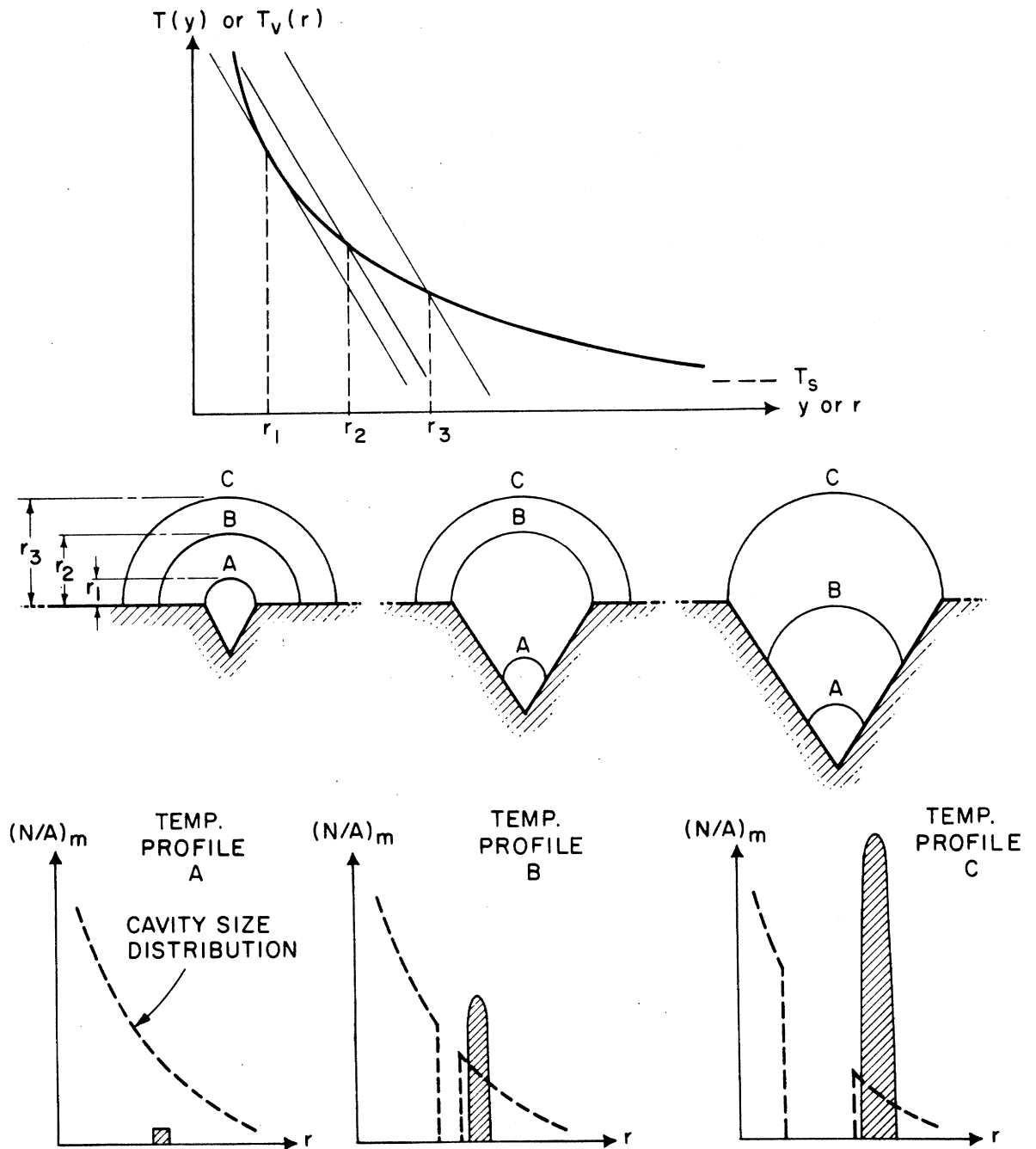


FIG. 27 ILLUSTRATION OF METASTABLE STATES FOR NUCLEI

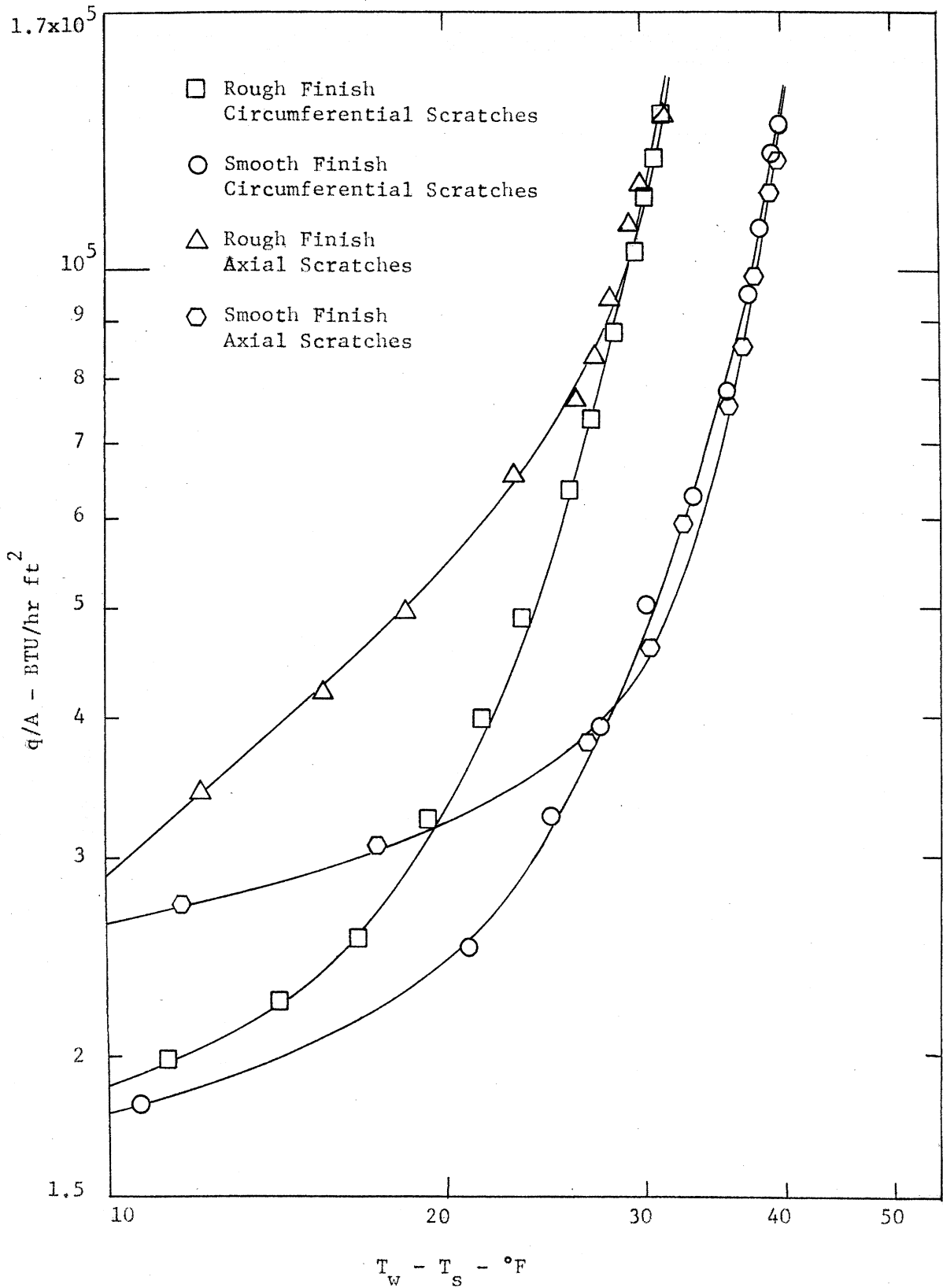


FIG. 28 INFLUENCE OF SURFACE FINISH WHEN POOL BOILING
FROM THE OUTSIDE OF A HORIZONTAL TUBE

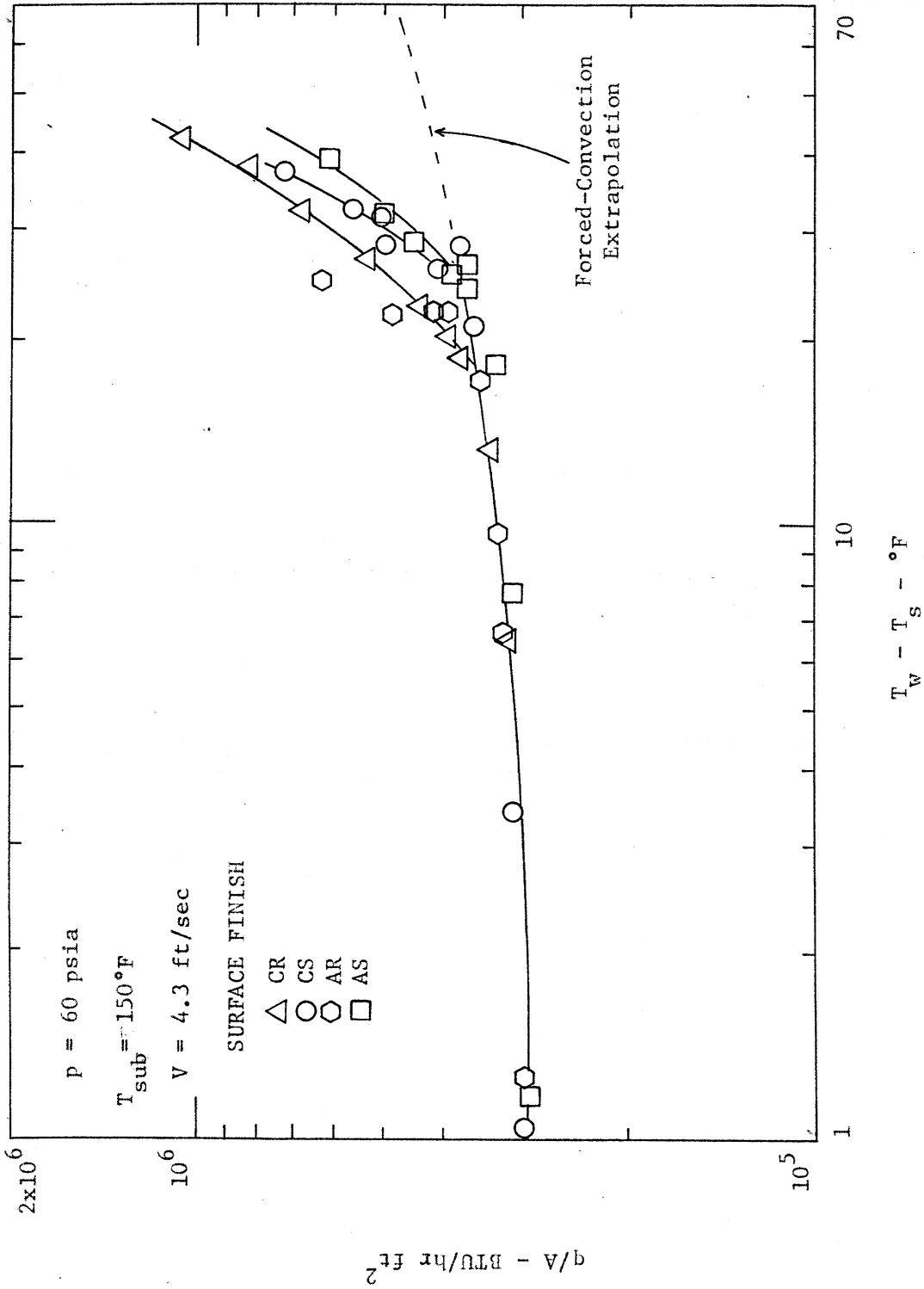


FIG. 29 FLOW SURFACE BOILING DATA - MODERATE HEAT FLUX

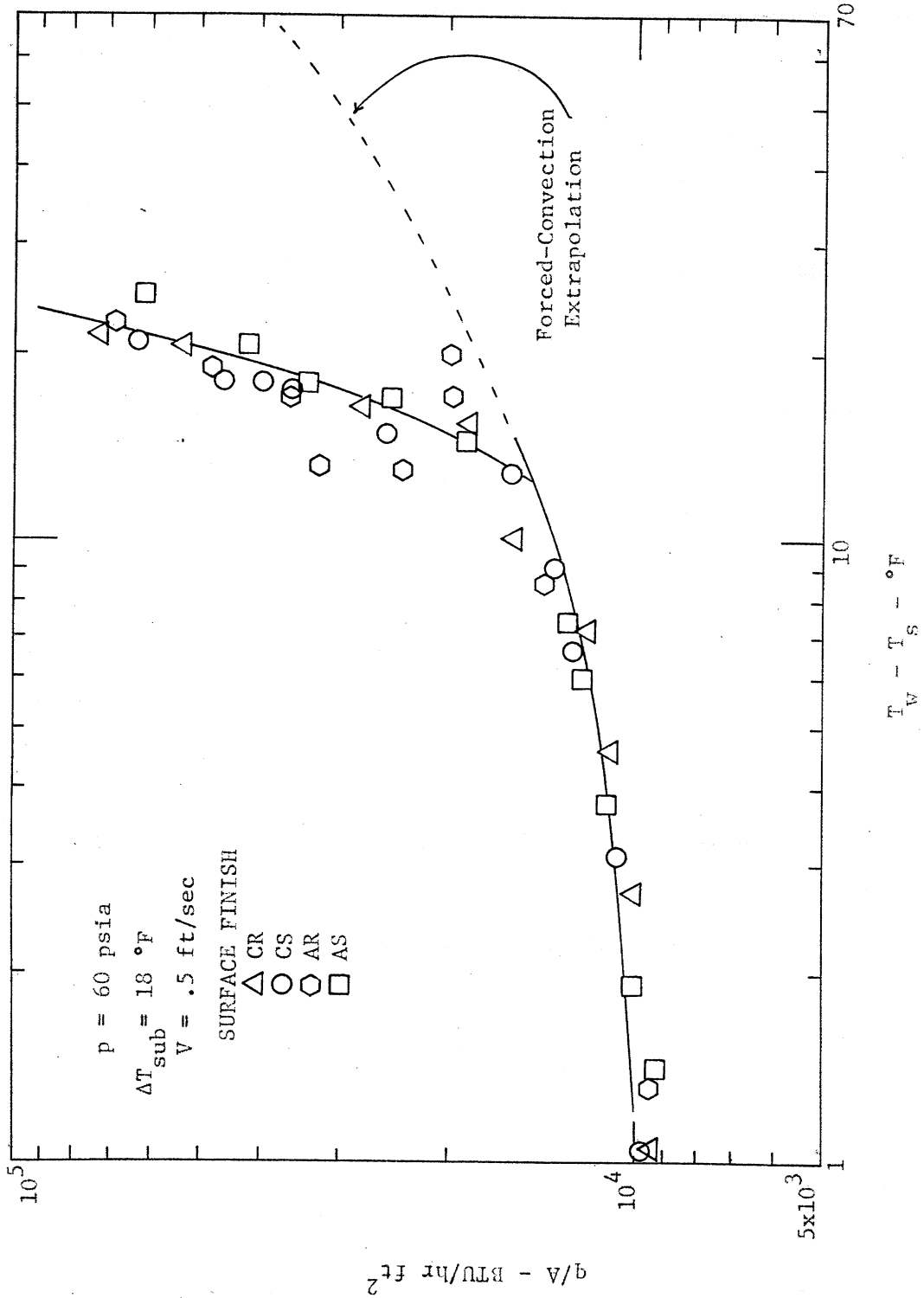


FIG. 31 FLOW SURFACE BOILING DATA - VERY LOW HEAT FLUX

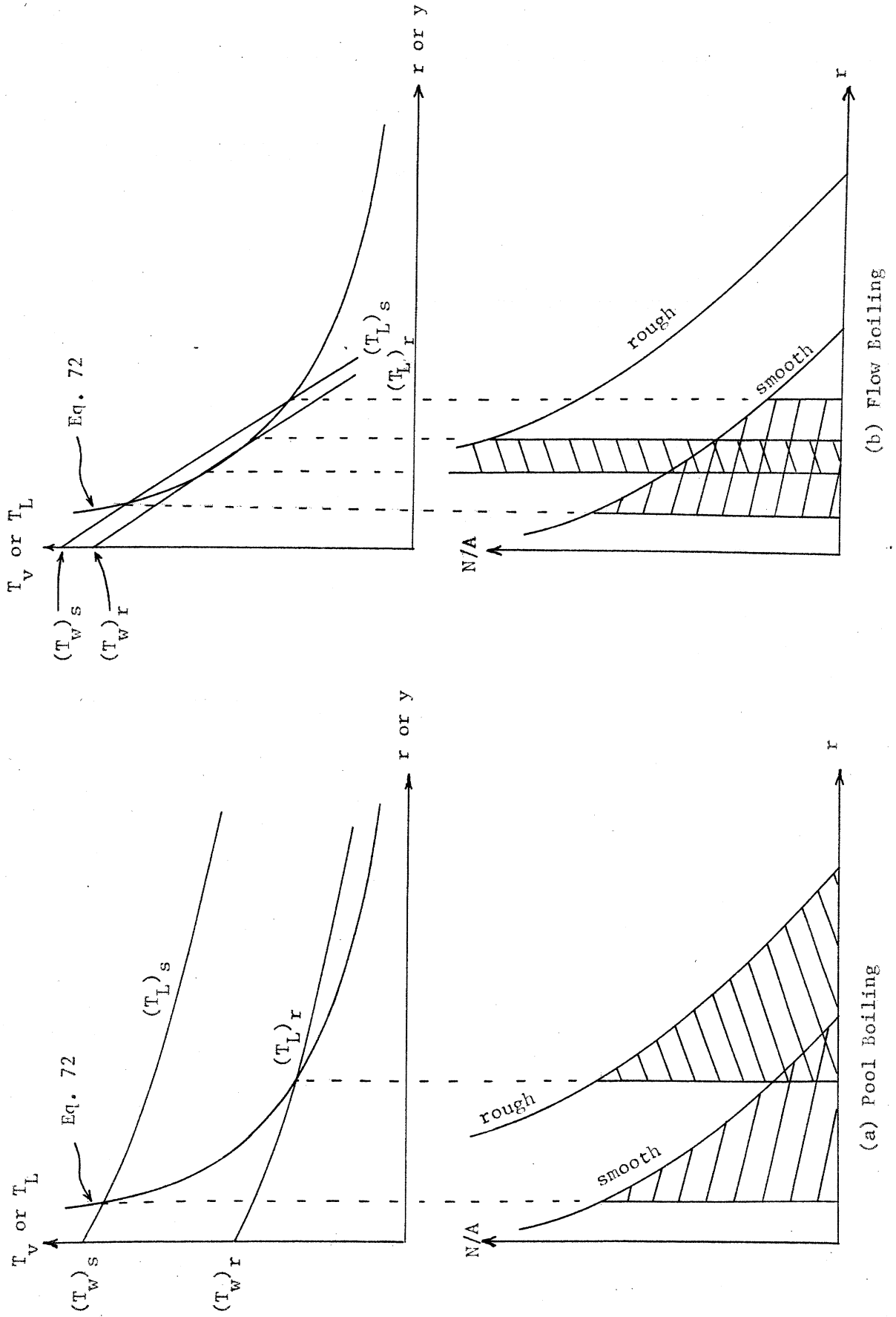


FIG. 32 EXPECTED INFLUENCE OF SURFACE FINISH - POOL vs. FLOW BOILING

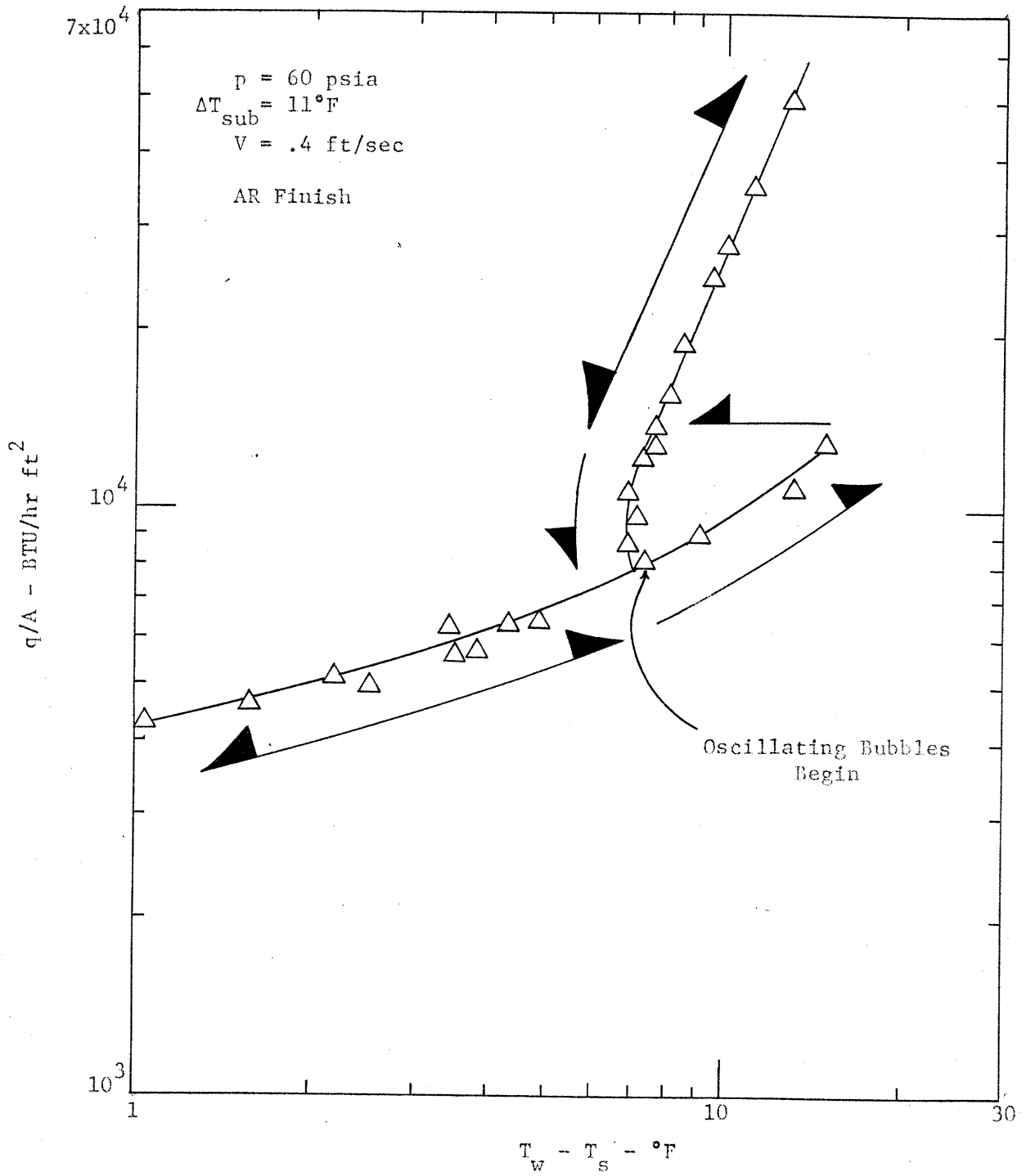


FIG. 33 DATA ILLUSTRATING HYSTERESIS IN FLOW BOILING

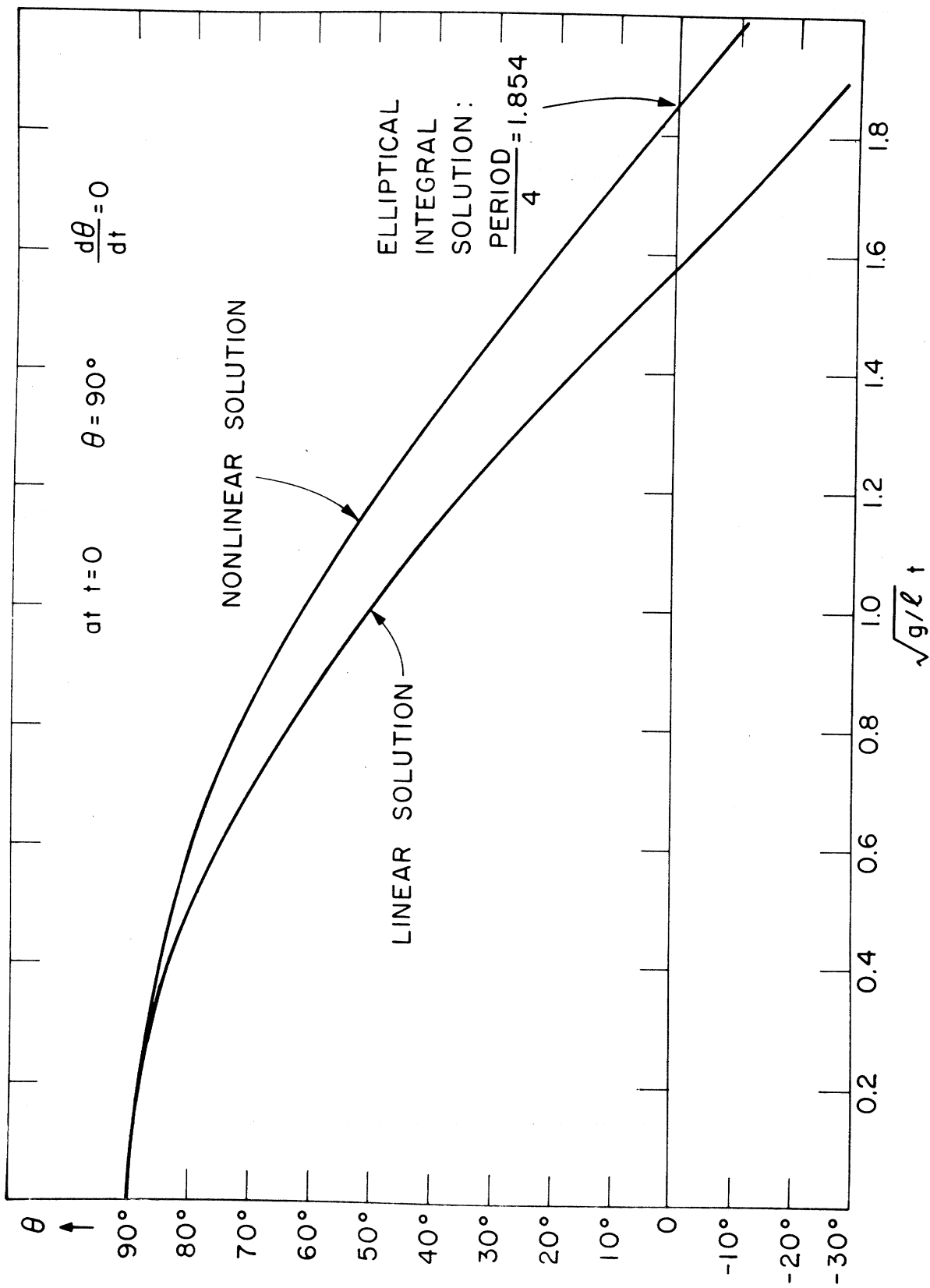


FIG. 34 COMPARISON OF LINEAR AND NONLINEAR SOLUTIONS FOR THE GRAVITY PENDULUM

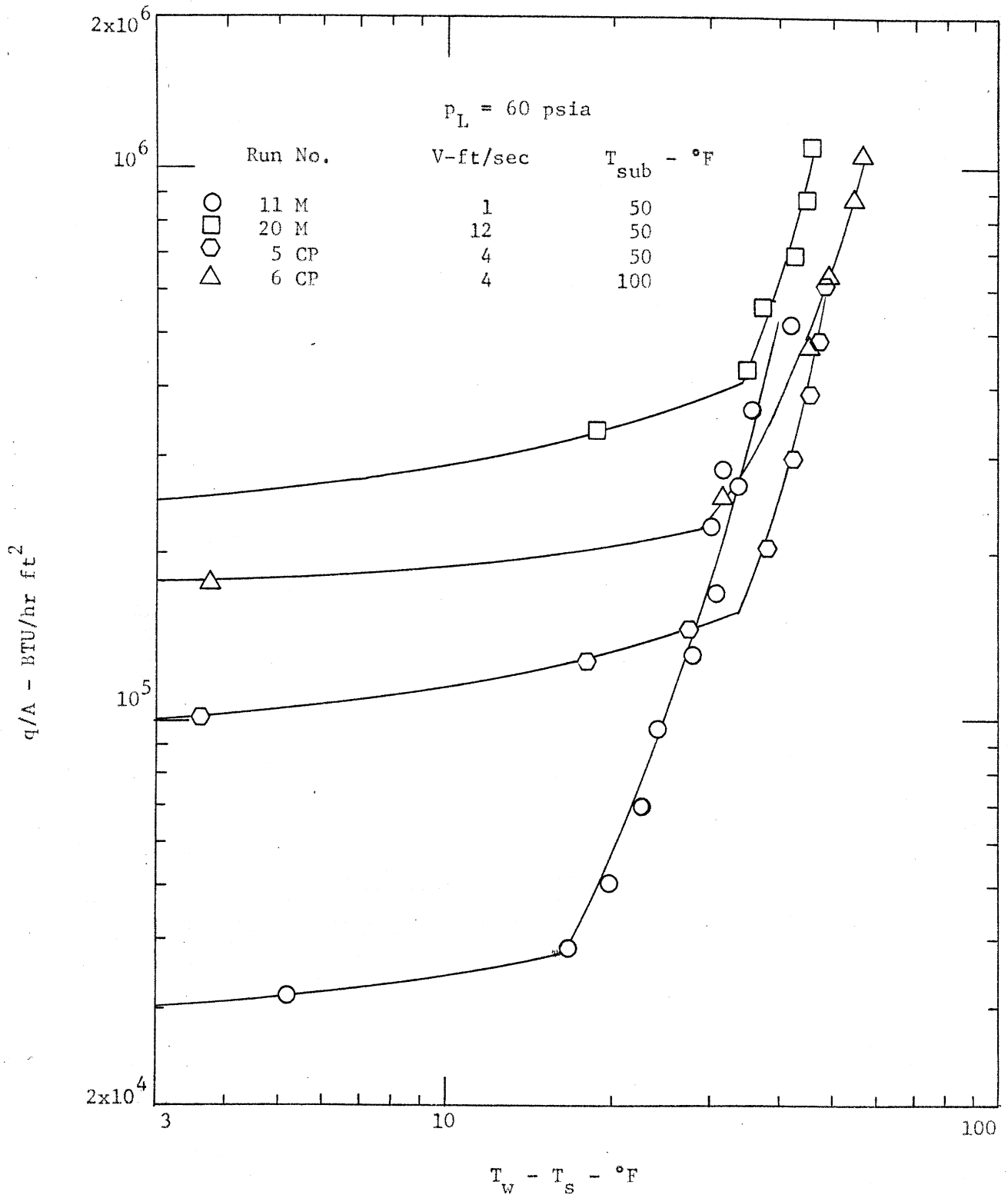


FIG. 35 SOME FLOW SURFACE BOILING DATA OF MCADAMS, et al.³⁰

BIOGRAPHICAL NOTE

Walter T. Brown, Jr., was born August, 18, 1937, in Kansas City, Missouri, the son of Mr. and Mrs. Walter T. Brown, now of Phoenix, Arizona. He attended primary and secondary schools in St. Louis, Missouri, and Toledo, Ohio. Following graduation from Libbey High School, Toledo, he attended the United States Military Academy at West Point.

After graduation from West Point in 1959, he completed training as a paratrooper and later as an Army Ranger. His next assignment was with the 82nd Airborne Division. From 1962 to 1963 he attended New Mexico State University, where he received his Master of Science degree in mechanical engineering. The following assignment was at the Army's missile test range at White Sands, New Mexico. There he served as the Chief of Engineering and Evaluation for three of the currently developing missile systems.

In September of 1964 he entered M. I. T., having earlier received a National Science Foundation Graduate Fellowship. Upon graduation from M. I. T., he will be assigned to the 25th Infantry Division in South Vietnam.

He is married to the former Margaret K. Hill. They have three children: Chip, 4 years, Rob, 2 years, and Meg, 8 months.